ASYMPTOTIC METHODS IN SEMICONDUCTOR DEVICE MODELING

Thesis by

Michael Jeffrey Ward

In Partial Fulfillment of the Requirements

for the Degree of

Doctor of Philosophy

California Institute of Technology

Pasadena, California

1988

Submitted May 19, 1988

Acknowledgements

I would like to sincerely thank my advisor, Donald Cohen, for allowing me great latitude in pursuing the invesigations pertaining to this thesis. I would also like to thank my mentor at I.B.M., Farouk Odeh, for three years of friendship and support. I am very grateful for their guidance and encouragement. Thanks are also due to Luis Reyna, of I.B.M., for many fruitful discussions and to John King, of R.P.I., for making his preprint available to me.

I gratefully acknowledge the financial support provided by a Natural Sciences and Engineering Council of Canada Scholarship and an I.B.M. Predoctoral Fellowship.

My stay at Caltech has been enriched by many members of the Applied Mathematics Department. Thanks to Jeff Aguilera, Bob Cox, Michael Landman, and Michael Rotenberry for many years of friendship. In particular, I thank Jeff Aguilera whose THEME package and expert assistance with TEX has saved me many hours of futility in texing this thesis.

Finally, I thank my wife Barbara for her love, patience, and understanding and my mother Alice and my uncle Gary for countless years of moral support.

Abstract

The behavior of metal oxide semiconductor field effect transistors (MOSFETs) with small aspect ratio and large doping levels is analyzed using formal perturbation techniques. Formally, we will show that in the limit of small aspect ratio there is a region in the middle of the channel under the control of the gate where the potential is one-dimensional. The influence of interface and internal layers in the one-dimensional potential on the averaged channel conductivity is closely examined in the large doping limit. The interface and internal layers that occur in the one-dimensional potential are resolved in the limit of large doping using the method of matched asymptotic expansions. The asymptotic potential in the middle of the channel is constructed for various classes of variable doping models including a simple doping model for the built-in channel device. Using the asymptotic one-dimensional potential, the asymptotic mobile charge, needed for the derivation of the long-channel I-V curves, is found by using standard techniques in the asymptotic evaluation of integrals. The formal asymptotic approach adopted not only provides a pointwise description of the state variables, but by using the asymptotic mobile charge, the lumped long-channel current-voltage relations, which vary uniformly across the various bias regimes, can be found for various classes of variable doping models.

Using the explicit solutions of some free boundary problems solved by Howison and King (1988), the two-dimensional equilibrium potential near the source and drain is constructed asymptotically in strong inversion in the limit of large doping. From the asymptotic potential constructed near the source and drain, a uniform analytical expression for the mobile charge valid throughout the channel is obtained. From this uniform expression for the mobile charge, we will show how it is possible to find the I-V curve in a particular bias regime taking into account the edge effects of the source and drain. In addition, the asymptotic potential for a two-dimensional n^+-p junction is constructed.

Table Of Contents

List Of Figures

List Of Tables

CHAPTER 1

Introduction To The Semiconductor Equations And The MOSFET

Since its invention in 1960, the metal oxide semiconductor field effect transistor (MOSFET) has been intensely studied by electrical engineers and computer scientists owing to its importance in the design of computer memory chips. Initially, highly simplified analytical models that were based on a multitude of approximations were used to determine the current-voltage relations of these devices. Many of the approximations used in these models cannot be derived from the governing semiconductor equations and do not provide a detailed description of internal device mechanisms. These early models nevertheless were relatively successful in predicting the lumped behavior of some long-channel devices in some bias regimes. Their predicted current-voltage relations are still extensively employed in circuit simulation packages. However, the trend towards device miniaturization and the design of short-channel devices, motivated by the desire to decrease the switching times, invalidates many of the approximations used in the earlier long-channel models.

For moderately short-channel devices, there are several adverse effects that occur, including loss of gate control on the channel conductivity and channel length modulation, that need to be understood quantitatively. As a partial remedy, variable doping implants are often used to reduce the effect of diminished gate control on the channel conductivity. A detailed quantitative analysis of the effect of variable doping on the channel conductivity in all bias ranges is, therefore, of considerable interest and is not encompassed within the framework of the earlier analytical long-channel models. By adopting a different approach to long-channel modeling, the effect of a variable implant on the channel conductivity can be understood quantitatively.

The problems associated with the design of very short-channel devices cannot be addressd by analytical long-channel modeling. For these devices, punchthrough between the source and drain becomes a possibility and even more importantly, the validity of the conventional drift-diffusion model must be more carefully examined.

The analysis of these very short-channel devices, which requires a full numerical discretization of the governing semiconductor equations at each bias point and is consequently not very useful for circuit simulation where closed form current-voltage relations are preferable, is not covered in this thesis.

In most of this thesis, we are primarily concerned with resolving the structure of solutions to the governing semiconductor equations for the MOSFET with small aspect ratio using formal perturbation techniques. With this perturbation approach the many assumptions employed in earlier long-channel modeling are found to be unnecessary. We emphasize that this asymptotic approach allows us to compute closed form current-voltage relations for two different classes of MOSFETs that vary uniformly across the various bias regimes. In addition, this approach also provides a pointwise description of the state variables, in contrast to the earlier long-channel models that only determined lumped characteristics. From this pointwise analytical theory some interesting physical effects that occur can now be investigated quantitatively. Finally, by combining our analytical long-channel expansions with a separate two-dimensional analysis of the governing equations in selected regions of the device, we will show how it is possible to investigate analytically the internal device mechanisms and find the lumped current-voltage relations for MOSFETs that begin to exhibit some two-dimensional short-channel effects.

Before discussing the existing long-channel analytical MOSFET models and the additional physical assumptions normally made, the basic governing semiconductor equations and the MOSFET are introduced. An excellent introduction to modern semiconductor devices and the relevant technology is given in Sze [31]. A more detailed treatment of the semiconductor physics underlying the performance of semiconductor devices is presented in Seeger [28].

1.1 The Governing Semiconductor Equations

In this section, we present the basic governing semiconductor equations, referred to as the drift-diffusion model, that describe the distribution of potential and the behavior of conduction electrons and holes in semiconductor devices. The basic semiconductor equations can be derived from Maxwell's equations supplemented by carrier current density relations and carrier continuity equations. The

current density relations are derived from approximations to the Boltzmann Transport Equation, which, for sufficiently large device dimensions, show that the flux of current for electrons and holes is due to both diffusion from concentration gradients and drift under the influence of the electric field. We shall not elaborate further on the derivation of these equations but instead refer the reader to Selberherr [29] where the basic semiconductor equations are derived and their range of validity is discussed.

The equations comprising the drift-diffusion model in a semiconducting material are

$$\epsilon_s \nabla \cdot \mathbf{E} = q(p - n + N)\,, \tag{1.1a}$$

$$\mathbf{J}_n = q u_n (n\mathbf{E} + \frac{kT}{q}\nabla n)\,, \tag{1.1b}$$

$$\mathbf{J}_p = q u_p (p\mathbf{E} - \frac{kT}{q}\nabla p)\,, \tag{1.1c}$$

$$\nabla \cdot \mathbf{J}_n = q(\frac{\partial n}{\partial t} + R - G)\,, \tag{1.1d}$$

$$\nabla \cdot \mathbf{J}_p = -q(\frac{\partial p}{\partial t} + R - G)\,, \tag{1.1e}$$

$$\mathbf{J} = \mathbf{J}_n + \mathbf{J}_p + \epsilon_s \frac{\partial \mathbf{E}}{\partial t}\,, \tag{1.1f}$$

$$\mathbf{E} = -\nabla \psi\,, \tag{1.1g}$$

where

n, p	are the electron and hole concentrations; respectively,
N	is the concentration of impurities;
$\mathbf{J}_n, \mathbf{J}_p$	are the electron and hole current densities, respectively;
$\mathbf{J}$	is the total current density;
$\mathbf{E}, \psi$	are the electric field and the electrostatic potential, respectively;
u_n, u_p	are the electron and hole mobilities, respectively;
R	is the recombination rate;
G	is the generation rate;

ϵ_s is the dielectric constant of the semiconducting material;

k is the Boltzmann's constant;

q is the elementary charge of a proton; and

T is the constant lattice temperature.

The combination $v_{\text{th}} \equiv kT/q$ is termed the thermal voltage.

To complete the specification of the drift-diffusion model, the recombination processes and the mobilities need to be modeled as functions of the carrier concentrations and the electric field. In addition, the spatial distribution of the impurities needs to be given. Since we shall investigate the electrical behavior of devices with various impurity profiles, we shall briefly discuss the model parameters commonly used in numerical simulations. A detailed discussion of the model parameters used in numerical simulations and their theoretical and experimental justification is provided in Selberherr [29].

The electrical behavior of a semiconductor device is greatly influenced by the spatial distribution of selected impurities, called dopants, that are implanted into the device. The net impurity concentration, N, is assumed to be completely ionized and does not contribute to the flow of current. The implant profile in a device arises from complicated diffusion-convection mechanisms that are dependent on the technological processes used for implanting the impurities. There are several process simulation packages available that model this problem and predict the final distribution of impurities for various technologies and from given initial conditions. As we are more concerned with device simulation rather than process simulation, the spatial distribution of impurities is assumed to be known.

The carrier mobilities, which are directly related to the mean free time between collisions, are determined by the various scattering mechanisms that predominate. Owing to the complexity of many of these mechanisms, empirical relations for the mobilities as a function of the electric field, doping concentration, and temperature are used in numerical simulations.

The net recombination rate, $R - G$, is the difference between the rates of recombination and generation of electron-hole pairs. There are several different recombination processes, each of which is modeled by a semi-empirical expression. The most basic recombination mechanism is referred to as the Shockley-Read-Hall

(SRH) process and has the form

$$R_{srh} = R - G = \frac{np - n_i^2}{\tau_n n + \tau_p p + \tau_c},$$

where τ_n, τ_p are the electron and hole mean lifetimes, respectively, which in general depend on both the type and concentration levels of the impurities present. The intrinsic carrier concentration, n_i, depends on the bandgap energy of the material, the density of states in the conduction and valence bands, and the lattice temperature.

Another recombination mechanism called impact ionization, which is a pure generation mechanism and is prevalent at high electric fields, can be modeled by

$$R_{imp} = R - G = -\alpha_n(|\mathbf{E}|)|\mathbf{J}_n| - \alpha_p(|\mathbf{E}|)|\mathbf{J}_p|,$$

where

$$\alpha_n(|\mathbf{E}|) = \alpha_{n_\infty} \exp(-E_n/|\mathbf{E}|) \quad \text{and} \quad \alpha_p(|\mathbf{E}|) = \alpha_{p_\infty} \exp(-E_p/|\mathbf{E}|).$$

Although not relevant to the MOSFET under normal operating conditions, this process is important in the study of breakdown phenomena associated with reverse bias junctions. To complete the formulation of the problem, the device geometry and boundary conditions relevant to the MOSFET must be specified. In addition, we shall give a brief introduction to how the MOSFET operates.

A cross sectional view of the MOSFET is shown in Figure 1.1. Electrical connections are made to the metal gate electrode and to the n-well reservoirs that comprise the source and drain regions. This device is designated an n-channel MOSFET, since for appropriate voltage biases the current flow between the source and drain is due to the transport of mobile conduction electrons parallel to the semiconductor-insulator interface. The conductivity of the channel between the source and drain is greatly influenced by the normal component of the electric field established by the voltage applied to the gate. Since the gate is isolated from the semiconductor by a layer of insulating material typically made of silicon dioxide, the modulating effect of the gate on the conductivity of the channel is purely by a field-effect mechanism. One of the primary goals of analytical modeling is to

determine the amount of current flow as a function of the source-drain bias for various ranges of gate voltage. These current-voltage relations are referred to as the device characteristics.

In general, the MOSFET is a four terminal device with voltages applied to the gate, source, drain, and substrate. Without loss of generality, we shall assume that the substrate and the source are kept at the same voltage. Allowing for a source-substrate bias simply introduces another parameter into the model and does not affect the structure of solutions to the governing equations. Furthermore, all voltage quantities are referenced with respect to the source. The device geometry and boundary conditions are now prescribed.

The n-well reservoirs of conduction electrons are formed by implanting large concentrations of donor impurities into the semiconducting material. The dopant concentration in these reservoirs, N_c, is taken to be constant. The shape of these wells is assumed to be known and is occasionally modeled either as a quarter circle or a rectangular region in device simulations. Across this boundary, the doping profile is assumed to vary rapidly and forms what is known as a p-n junction.

The boundaries of the device are composed of both physical boundaries, which include contacts and insulating segments, and artificial boundaries required for numerical simulations. Neglecting any surface recombination effects along the semiconductor-insulator interface BC, we assume that there is no flux of carriers normal to the interface so that

$$\mathbf{J}_n \cdot \hat{\eta} = 0 \qquad \text{and} \qquad \mathbf{J}_p \cdot \hat{\eta} = 0 \quad \text{on} \quad x_1 = 0\,,$$

where $\hat{\eta}$ is the unit normal to the interface BC. Furthermore, assuming no interface charges, the electrostatic potential and the electric displacement vector are continuous across the interface BC so that

$$\psi\,|_{\text{sem}} = \psi\,|_{\text{ins}}\,,$$
$$\epsilon_s \frac{\partial \psi}{\partial x_1}\,|_{\text{sem}} = \epsilon_i \frac{\partial \psi}{\partial x_1}\,|_{\text{ins}}\,,$$

where ϵ_s and ϵ_i are the dielectric constants of the semiconductor and the oxide, respectively. Neglecting interface charges is not restrictive since their inclusion simply introduces another parameter into the model.

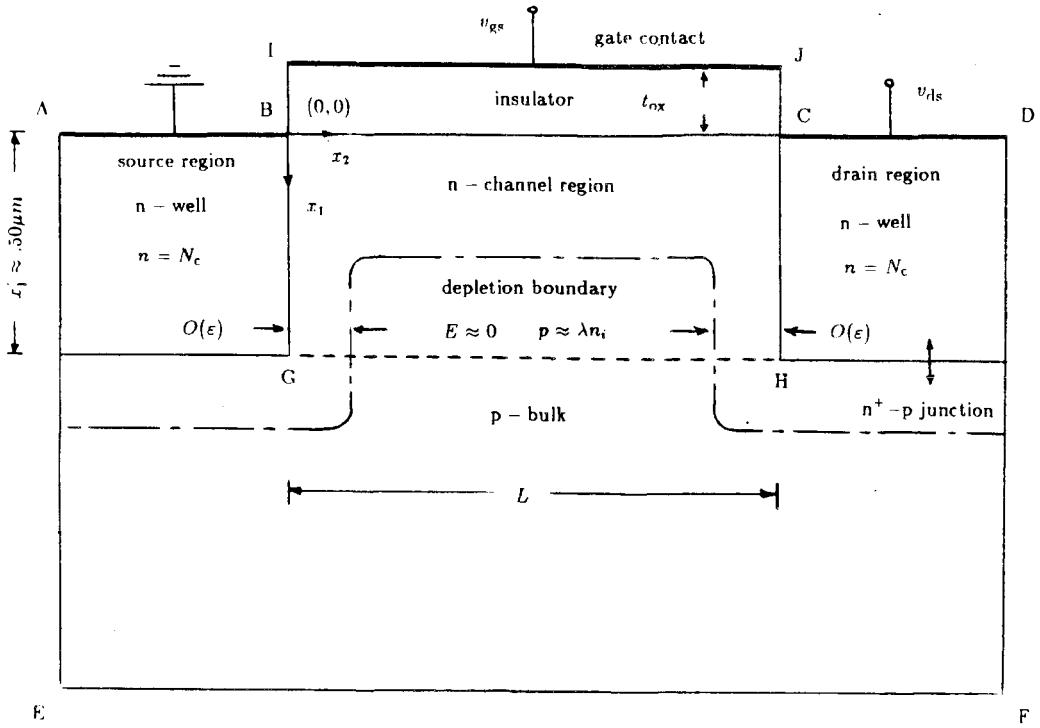

FIGURE 1.1. Cross Sectional View of the MOSFET

The source and drain contacts AB, CD are assumed to be ohmic and thus the relevant boundary conditions for the carrier concentrations on these segments are

$$np = n_i^2 \quad \text{thermal electronic equilibrium},$$
$$n - p - N_c = 0 \quad \text{vanishing space charge}.$$

Solving the resulting quadratic equations on these segments we obtain the Dirichlet boundary conditions

$$n = \frac{1}{2}(N_c + \sqrt{N_c^2 + 4n_i^2}) \sim N_c,$$
$$p = \frac{1}{2}(-N_c + \sqrt{N_c^2 + 4n_i^2}) \sim n_i^2/N_c,$$

for $N_c/n_i \approx 10^8 \gg 1$. In addition, we have a Dirichlet boundary condition for the

electrostatic potential on the contacts AB, CD so that

$$\psi = v_{\rm th} \ln \left(\frac{N_{\rm c} + \sqrt{N_{\rm c}^2 + 4n_i^2}}{2n_i} \right) \sim v_{\rm th} \ln \frac{N_{\rm c}}{n_i} \quad \text{on source AB,}$$

$$\psi = v_{\rm th} \ln \left(\frac{N_{\rm c} + \sqrt{N_{\rm c}^2 + 4n_i^2}}{2n_i} \right) + v_{\rm ds} \sim v_{\rm th} \ln \frac{N_{\rm c}}{n_i} + v_{\rm ds} \quad \text{on drain CD,}$$

for $N_{\rm c}/n_i \gg 1$. The difference in the applied bias between the source and the drain, $v_{\rm ds}$, is called the source-drain bias.

The quantity

$$\psi_{\rm bi} = v_{\rm th} \ln \left(\frac{N_{\rm c} + \sqrt{N_{\rm c}^2 + 4n_i^2}}{2n_i} \right)$$

is called the built-in voltage.

The oxide bounded by BIJC is assumed to be charge neutral, and thus in this region the electrostatic potential satisfies Laplace's equation

$$\nabla^2 \psi = 0 .$$

The boundary condition for the potential on the gate contact IJ is $\psi = v_{\rm gs} - v_{\rm ref}$, where $v_{\rm gs}$ is the gate voltage referenced with respect to the source and $v_{\rm ref}$ is some reference voltage.

In most numerical device simulations, the boundary conditions on the artificial boundary segments AE, DF, EF, BI and CJ are taken to be

$$\mathbf{J}_n \cdot \hat{\eta} = 0 \quad , \quad \mathbf{J}_p \cdot \hat{\eta} = 0 \quad , \quad \text{and} \quad \mathbf{E} \cdot \hat{\eta} = 0 .$$

Finally, to complete the formulation of the drift-diffusion model, initial conditions on the electron and hole concentrations are given in the semiconducting material at time t=0.

Numerical device simulation efforts for the MOSFET are focused on developing efficient numerical methods to solve the resulting set of nonlinear parabolic partial differential equations for n, p and ψ with the associated boundary and initial conditions. The analysis of the numerical algorithims used in device simulations has

received significant attention from numerical analysts in the last few years. An excellent overview of numerical device simulation is presented in Fichtner *et. al.* [13]. A more detailed discussion of the numerical techniques used to solve the governing equations is given in Bank *et. al.* [3].

Some analytical investigations of the governing semiconductor equations under various simplifying assumptions have also recently appeared in the mathematical literature. The book by Markovich [18] contains many of the known existence, uniqueness and regularity results for solutions to the time independent governing semiconductor equations under various model assumptions. The rigorous asymptotic approach to semiconductor device modeling adopted by Markovich is presented in [19]. In contrast to these rigorous results, a detailed study using formal perturbation techniques for the one-dimensional p-n junction with SRH recombination under forward bias is given by Please in [23].

In order to develop analytical models for the MOSFET that predict the device characteristics, the model equations as well as the device geometry need to be simplified. For simplicity, the device geometry is simplified to the rectangular region whose boundaries are the interface BC and the lines BG, CH, and GH as shown in Figure 1.1. The boundary conditions used on BG and CH are those normally imposed on the source and drain, respectively. The boundary condition imposed on the segment GH is prescribed later. The additional physical simplifications, as well as a critique of the existing analytical models that predict the electrical behavior of long-channel devices, are discussed in the next section.

1.2 The Gradual Channel Approximation And Scalings

The first models that derived the device characteristics of a long-channel MOSFET under constant doping for various ranges of gate bias were proposed by Pao and Sah [21] and Barron [4]. Since that time there have been many variants of these models, most notably the charge sheet approximation by Brews [6] that provided an alternative formulation to the original Pao-Sah model. In this thesis, these prior analytical models are collectively referred to as the conventional gradual channel approximation GCA. We refrain from describing these models in detail as there are excellent review articles on the subject by Brews [5] and Engl [11]. Instead, we focus our discussion on the model assumptions normally made

and the inadequacies of these models in characterizing certain interesting physical effects that occur in MOSFETs. In addition, some mathematical questions raised by these models are discussed. In all the existing analytical models, it is assumed that there is no recombination and that the current flow due to holes is negligible everywhere in the channel region.

One of the main mathematical questions concerns the range of validity of the conventional GCA. Specifically, what are the necessary restrictions on the doping concentration, channel length, and source-drain bias to ensure that the scaled MOSFET behaves similarly to a long-channel device without exhibiting significant short-channel effects? By an appropriate scaling of the governing equations, this question shall be addressed. Formally, we shall show that for certain parameter ranges there is a region in the middle of the channel away from the source and drain where the potential distribution is one-dimensional and is controlled by the input gate voltage.

In the conventional GCA for constant channel doping, a first integral of the one-dimensional Poisson equation normal to the interface is used in conjunction with the well known depletion approximation to compute the mobile charge available for current conduction. In the study of a related semiconductor device, the one-dimensional p-n junction, Please [23] showed that the depletion approximation represents the leading order term in the asymptotic expansion of the potential for large channel doping in regions where the space charge density is dominated by the impurity concentration. However, for the MOSFET, there are several other layers in addition to this region which the conventional GCA, by simply obtaining a first integral of the Poisson equation, does not resolve. By failing to resolve these additional boundary layers, some interesting physical effects cannot be understood quantitatively. Moreover, in the case of realistic variable doping profiles, a first integral of the Poisson equation does not exist. Using some techniques available in the asymptotic expansion of integrals, we shall compute the amount of mobile charge available for current conduction in the limit of large doping for all relevant ranges of gate bias. This computation is essential to derive device characteristics that are smooth functions of the gate voltage.

Although the conventional GCA is useful in deriving device characteristics for several ranges of gate bias, currently there is no theory that uniformly encompasses

the many different bias regimes that occur in MOSFETs. Furthermore, with these lumped models there are certain physical effects, such as pinchoff and non-tangential current flow, that occur and are not explained quantitatively.

Pinchoff, which manifests itself in several different ways depending on the doping profile, is normally characterized by the vanishing of the channel of conduction electrons at some position along the channel and thus sets a limit on the amount of current flow for given source-drain bias. This phenomenon is understood only qualitatively within the framework of the GCA. Specifically, the GCA can only predict the minimum conditions on the gate and source-drain biases for the occurrence of pinchoff at the end of the channel. It is then assumed that further increases in the source-drain bias are not reflected in higher current levels. These lumped models are insufficient to characterize pinchoff after these minimum conditions are attained. In Chapter 5, a more careful definition of pinchoff is given for two different types of MOSFETs, and we shall show that by determining the carrier concentration explictly along the full extent of the channel, the I-V curve associated with a device operating in the pinchoff regime can easily be obtained.

In the conventional GCA, the current flow in the channel away from the source and drain is assumed to be entirely tangential. From our perturbation techniques, we shall determine the range of validity of this approximation and shall explictly exhibit deviations from this behavior in certain bias regimes. Specifically, we shall compute the current density in the direction normal to the interface and show that this component of the current density vector is significant in the channel near the drain for certain ranges of gate bias.

The conventional GCA gives no information on the distribution of potential and the electron concentration in the vicinity of the source and drain. Even with our perturbation techniques, the general structure of the solutions in these regions in all bias ranges does not appear to be amenable to analytical methods. However, we shall see in Chapter 6 that the explicit construction of the equilibrium potential under inversion conditions can be obtained using the explicit solutions of some free boundary problems provided recently by Howison and King [17]. Using these analytical results, a uniform expression for the mobile charge valid throughout the channel will be written. Using this expression for the mobile charge, we will show how it is possible to find the $I - V$ curves, incorporating some two-dimensional

Scaling Factor	Typical Value at 20°
$n = n_i\bar{n}, \quad p = n_i\bar{p}$	$1.45 \times 10^{10}\,\mathrm{cm}^3$
$\psi = \dfrac{kT}{q}\bar{\psi}$	0.0253 V
$x_1 = L_\mathrm{d}\bar{x}, \quad L_\mathrm{d} = \left(\dfrac{kT\epsilon_\mathrm{s}}{n_i q^2}\right)^{1/2}$	$33.8\,\mu\mathrm{m}$
$x_2 = Ly$	$10 - 90\,\mu\mathrm{m}$
$u_n = \mu_{nc}\bar{u}_n$	$1400\,\mathrm{cm}^2/\mathrm{V}\cdot\mathrm{sec}$
$u_p = \mu_{pc}\bar{u}_p$	$500\,\mathrm{cm}^2/\mathrm{V}\cdot\mathrm{sec}$
$t = \bar{t}/\omega \quad \omega = qn_i\mu_{nc}/\epsilon_\mathrm{s}$	$3.08 \times 10^6\,\mathrm{HZ}$
$\tau_n = \dfrac{\epsilon_\mathrm{s}}{qn_i\mu_{nc}}\bar{\tau}_n$	$3.42 \times 10^{-7}\,\mathrm{sec}$
$\tau_p = \dfrac{\epsilon_\mathrm{s}}{qn_i\mu_{nc}}\bar{\tau}_p$	$3.42 \times 10^{-7}\,\mathrm{sec}$
$\tau_\mathrm{c} = \dfrac{\epsilon_\mathrm{s}}{q\mu_{nc}}\bar{\tau}_\mathrm{c}$	$4.70 \times 10^3\,\mathrm{sec/cm}^3$
$\mathbf{J}_n = \dfrac{kTn_i\mu_{nc}}{L_\mathrm{d}}\bar{\mathbf{J}}_n$	$2.43 \times 10^{-5}\,\mathrm{coul/cm}^2\cdot\mathrm{sec}$
$\mathbf{J}_p = \dfrac{kTn_i\mu_{pc}}{L_\mathrm{d}}\bar{\mathbf{J}}_p$	$8.60 \times 10^{-6}\,\mathrm{coul/cm}^2\cdot\mathrm{sec}$

TABLE 1.1. Table of Scaling Values

effects, in a particular bias regime. These special analytical results, that we shall discuss, are beneficial in that the explicit dependence of the mobile charge, and hence the $I - V$ curves on the two-dimensional device geometry is available.

To begin the analysis, we introduce a singular perturbation scaling of the governing semiconductor equations. For generality, the scalings are introduced for the full system of equations under SRH recombination; however, as in all existing analytical models for the MOSFET, we shall eventually focus only on the transport of electrons and the distribution of potential with no recombination.

1.3 The Singular Perturbation Scaling

Following Demari [10], the governing semiconductor equations are scaled by introducing a set of dimensionless variables that are conveniently summarized in Table 1.1. Typical values of the scaling constants are given for silicon at room temperature.

With these scalings, the semiconductor equations under SRH recombination only become

$$\bar{\nabla}^2\bar{\psi} = \bar{n} - \bar{p} - \frac{N(L_{\rm d}\bar{x})}{n_i}\,, \tag{1.2a}$$

$$\bar{\mathbf{J}}_n = \bar{u}_n(\bar{\nabla}\bar{n} - \bar{n}\bar{\nabla}\bar{\psi})\,, \tag{1.2b}$$

$$\bar{\mathbf{J}}_p = -\bar{u}_p(\bar{\nabla}\bar{p} + \bar{p}\bar{\nabla}\bar{\psi})\,, \tag{1.2c}$$

$$\bar{\nabla}\cdot\bar{\mathbf{J}}_n = (\frac{\partial\bar{n}}{\partial\bar{t}} + \bar{R})\,, \tag{1.2d}$$

$$\mu_{\rm c}\bar{\nabla}\cdot\bar{\mathbf{J}}_p = -(\frac{\partial\bar{p}}{\partial\bar{t}} + \bar{R})\,, \tag{1.2e}$$

where the scaled SRH recombination mechanism is

$$\bar{R}(\bar{n},\bar{p}) = \frac{\bar{n}\bar{p} - 1}{\bar{\tau}_n\bar{n} + \bar{\tau}_p\bar{p} + \bar{\tau}_{\rm c}}\,,$$

and the gradient operator in these new variables is

$$\bar{\nabla} \equiv \left(\frac{\partial}{\partial\bar{x}}, \frac{L_{\rm d}}{L}\frac{\partial}{\partial y}\right).$$

The constant $\mu_{\rm c}$ is simply $\mu_{\rm c} = \mu_{pc}/\mu_{nc}$. In the literature $L_{\rm d}$, is referred to as the intrinsic Debye length.

In applications, the ratio of the maximum dopant concentration in the channel to the intrinsic concentration, n_i, is normally very large, typically ranging bewteen 10^4 and 10^7. Therefore, we introduce a large parameter, λ, by

$$\frac{N(L_{\rm d}\bar{x})}{n_i} = \lambda\bar{N}(\bar{x})\,.$$

However, for $\lambda \gg 1$, we anticipate rapid variations in the electrostatic potential in the direction normal to the semiconductor-insulator interface. From the analysis

of the one-dimensional problem, these variations occur on a scale of $O(\sqrt{\ln\lambda/\lambda})$. This information leads us to consider further scalings of the form

$$\bar{\psi} = w \ln\lambda \tag{1.3a}$$

$$x = \bar{x}/\sqrt{\frac{\ln\lambda}{\lambda}} \tag{1.3b}$$

in which both x and w are $O(1)$ as $\lambda \to \infty$. Moreover, it is important to note that the carrier concentrations can range over many orders of magnitude. We therefore introduce new dependent variables ϕ_n and ϕ_p that are related to the carrier concentrations by

$$\bar{n} = e^{\ln\lambda(w-\phi_n)} \qquad \text{and} \qquad \bar{p} = e^{-\ln\lambda(w-\phi_p)}\,.$$

Physically, these variables, termed the quasi-Fermi potentials, measure the departure from thermal electronic equilibrium of the time independent potential. Thermal electronic equilibrium, in which there is no current flow in the device, is characterized by $\phi_n \equiv 0$ and $\phi_p \equiv 0$. The spatial variations of the quasi-Fermi potentials in the channel constitute the driving force behind the flow of current. These variables are preferable to using the carrier concentrations as dependent variables since the boundary condition for each of these variables on the semiconductor-insulator interface is now a pure Neumann condition. By examining the boundary conditions for the carrier concentrations in the simplified geometry, the boundary conditions for the quasi-Fermi potentials are immediately seen to be

$$\phi_n = 0 \quad \text{and} \quad \phi_p = 0 \quad \text{on } y = 0\,, \tag{1.4a}$$

$$\phi_n = \frac{\bar{v}_{\rm ds}}{\ln\lambda} \quad \text{and} \quad \phi_p = \frac{\bar{v}_{\rm ds}}{\ln\lambda} \quad \text{on } y = 1\,, \tag{1.4b}$$

$$\frac{\partial\phi_n}{\partial x} = 0 \quad \text{and} \quad \frac{\partial\phi_p}{\partial x} = 0 \quad \text{on } x = 0\,, \tag{1.4c}$$

where $\bar{v}_{\rm ds} = v_{\rm ds}/v_{\rm th}$. The boundary conditions on GH are specified in Chapter 5. With this formulation, not only are all the dependent variables of the same order of magnitude, but the non-ohmic device behavior can also be more easily obtained.

Assuming that the time scale associated with the externally applied biases is much longer than the recombination and dieletric relaxation times, we focus

on the long time behavior of the carrier concentrations and the distribution of potential. Ignoring the initial transients and dropping the overbar notation, the static semiconductor equations in these new variables become

$$\tilde{\nabla}^2 w = \frac{1}{\lambda}(e^{\ln\lambda(w-\phi_n)} - e^{-\ln\lambda(w-\phi_p)}) + \ d(x)\,, \tag{1.5a}$$

$$\tilde{\nabla}^2\phi_n + \tilde{\nabla}\phi_n \cdot \left(\frac{\tilde{\nabla}\mu_n}{\mu_n} + \ln\lambda\tilde{\nabla}(w-\phi_n)\right) = -\frac{1}{\lambda\mu_n}H_n(\phi_n,\phi_p,w)\,, \tag{1.5b}$$

$$\tilde{\nabla}^2\phi_p + \tilde{\nabla}\phi_p \cdot \left(\frac{\tilde{\nabla}\mu_p}{\mu_p} - \ln\lambda\tilde{\nabla}(w-\phi_p)\right) = \frac{1}{\lambda\mu_c\,\mu_n}H_p(\phi_n,\phi_p,w)\,. \tag{1.5c}$$

The scaled current densities in the x_1 and x_2 directions now take the simpler form

$$\bar{\mathbf{J}}_n = -(\lambda\ln\lambda)^{1/2}\mu_n e^{\ln\lambda(w-\phi_n)}\tilde{\nabla}\phi_n\,, \tag{1.6a}$$

$$\bar{\mathbf{J}}_p = -(\lambda\ln\lambda)^{1/2}\mu_p e^{-\ln\lambda(w-\phi_p)}\tilde{\nabla}\phi_p\,. \tag{1.6b}$$

With this scaling, the SRH recombination mechanism becomes

$$H_n(\phi_n,\phi_p,w) = e^{-\ln\lambda(w-\phi_n)}H(\phi_n,\phi_p,w)\,,$$
$$H_p(\phi_n,\phi_p,w) = e^{\ln\lambda(w-\phi_p)}H(\phi_n,\phi_p,w)\,,$$

where

$$H(\phi_n,\phi_p,w) = \frac{e^{\ln\lambda(\phi_p-\phi_n)}-1}{\bar{\tau}_n e^{\ln\lambda(w-\phi_n)} + \bar{\tau}_p e^{-\ln\lambda(w-\phi_p)} + \bar{\tau}_c}\,.$$

The scaled electron and hole mobilities are μ_n and μ_p, respectively. The normalized doping profile is $d(x) = -\bar{N}(x\sqrt{\ln\lambda/\lambda})$, and the new gradient operator becomes

$$\tilde{\nabla} \equiv \left(\frac{\partial}{\partial\bar{x}}, \varepsilon\frac{\partial}{\partial\bar{y}}\right)\,, \qquad \text{where} \qquad \varepsilon = \frac{L_d}{L}\sqrt{\frac{\ln\lambda}{\lambda}}\,.$$

Physically, ε represents an aspect ratio of the device. Alternative scalings of the governing equations are given in Markovich [19].

From this scaling, the validity of any one-dimensional analysis normal to the interface is seen to be restricted to channel lengths and maximum dopant concentrations satisfying $\varepsilon \ll 1$. Numerical values of ε for silicon at room temperature

with a channel length of $L = 10^p$ microns are computed for various dopant concentrations. With $\varepsilon \equiv \varepsilon_0(\lambda)10^{-p}$ we calculate

$$\varepsilon_0 = \begin{cases} 1.03 & \text{for} \quad \lambda = 10^4 \\ 0.126 & \text{for} \quad \lambda = 10^6 \\ 0.0145 & \text{for} \quad \lambda = 10^8 . \end{cases}$$

Assuming that $\lambda = 10^6$ is a representative value of the channel doping and enforcing the condition that $\varepsilon \leq .01$, the validity of any one-dimensional analysis in the middle of the channel is seen to be restricted to the consideration of 10 micron or longer devices. Although this criterion is rather arbitrary, comparison with numerical simulations shows that it is quite satisfactory in practice. For submicron devices with the same channel doping, the governing equations are fully two-dimensional, and numerical methods are required to accurately solve for the potential and the carrier concentrations.

Since the voltage quantities are scaled with respect to the thermal voltage, the influence of large source-drain biases that can affect the validity of any one-dimensional approximation is not immediately apparent. Physically, even for $\varepsilon \ll 1$, large source-drain biases can cause the device to exhibit significant two-dimensional behavior in the channel normally characteristic of only shorter devices. As will be discussed in Chapters 5 and 6, this effect is reflected in the breakdown of the regular asymptotic expansion in the aspect ratio ε in the middle of the channel for large source-drain biases.

1.4 The Modeling Of The Insulator

We recall that the surface potential is not specified *a priori* but is a consequence of the voltage applied to the gate. In order to proceed analytically, without deriving cumbersome integral equations coupling the potential in the insulator to the potential in the semiconducting material, the potential distribution in the insulator is instead modeled based on physical observations. In several MOSFET simulation packages and in all previous analytical models, the two-dimensional Laplace's equation is not solved in the insulator. Instead, a one-dimensional voltage drop perpendicular to the gate is assumed. However, as remarked by Selberherr [29], if the channel length is not long compared to the oxide thickness t_{ox}, the simulation errors introduced with such an approximation are intolerably

large. Plots of the surface potential from numerical calculations by Greenfield [15] indicate that in thermal electronic equilibrium the surface potential is constant in the middle of the channel and has rapid variations near the source and drain regions. Motivated by these observations, we now introduce a model for the potential distribution in the insulator.

We begin by scaling $x_1 = t_{ox}\hat{x}$ and $x_2 = Ly$, so that Laplace's equation in the insulator becomes

$$\frac{\partial^2 \hat{\psi}}{\partial \hat{x}^2} + d^2 \frac{\partial^2 \hat{\psi}}{\partial y^2} = 0\,,$$

where $d = t_{ox}/L$ and $\hat{\psi}(\hat{x}, y) = \psi(t_{ox}\hat{x}, Ly)$. Using a typical oxide thickness of $t_{ox} \approx 0.025$ microns and a channel length of 10 microns, we notice that $d \approx 0.0025$. Since the aspect ratio d is very small, we look for a solution to Laplace's equation that reduces to the one-dimensional approximation $\partial^2\hat{\psi}/\partial\hat{x}^2 \approx 0$ away from the artificial segments BI, CJ and that satisfies $\hat{\psi}(0,0) = \psi_{bi}$ and $\hat{\psi}(0,1) = \psi_{bi} + v_{ds}$, as well as the Dirichlet boundary condition on the gate. Assuming an exponential boundary layer behavior in the surface potential near the source and drain regions, a solution for $d \ll 1$ to Laplace's equation in the insulator that is monotonic in the x_1 direction is given by

$$\hat{\psi}(\hat{x}, y) = (v_{gs} - v_{ref} - E_x t_{ox}(\hat{x} + 1)) + B(\hat{x})e^{-\pi y/2d} + C(\hat{x})e^{-\pi(1-y)/2d}\,, \qquad (1.7)$$

where

$$B(\hat{x}) = \left(\psi_{bi} + t_{ox}E_x - v_{gs} + v_{ref}\right) \sin\left(\frac{\pi}{2}(\hat{x} + 1)\right),$$

and

$$C(\hat{x}) = \left(\psi_{bi} + v_{ds} + t_{ox}E_x - v_{gs} + v_{ref}\right) \sin\left(\frac{\pi}{2}(\hat{x} + 1)\right).$$

As we shall see in Chapter 2, the unknown constant E_x, which represents the magnitude of the electric field in the x_1 direction away from the source and drain, shall be determined from the one-dimensional analysis of the equilibrium potential. As the ratio of the oxide thickness to the channel length increases, the boundary layers become less prominent and the region over which we can assume a one-dimensional voltage drop becomes narrower. This description of the oxide is consistent with Selberherr's observations. It is also noteworthy that on

the artificial boundary segments in the oxide, Mock [20] uses a linear interpolant between the specified voltages as boundary data for his numerical simulations. By examining (1.7), the boundary data that we use is only slightly more complicated on these segments.

Away from the artificial boundary segments $\psi(x_1, x_2) \approx (v_{\rm gs} - v_{\rm ref}) - E_{\rm x}(x_1 + t_{\rm ox})$ and thus defining $\psi = \psi_s$ on the interface $x_1 = 0$, we have

$$\frac{\partial \psi}{\partial x_1} \cong \frac{\psi_s - v_{\rm gs} + v_{\rm ref}}{t_{\rm ox}}.$$

Then, using the continuity of the electric displacement vector across the interface, we obtain the mixed boundary condition

$$-\epsilon_{\rm s}\frac{\partial \psi}{\partial x_1} + \epsilon_{\rm i}\frac{\psi_s - v_{\rm gs} + v_{\rm ref}}{t_{\rm ox}} = 0 \qquad \text{on} \quad x_1 = 0\,.$$

Assuming that $d = O(\varepsilon)$ and using the one-dimensional theory for the equilibrium potential in the middle of the channel, a unique surface potential ψ_s^0 for a given gate voltage can be computed. With this value for the surface potential, the constant electric field $E_{\rm x}$ in the middle of the insulator is known, and thus the solution to Laplace's equation in the insulator becomes

$$\psi(x_1, y) = (\psi_s^0 - (v_{\rm gs} - v_{\rm ref} - \psi_s^0)\frac{x_1}{t_{\rm ox}}) + B(x_1)e^{-\pi y/2d} + C(x_1)e^{-\pi(1-y)/2d}, \quad (1.8)$$

where

$$B(x_1) = (\psi_{\rm bi} - \psi_s^\circ)\sin\left(\frac{\pi}{2}(\frac{x_1 + t_{\rm ox}}{t_{\rm ox}})\right),$$

and

$$C(x_1) = (\psi_{\rm bi} + v_{\rm ds} - \psi_s^\circ)\sin\left(\frac{\pi}{2}(\frac{x_1 + t_{\rm ox}}{t_{\rm ox}})\right).$$

To obtain the normalized boundary condition along the interface, we non dimensionalize by taking

$$x_1 = L_{\rm d}\sqrt{\frac{\ln\lambda}{\lambda}}\,x \quad \text{and} \quad \psi = v_{\rm th}\ln\lambda\, w\,,$$

and we introduce the normalized capacitance, $c_{\rm ox}$, by

$$c_{\rm ox} = \frac{\epsilon_{\rm i}}{t_{\rm ox}}\frac{L_{\rm d}}{\epsilon_{\rm s}}.$$

With these substitutions, the following mixed boundary condition holds on the interface away from the source and drain;

$$-\frac{\partial w}{\partial x} + c_{\rm ox}\sqrt{\frac{\ln\lambda}{\lambda}}w_s = c_{\rm ox}\sqrt{\frac{\ln\lambda}{\lambda}}\frac{(\bar{v}_{\rm gs} - \bar{v}_{\rm ref})}{\ln\lambda},$$

where $\bar{v}_{\rm gs} = v_{\rm gs}/v_{\rm th}$ and $\bar{v}_{\rm ref} = v_{\rm ref}/v_{\rm th}$. The reference voltage is chosen so that $\bar{v}_{\rm gs} \approx 0$ when $w_s = -1$, which in Chapter 2 will be seen to correspond to flatband conditions. The choice $v_{\rm ref} = 0$ then implies

$$-\frac{\partial w}{\partial x} + c_{\rm ox}\sqrt{\frac{\ln\lambda}{\lambda}}(w_s + 1) = c_{\rm ox}\sqrt{\frac{\ln\lambda}{\lambda}}\frac{\bar{v}_{\rm gs}}{\ln\lambda}.$$

Using the material constants $\epsilon_{\rm s} = 11.9$ and $\epsilon_{\rm i} = 3.9$ for silicon and silicon dioxide, respectively, and a representative oxide thickness of $t_{\rm ox} \cong .025$ microns, we find that $c_{\rm ox} \cong 450$.

With this insulator model, the boundary conditions for the potential are now specified. The boundary conditions on the source and drain contact for the scaled potential are

$$w = w_{\rm bi} \equiv \frac{\ln(N_{\rm c}/n_{\rm i})}{\ln\lambda} \quad \text{on} \quad y = 0, \tag{1.9a}$$

$$w = w_{\rm bi} + \frac{\bar{v}_{\rm ds}}{\ln\lambda} \quad \text{on} \quad y = 1. \tag{1.9b}$$

From the modeling of the insulator, the surface potential along the full extent of the interface is then given by

$$w(0,y) = w_s + (w_{\rm bi} - w_s)\,e^{-\pi y/2d} + (w_{\rm bi} + \frac{\bar{v}_{\rm ds}}{\ln\lambda} - w_s)e^{-\pi(1-y)/2d}, \tag{1.10}$$

where w_s is determined from the outer ε solution to the potential satisfying

$$-\frac{\partial w}{\partial x} + c_{\rm ox}\sqrt{\frac{\ln\lambda}{\lambda}}(w_s + 1) = c_{\rm ox}\sqrt{\frac{\ln\lambda}{\lambda}}\frac{\bar{v}_{\rm gs}}{\ln\lambda} \tag{1.11}$$

on the semiconductor-insulator interface $x = 0$ in the middle of the channel away from the source and drain. This boundary condition along the interface is used in Chapter 6 when we solve analytically for the equilibrium potential in the vicinity of the source and drain. A plot of the surface potential along the interface is

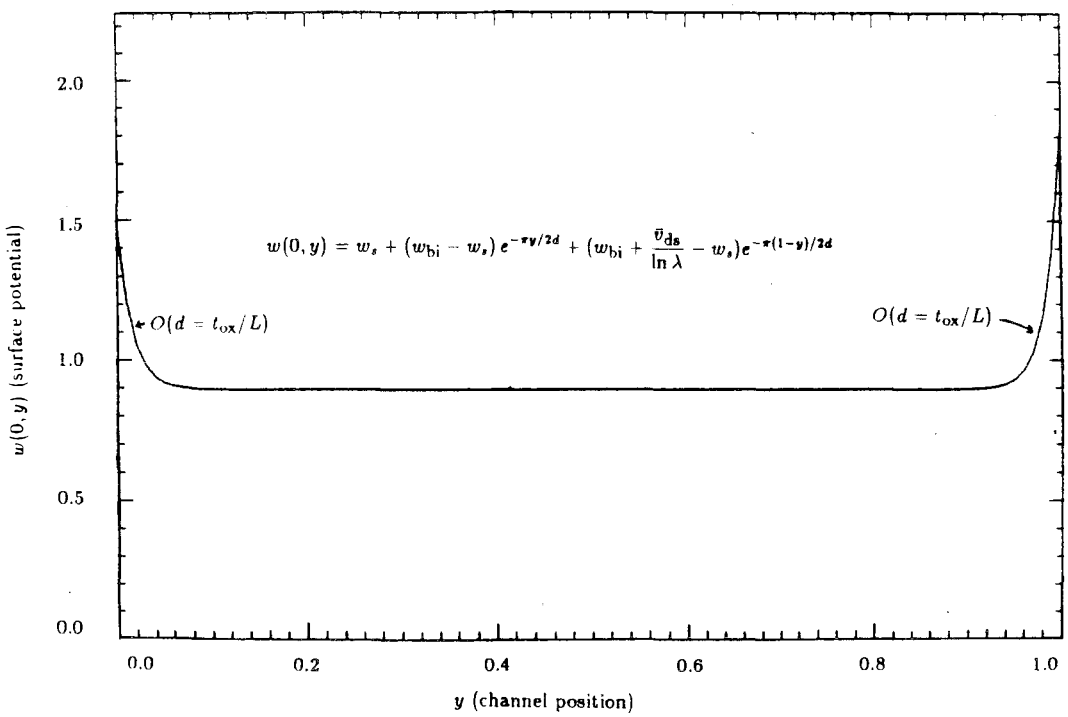

FIGURE 1.2. Surface Potential Along the Interface BC

shown in Figure 1.2. The boundary condition for the potential on the segment GH is specified in the next chapter.

For certain ranges of gate voltage under a non-zero source-drain bias the surface potential is not constant in the middle of the channel. The drift current induced in the channel by this variation in the surface potential is analyzed in Chapter 5.

We now begin our analysis by examining the equilibrium problem in the middle of the channel for a wide range of gate biases. As we shall see in Chapter 5, it is essential to resolve the layer structure as $\lambda \to \infty$ associated with this problem to characterize quantitatively the electron current flow and the device characteristics under a non-zero source-drain bias.

CHAPTER 2

Asymptotic Theory Of The One-Dimensional Equilibrium Potential: I

In Chapters 2 and 3 the nonlinear Poisson equation in equilibrium is analyzed in the middle of the channel in the limit $\lambda \to \infty$ for two classes of doping profiles. Using singular perturbation techniques, the intricate boundary and internal layer structure of the potential for $\lambda \gg 1$ is resolved for various ranges of gate voltage. In studying the dependence of the potential on the gate voltage, it will be shown that different qualitative behavior in the solution near the semiconductor-insulator interface is possible for different ranges of gate voltage. This behavior is a direct result of the several possible dominant balances in the potential equation that can hold near the interface. Finally, using techniques in the asymptotic expansion of integrals, we shall compute asymptotically the amount of mobile charge available for the conduction of current under a non-zero source-drain bias.

The device type and its associated operating characteristics are determined by the implant profile. The two classes of devices that are considered are the enhancement mode device and the built-in channel device. The enhancement device studied in this chapter is obtained by implanting only acceptor impurities such as boron into the substrate; whereas a built-in channel device, which is considered in Chapter 3, is obtained by implanting both acceptor and donor impurities. The layer structure of the potential for $\lambda \gg 1$ will be resolved for both of these cases.

2.1 Enhancement Mode Device – Asymptotic Potential

The doping profile for the enhancement mode device is modeled by

$$d(x) = \beta + (1-\beta) f(x:\sigma)\,,$$

where:

$$(i)\ \ 0 < \beta \leq 1, \quad \sigma > 0, \text{ with } \beta, \sigma \text{ independent of } \lambda,$$

$$(ii)\ \ d(0) = 1, \quad d'(x) \leq 0, \text{ and } d(x) \to \beta \text{ as } x \to \infty,$$

$$(iii)\ \ x^n f(x:\sigma) \to 0 \text{ as } x \to \infty \quad \text{for all integers } n > 0\,,$$

and σ, referred to as the straggle, represents the scale of the variable doping profile. Normally, $f(x:\sigma)$ is taken as $f(x) = \exp(-(x/\sigma)^2)$ and typically $\beta \in [.01, 1.0]$ and $\sigma \in [.10, 10.0]$. For other doping profiles, the location of maximum dopant concentration, referred to as the projected range, occurs away from the semiconductor-insulator interface. The results that we shall present for the asymptotic potential can also be generalized to include implant profiles with non-zero projected range.

From Chapter 1 equation (1.5 a), the nonlinear Poisson equation in equilibrium, $\phi_n \equiv 0$ and $\phi_p \equiv 0$, is

$$w_{xx} + \varepsilon^2 w_{yy} = \frac{2}{\lambda}\sinh(w\,\ln\lambda) + d(x), \tag{2.1}$$

and the boundary conditions are

$$-w_x + c_{\rm ox}\left(\frac{\ln\lambda}{\lambda}\right)^{1/2}(w_s+1) = c_{\rm ox}\left(\frac{\ln\lambda}{\lambda}\right)^{1/2}\frac{\bar{v}_{\rm gs}}{\ln\lambda} \qquad \text{on } x=0\,,$$

and

$$\lim_{x\to\infty} w(x) = -\frac{1}{\ln\lambda}\sinh^{-1}(\frac{\beta\lambda}{2}) \qquad \text{with } \beta\lambda \gg 1\,,$$

where $w_s = w(0,y)$ is the surface potential that is independent of y in the middle of the channel. In this Chapter, asymptotic expansions as $\lambda \to \infty$ are constructed for the outer solution to (2.1), defined by setting $\varepsilon = 0$, for various ranges of gate voltage, $\bar{v}_{\rm gs}$. The operating regime of the device is characterized by the value of the gate voltage or, more conveniently, the surface potential. The terminology and classification introduced below for constant doping, $\beta = 1$, can be found in the literature, i.e., Sze [31]:

$$\begin{aligned}
w_s(\bar{v}_{\rm gs}) &> 1 && \text{Strong Inversion}\\
0 \le w_s(\bar{v}_{\rm gs}) &\le 1 && \text{Weak Inversion}\\
-1 + O(1/\ln\lambda) \ll w_s(\bar{v}_{\rm gs}) &< 0 && \text{Depletion}\\
|w_s(\bar{v}_{\rm gs}) + 1| &= O(1/\ln\lambda) && \text{Near Flatband}\\
w_s(\bar{v}_{\rm gs}) &\ll -1 + O(1/\ln\lambda) && \text{Accumulation}\,.
\end{aligned}$$

The voltage normalization for constant doping is such that $\bar{v}_{\rm gs} \approx 0$ at flatband where $w_s \approx -1$.

The regimes relevant to an n-channel device that are studied are inversion, both weak and strong, and depletion. The asymptotic potential for the remaining two regimes, due to their relevance to the built-in channel device, will also be constructed.

For gate voltages corresponding to strong inversion, a significant amount of n-carriers are present near the semiconductor-insulator interface. Under this condition, the interface is said to be strongly inverted and the thin layer containing these charges is called the inversion layer.

For gate voltages corresponding to weak inversion or depletion, the total semiconductor space charge density near the interface is dominated by the immobile acceptor ions. The region containing these charges is called the depletion layer. For gate voltages corresponding to weak inversion, a small leakage current flows in the channel upon application of a source-drain bias. Alternatively, for gate voltages corresponding to the depletion regime, there are virtually no mobile n-carriers near the interface available for current conduction.

The conventional GCA under constant doping is based on the first integral of the one-dimensional Poisson equation with $\varepsilon = 0$, combined with the depletion approximation first introduced by Shockley [30]. Although this method is useful for finding the total charge on the semiconductor as predicted by the one-dimensional theory, it has several drawbacks, some of which were discussed in Chapter 1.

Instead, by resolving the boundary layers in the potential, the more realistic case of a variable implant can be treated for all bias ranges. In addition, the conjecture based on numerical experiments that the width of the depletion layer is insensitive to gate voltages above some threshold will be proved asymptotically. This result has implications concerning the dependence of the mobile charge near the interface on the gate voltage. Most importantly, the information obtained from this approach is invaluable in analyzing the device in non-equilibrium conditions and in quantifying observed physical effects such as pinchoff.

In order to determine the dominant balance that holds near the interface, it is convenient to suppose that the surface potential, w_s, is specified. Later, the surface potential will be related to the gate voltage. The matching techniques employed are first illustrated for the constant doping case, $\beta = 1$. The agreement between the leading order asymptotic solution and direct numerical calculations

of the potential will be seen to be excellent. A schematic plot of the potential is shown below for strong inversion under constant doping. We begin our analysis with weak inversion.

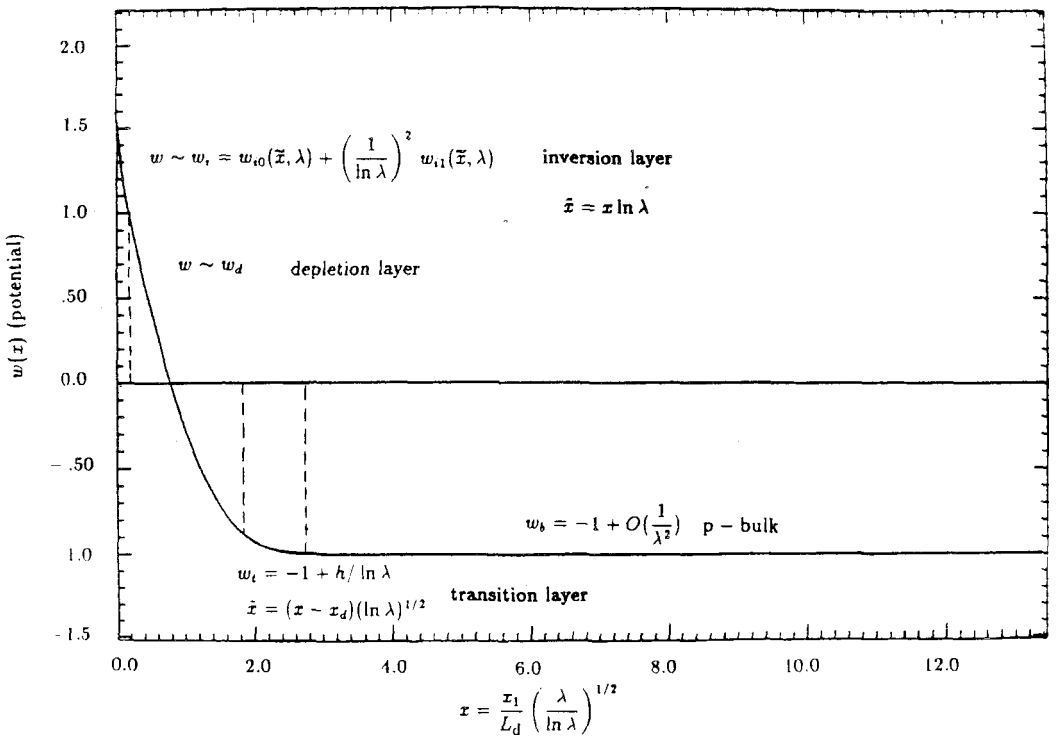

FIGURE 2.1. Schematic Plot of the Equilibrium Potential

Weak Inversion-Depletion $(-1+O(1/\ln\lambda) \ll w_s \leq 1)$ constant doping. In this case, the dominant contribution to the space charge density near the interface arises from the immobile acceptor ions. Therefore, near the interface, the nonlinearity in the Poisson equation can be neglected. The analysis of the matching for this case closely parallels that of Please [23].

Near the interface, the depletion layer potential for constant doping satisfying $w_d(0) = w_s$ is expanded as

$$w_d = \frac{1}{2}x^2 + ax + w_s\,,$$

where

$$a = \sum_{i=0}^{\infty} a_i (\ln \lambda)^{-i}\,,$$

with as yet unknown coefficients a_i. The important feature is that the presence of $(\ln\lambda - 1)^{1/2}$ terms that will appear in the analysis require an infinite order expansion in powers of $\ln\lambda$ to successfully match. The failure to match to an infinite order in $\ln\lambda$ makes the potential and thus the total charge highly inaccurate near flatband.

In the p-bulk, an expansion of the boundary condition at infinity for $\lambda \gg 1$ provides $w_b = -1 + O(1/\lambda^2 \ln\lambda)$.

As in the study of the p-n junction by Please [23], the depletion layer potential is matched to the bulk by means of a transition layer centered at some unknown depth x_d referred to as the depletion width. The matching of the depletion layer to the bulk determines both the depletion width and the coefficients, a_i, of the depletion layer expansion.

In this internal layer, we define transition layer variables by

$$x_t = \frac{x - x_d}{\nu_d(\lambda)} \qquad \text{and} \qquad w_t(x_t) = w(x_t\nu_d(\lambda) + x_d)\,,$$

and

$$w_t(x_t) = -1 + \sigma_d(\lambda)h(x_t)\,,$$

where $h(x_t) = h_0(x_t) + h_1(x_t)/\lambda^2 + \cdots$. Upon substituting this expansion into the original equation (2.1), the appropriate scalings are immediately seen to be

$$\nu_d(\lambda) = \left(\frac{1}{\ln\lambda}\right)^{1/2} \qquad \text{and} \qquad \sigma_d(\lambda) = \frac{1}{\ln\lambda}\,,$$

so that the transition layer equation for h_0 becomes

$$h_0'' = 1 - e^{-h_0}\,. \tag{2.2}$$

To match to the bulk potential, we require $h_0(\infty) = 0$. It is not possible to integrate (2.2) explicitly; a first integral, however, provides the implicit expression

$$-\sqrt{2}x_t = \int_1^{h_0} (e^{-y} + y - 1)^{-1/2}\,dy\,. \tag{2.3}$$

The lower limit of the integral can be chosen arbitrarily as $O(1)$ changes in its value are reflected in $O((\ln\lambda)^{-1/2})$ changes in the depletion width.

Even though the transition layer solution is not known explicitly, all we require for matching are the asymptotics out of this layer. Defining an intermediate variable, x_η, via

$$x_\eta = \frac{x - x_d}{\eta(\lambda)}, \qquad \text{where} \qquad \frac{1}{(\ln\lambda)^{1/2}} \ll \eta(\lambda) \ll 1,$$

and expanding the implicit transition layer solution (2.3) as $x_t \to -\infty$, or alternatively as $h \to \infty$, provides

$$w_t \sim -1 + \frac{1}{2}x_\eta^2\eta^2 - \frac{x_\eta \eta\, c}{\sqrt{2}}(\ln\lambda)^{-1/2} + (\frac{c^2}{4} + 1)(\ln\lambda)^{-1} + \cdots, \tag{2.4}$$

where

$$c = \int_1^\infty \left[(y-1)^{-1/2} - (e^{-y} + y - 1)^{-1/2}\right] dy. \tag{2.5}$$

The value of c from numerical integration to five significant digits is $c = .81785$.

Similarly, expanding the depletion layer potential in terms of the intermediate variable gives

$$w_d \sim \frac{1}{2}x_d^2 + ax_d + w_s + x_\eta\eta(a + x_d) + \frac{1}{2}x_\eta^2\eta^2 + \cdots.$$

To match, we must also expand the depletion width as

$$x_d = \sum_{i=0}^{\infty} x_{di}(\ln\lambda)^{-i/2}$$

and equate powers of $\eta(\lambda)$ in the above expressions. Matching the transition and depletion layer potentials to an infinite order in $\ln\lambda$ by solving the resulting algebraic equations gives

$$\begin{aligned} a &= -\sqrt{2}(w_s + 1 - 1/\ln\lambda)^{1/2}, \\ x_d &= -\frac{c}{\sqrt{2}}(\ln\lambda)^{-1/2} + \sqrt{2}(w_s + 1 - 1/\ln\lambda)^{1/2}, \end{aligned} \tag{2.6}$$

of which the first few terms for $\ln\lambda \gg 1$ are

$$\begin{aligned} a &\sim -\sqrt{2}(w_s+1)^{1/2}\left[1 - \frac{1}{2(w_s+1)\ln\lambda} + \cdots\right], \\ x_d &\sim -\frac{c}{\sqrt{2}}(\ln\lambda)^{-1/2} + \sqrt{2}(w_s+1)^{1/2}\left[1 - \frac{1}{2(w_s+1)\ln\lambda} + \cdots\right]. \end{aligned}$$

The leading order term in this expansion is equivalent to the depletion approximation in which the transition layer is neglected, and the leading order depletion

layer potential is patched for C^1 continuity to the bulk at some unknown location. Using the expression for a, the depletion layer potential is

$$w_d = \frac{1}{2}x^2 - \sqrt{2}(w_s + 1 - 1/\ln\lambda)^{1/2}\, x + w_s\,.$$

From this expression, we see that the expansion breaks down near flatband where $w_s = -1 + O(1/\ln\lambda)$. When this condition occurs, the transition layer equation is valid up to the interface as there is no region of depleted carriers.

We now consider strong inversion characterized by a different balance in the Poisson equation for $\lambda \gg 1$ near the interface. This layer is not present for p-n junctions unless the junction is strongly one-sided.

Strong Inversion ($w_s \geq 1$), constant doping. In the inversion layer near the interface, the contribution to the space charge density is dominated by the n-carriers. In this layer, we consider stretched variables defined by

$$\tilde{x} = \frac{x}{\nu(\lambda)} \qquad \text{and} \qquad w_i(\tilde{x}) = w(\tilde{x}\nu(\lambda))\,,$$

where $w_i(\tilde{x})$ is expanded as

$$w_i(\tilde{x}) = w_{i0}(\tilde{x},\lambda) + \sigma(\lambda)w_{i1}(\tilde{x},\lambda) + \cdots\,,$$

and $\sigma(\lambda)$, $\nu(\lambda) \to 0$ as $\lambda \to \infty$ are scalings to be determined. Substituting this expansion into (2.1) then yields

$$\frac{1}{\nu^2(\lambda)}(w_{i0}'' + \sigma(\lambda)w_{i1}'' + \cdots) = \frac{2}{\lambda}\sinh\left((w_{i0} + \sigma(\lambda)w_{i1} + \cdots)\ln\lambda\right) + 1\,.$$

The appropriate boundary layer scalings in this layer are assumed to satisfy

$$\sigma(\lambda) = \nu^2(\lambda) \qquad \text{and} \qquad \sigma(\lambda)\ln\lambda \ll 1\,,$$

so that upon linearizing the exponential we obtain the layer equations:

$$w_{i0}'' = \frac{\nu^2(\lambda)}{\lambda}\, e^{w_{i0}\ln\lambda} \qquad w_{i0}(0) = w_s, \tag{2.7a}$$

$$w_{i1}'' - \left[\frac{\nu^2(\lambda)\ln\lambda}{\lambda}\, e^{w_{i0}\ln\lambda}\right] w_{i1} = 1 \qquad w_{i1}(0) = 0\,. \tag{2.7b}$$

We remark that the leading order equation gives no information about the scale of the inversion layer since a shift in w_{i0} can be absorbed into the length scale. An

exact solution of $(2.7a)$, which is linear as $\tilde{x} \to \infty$ and that satisfies the required boundary condition on $\tilde{x} = 0$, is

$$w_{i0} = w_s - \frac{2}{\ln \lambda} \ln \left(\frac{1}{\alpha} \sinh(\alpha \sqrt{\frac{A}{2}} \tilde{x} + \gamma) \right) , \tag{2.8}$$

where

$$A(\lambda) = \nu^2(\lambda) \lambda^{w_s - 1} \ln \lambda \, , \tag{2.9a}$$

and

$$\gamma = \sinh^{-1}(\alpha) \, . \tag{2.9b}$$

Substituting w_{i0} into the boundary layer equation at the next order $(2.7b)$ then gives

$$w_{i1}'' - \frac{\nu^2(\lambda) \lambda^{w_s - 1} \alpha^2 \ln \lambda}{\sinh^2 (\alpha \sqrt{A} \tilde{x} / \sqrt{2} + \gamma)} w_{i1} = 1 \, . \tag{2.10}$$

The unknown constant α and the scaling $\nu(\lambda)$ will be found by matching to the depletion layer.

Now in the depletion layer, the contribution to the space charge density of the nonlinear terms in the Poisson equation can be neglected. Consequently, in this region we again assume the asymptotic expansion

$$w_d = \frac{1}{2} x^2 + a x + b \, ,$$

where $a = a(\lambda)$, $b = b(\lambda)$ both $O(1)$ are to be found by matching.

To match to the depletion layer, we define an intermediate variable x_η by

$$x_\eta = \frac{x}{\eta(\lambda)} \, ,$$

where $\nu(\lambda) \ll \eta(\lambda) \ll 1$. The depletion layer potential in terms of an intermediate variable becomes

$$w_d = b + a x_\eta \eta + \frac{1}{2} x_\eta^2 \eta^2 \, . \tag{2.11}$$

Similarly, we expand the inversion layer potential in terms of the intermediate variable $x_\eta = \frac{1}{\eta} \tilde{x} \nu$. Assuming that $\alpha (\ln \lambda)^{1/2} \lambda^{(w_s - 1)/2} \eta(\lambda) \gg 1$ and using the

large argument expansion of y,

$$\ln\left(\frac{1}{\alpha}\sinh(y)\right) \sim -\ln(2\alpha) + y - e^{-2y} + \cdots ,$$

(2.8) becomes

$$w_{i0} \sim w_s + \frac{2}{\ln\lambda}\ln\left(\frac{2\alpha}{\alpha+\sqrt{\alpha^2+1}}\right) - \sqrt{\frac{2}{\ln\lambda}}\,\alpha\lambda^{(w_s-1)/2}x_\eta\eta + \text{T.S.T.} \quad . \tag{2.12}$$

Comparing the $O(\eta(\lambda))$ terms in (2.11) and (2.12), we see that to match we must set

$$\alpha = \lambda^{(1-w_s)/2}\sqrt{\ln\lambda}\,\alpha_0 , \tag{2.13}$$

where $\alpha_0(\lambda) = O(1)$ is to be found in the matching process.

Using the form of α in the higher order boundary layer equation (2.10) we obtain

$$w_{i1}'' - \frac{\alpha_0^2\,\nu(\lambda)^2\,(\ln\lambda)^2}{\sinh^2(\alpha_0\,\nu(\lambda)\ln\lambda\,\tilde{x}/\sqrt{2}+\gamma)}w_{i1} = 1 , \tag{2.14}$$

which suggests the scaling $\nu(\lambda) = 1/\ln\lambda$ so that consequently $\sigma(\lambda) = (1/\ln\lambda)^2$. The asymptotics out of the inversion layer as $\tilde{x} \to \infty$ for w_{i1} are

$$w_{i1} \sim \frac{1}{2}\tilde{x}^2 + a_{i1}\tilde{x} + b_{i1} ,$$

where, in order to match to the depletion layer, the linear growth must be suppressed by imposing $a_{i1} = 0, b_{i1} = 0$. Using a dominant balance argument on w_{i1} as $\tilde{x} \to \infty$, we then find

$$w_{i1} \sim \frac{1}{2}\tilde{x}^2\left(1 + 2\exp(-\sqrt{2}\alpha_0\tilde{x} - 2\gamma)\right) .$$

As a remark, the equation for w_{i1} can be reduced to quadratures via the transformation

$$z = -\coth(\frac{\alpha_0}{\sqrt{2}}\tilde{x} + \gamma) ,$$

$$u = w_{i1} - \frac{1}{2}\tilde{x}^2 ,$$

giving the forced Legendre's equation

$$(1-z^2)u''(z) - 2zu'(z) + 2u = -\frac{2}{\alpha_0^2}(\coth^{-1}(z) + \gamma)^2$$

on $z \in [-\coth\gamma, -1)$, with $u(-\coth\gamma) = 0$. However, since $u \to 0$ exponentially as $z \to -1$ the details of this solution are unnecessary to successfully complete the matching.

Using the form of α as well as the asymptotics of w_{i1} as $\tilde{x} \to \infty$, the expansion of the potential out of the inversion layer becomes

$$w_i \sim 1 + K(\lambda, w_s, \alpha_0) - \sqrt{2}\alpha_0 x_\eta \eta + \frac{1}{2} x_\eta^2 \eta^2 , \tag{2.15}$$

where

$$K(\lambda, w_s, \alpha_0) = \frac{\ln(\ln \lambda)}{\ln \lambda} + \frac{2}{\ln \lambda} \left[\ln(2\alpha_0) - \sinh^{-1}(\alpha) \right] . \tag{2.16}$$

By comparing the two expressions (2.15) and (2.11), we require

$$b = 1 + K(\lambda, w_s, \alpha_0) \qquad \text{and} \qquad a = -\sqrt{2}\alpha_0 . \tag{2.17}$$

In order to solve for the matching parameters a further equation is needed and is obtained from matching the depletion layer solution to the bulk. The analysis is similar to that of weak inversion.

Constructing an internal layer as in weak inversion at the depletion edge and expanding both the depletion and transition layer potentials in terms of an intermediate variable gives

$$w_d \sim \frac{1}{2} x_d^2 + a x_d + 1 + K(\lambda, w_s, \alpha_0) + x_\eta \eta (a + x_d) + \frac{1}{2} x_\eta^2 \eta^2 ,$$

$$w_t \sim -1 + \frac{1}{2} x_\eta^2 \eta^2 - \frac{x_\eta \eta c}{\sqrt{2}} (\ln \lambda)^{-1/2} + (\frac{c^2}{4} + 1)(\ln \lambda)^{-1} .$$

The solutions of the two algebraic equations obtained from equating coefficients of $\eta(\lambda)$ are

$$a = -\sqrt{2}(2 + K(\lambda, w_s, \alpha_0) - 1/\ln \lambda)^{1/2} ,$$

$$x_d = -\frac{c}{\sqrt{2}} (\ln \lambda)^{-1/2} + \sqrt{2}(2 + K(\lambda, w_s, \alpha_0) - 1/\ln \lambda)^{1/2} ,$$

where c is given by (2.5). Finally, the matching parameter in the inversion layer, α_0, is now determined from (2.17). We find

$$\alpha_0 = (2 + K(\lambda, w_s, \alpha_0) - 1/\ln \lambda)^{1/2} , \tag{2.18}$$

which is a weakly nonlinear equation for α_0 that can be solved approximately by the method of undetermined coefficients or numerically by iteration. Once α_0 is

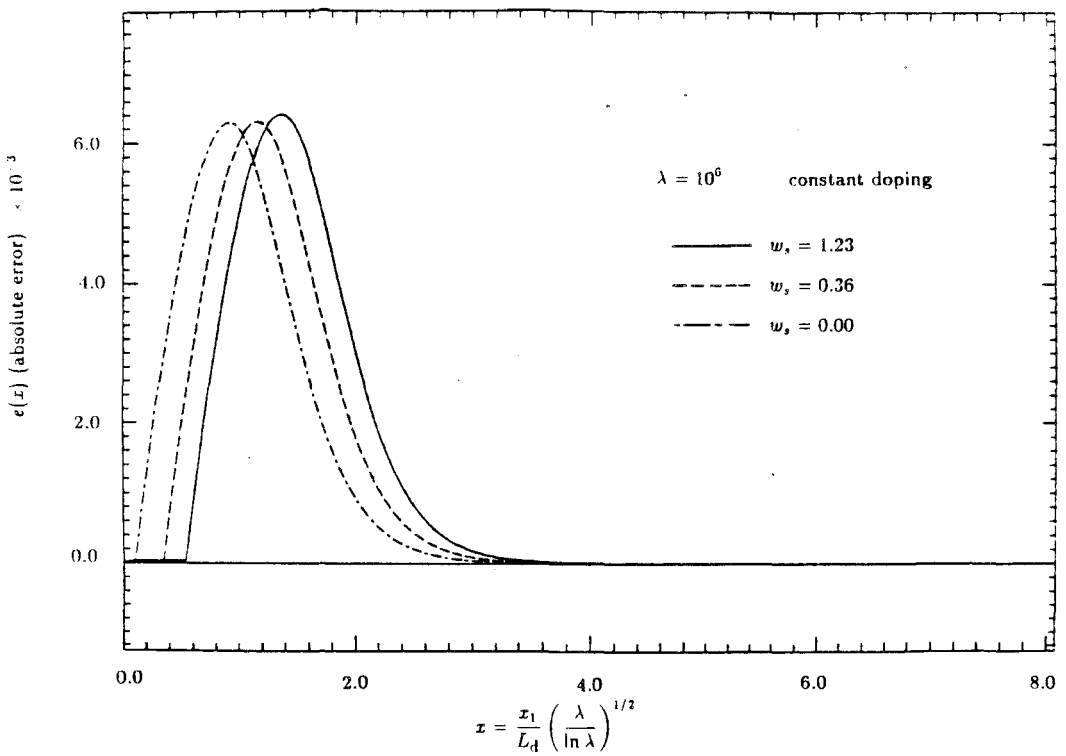

FIGURE 2.2. Comparison of the Asymptotic and the Numerical Equilibrium Potential

found, the switchback term $K(\lambda, w_s, \alpha_0)$ is known and thus the depletion width and the matching parameter a are determined. As a remark, the approximation $\alpha_0 \approx \sqrt{2}$ for realistic doping levels is quite poor, even though $K \ll 1$ for $\lambda \gg 1$, since $K \approx .20$ for $\lambda = 10^6$.

Another important remark is to notice that the order of $K(\lambda, w_s, \alpha_0)$ in the depletion layer expansion depends on the surface potential. In very strong inversion, typically when $w_s \gg 1 + \ln(\ln\lambda)/\ln\lambda$, α is transcendentally small in $\ln\lambda$ as $\lambda \to \infty$. This implies that in this regime, $K(\lambda, w_s, \alpha_0) = O(\ln(\ln\lambda)/\ln\lambda)$ so that the matching parameters α_0, a, and the depletion width are highly insensitive to the surface potential, w_s. Therefore, for this range of surface potential, $\alpha_0 \sim (2 + \ln(\ln\lambda)/\ln\lambda - 1/\ln\lambda)^{1/2}$ is a good approximation. Alternatively, as $w_s \to 1^+$, the expansion $\sinh^{-1}(\alpha) \sim \ln(2\alpha) + 1/4\alpha^2$ for $\alpha \gg 1$ applies and consequently $K \sim (1/\ln\lambda)^2$. Therefore, in this limit, $a \sim (2 - 1/\ln\lambda)^{1/2}$ which agrees asymptotically with the weak inversion expression (2.6) when $w_s = 1$.

To compare our asymptotics with the numerical solution to (2.1), the BVP is solved numerically by finite differences on a uniform mesh with the boundary

condition as $x \to \infty$ imposed at a few depletion widths from the interface. The mesh is taken to be sufficiently fine to resolve the inversion layer. From Figure 2.2, the error, defined as the magnitude of the difference between the numerical and asymptotic potential for $\lambda = 10^6$, is roughly 0.6×10^{-2} in both weak and strong inversion. We now consider the case of accumulation.

Accumulation ($w_s \ll -1 + O(1/\ln\lambda)$) constant doping. In contrast to the previous case, an inversion layer is to be matched not to the depletion layer but rather to the bulk solution. In this regime, the contribution to the space charge density of the n-carriers can be neglected everywhere. For convenience, we define $v(x) = -w(x)$ and $v_s = -w_s$ so that the nonlinear Poisson equation becomes

$$v''(x) = \frac{1}{\lambda} e^{v \ln\lambda} - 1 \quad \text{with} \quad v(0) = v_s \ , \ v(\infty) = 1 \, . \tag{2.19}$$

In the inversion layer, we define $\tilde{x} = x \ln\lambda$, so that the leading order equation becomes

$$v_i''(\tilde{x}) = \frac{1}{\lambda(\ln\lambda)^2} e^{v_i \ln\lambda} \, .$$

Two solutions that satisfy this equation are

$$v_1(\tilde{x}) = 1 + \frac{1}{\ln\lambda}\ln(c_1^2) + \frac{2}{\ln\lambda}\ln\left(\sec\left(\frac{c_1}{\sqrt{2}}(\ln\lambda)^{-1/2}\tilde{x} - x_d\right)\right) \, ,$$

$$v_2(\tilde{x}) = 1 + \frac{1}{\ln\lambda}\ln(c_2^2) - \frac{2}{\ln\lambda}\ln\left(\sinh\left(\frac{c_2}{\sqrt{2}}(\ln\lambda)^{-1/2}\tilde{x} + \gamma\right)\right) \, ,$$

where

$$c_1 = \cos(x_d)\lambda^{(v_s-1)/2} \qquad \text{and} \qquad c_2 = \sinh(\gamma)\lambda^{(v_s-1)/2}$$

are needed to satisfy the boundary condition on the interface. Recall that v_2 was used to match the inversion to the depletion layer in the previous bias regime. We now show why, in this case, v_1 is the layer solution needed to match to the bulk.

To obtain some insight into the differences between the boundary layer solutions v_1 and v_2, we compare the slope at the origin between v_1, v_2 and the expression obtained from integrating (2.19) once with $v(\infty) = 1$. In the original

variable $x = \tilde{x}/\ln\lambda$, we have

$$v'(x=0) = -\sqrt{2}\left(\frac{1}{\lambda\ln\lambda}e^{v_s\ln\lambda} - v_s + 1 - \frac{1}{\ln\lambda}\right)^{1/2},$$
$$v_2'(x=0) = -\left(\frac{2}{\ln\lambda}\right)^{1/2}\lambda^{(v_s-1)/2}\left(1 + c_2^2/\lambda^{v_s-1}\right)^{1/2},$$
$$v_1'(x=0) = -\left(\frac{2}{\ln\lambda}\right)^{1/2}\lambda^{(v_s-1)/2}\left(1 - c_1^2/\lambda^{v_s-1}\right)^{1/2}.$$

Setting $v_s = 1 + \ln(\ln\lambda)/\ln\lambda$, then implies

$$v'(x=0) = -\sqrt{2}\left(1 - \ln(\ln\lambda)/\ln\lambda - 1/\ln\lambda\right)^{1/2},$$
$$v_2'(x=0) = -\sqrt{2}\left(1 + c_2^2/\ln\lambda\right)^{1/2},$$
$$v_1'(x=0) = -\sqrt{2}\left(1 - c_1^2/\ln\lambda\right)^{1/2}.$$

Comparing the first two expressions above we notice that choosing v_2 as the boundary layer solution would imply $c_2^2 < 0$. Alternatively, comparing the first and third expressions we then anticipate that v_1 is the required boundary layer solution and that $c_1^2 \sim \ln(\ln\lambda) + 1$ for this value of the surface potential. A similar argument shows that the ln(sec) solution would have been inappropriate for matching the inversion layer to the depletion layer.

To determine how the inversion layer must match to the bulk, we notice that by using v_1 it is possible to patch to the bulk for C^1 continuity at some unknown location and determine a real value for the constant c_1. Setting $v_1(\tilde{x}_0) = 1$ and $v_1'(\tilde{x}_0) = 0$ gives

$$x_d = \frac{\tilde{x}_0}{\sqrt{2}}(\ln\lambda)^{-1/2} \qquad \text{and} \qquad c_1 = 1.$$

Satisfying the boundary condition on the interface and using $v_s \gg 1 + O(1/\ln\lambda)$ then implies

$$x_d \sim \frac{\pi}{2} + \lambda^{(1-v_s)/2} + O(\lambda^{(1-v_s)}) \quad \text{and} \quad \tilde{x}_0 \sim \frac{\pi}{\sqrt{2}}(\ln\lambda)^{1/2},$$

which shows that the patching is done on a scale wider than the inversion layer. In addition, since the argument of the secant in the boundary layer solution v_1 must remain bounded for the logarithm to exist, we anticipate that the inversion

layer matches to the bulk via a transition layer in a triple-deck fashion. We now explicitly illustrate the matching for this case when $v_s = 1 + \ln(\ln\lambda)/\ln\lambda$.

The transition layer solution between the inversion layer and the bulk is defined by

$$v = 1 + h/\ln\lambda \qquad \text{and} \qquad \tilde{x}_t = x(\ln\lambda)^{1/2}\,,$$

giving $h'' = e^h - 1$ with the boundary condition $h(\infty) = 0$ needed to match to the bulk. Integrating the equation for h once gives

$$-\sqrt{2}\tilde{x}_t = \int_{h(0)}^{h} (e^y - y - 1)^{-1/2}\, dy\,.$$

Expanding the integral in terms of an intermediate variable

$$\tilde{x}_t = x_\eta \eta (\ln\lambda)^{1/2} \quad \text{where} \quad 1/\ln\lambda \ll \eta \ll (1/\ln\lambda)^{1/2}$$

then implies

$$v \sim 1 + \frac{h(0)}{\ln\lambda} - \sqrt{\frac{2}{\ln\lambda}} x_\eta \eta \left(e^{h(0)} - h(0) - 1\right)^{1/2} + \frac{x_\eta^2 \eta^2}{2}\left(e^{h(0)} - 1\right)\,. \tag{2.20}$$

Now for the inversion layer we have $\tilde{x} = x_\eta \eta \ln\lambda$ so that the inversion layer potential v_1 becomes

$$v_1(\tilde{x}) = 1 + \frac{1}{\ln\lambda}\ln(c_1^2) + \frac{2}{\ln\lambda}\ln\left(\sec(\frac{c_1}{\sqrt{2}}(\ln\lambda)^{1/2} x_\eta \eta - x_d)\right)\,.$$

Assuming that $c_1\eta(\ln\lambda)^{1/2} \ll 1$ and using the two expansions

$$\sec(z+\varepsilon) \sim \sec(z) + \varepsilon\sec(z)\tan(z) + \frac{\varepsilon^2}{2}(2\sec^2(z) - \sec(z)) + \cdots\,,$$

$$\ln(1+\varepsilon) \sim \varepsilon - \frac{1}{2}\varepsilon^2 + \cdots\,,$$

both valid for $\varepsilon \ll 1$, we obtain

$$v_1 \sim 1 + \frac{\ln(c_1^2\sec^2(x_d))}{\ln\lambda} - \frac{\sqrt{2}\,c_1}{(\ln\lambda)^{1/2}}\left(\sec^2(x_d) - 1\right)^{1/2} x_\eta\eta + \frac{c_1^2}{2}x_\eta^2\eta^2\sec^2(x_d) + \cdots\,. \tag{2.21}$$

Matching the two expressions (2.21) and (2.20) when $v_s = 1 + \ln(\ln\lambda)/\ln\lambda$ gives

$$h(0) = \ln(\ln\lambda) \quad \text{and} \quad c_1^2 = \ln(\ln\lambda) + 1\,.$$

Then from the equation imposed by the boundary condition, namely $c_1^2 \sec^2(x_d) = \ln\lambda$, and with $\sec(\pi/2+\varepsilon) \sim -1/\varepsilon$ for $\varepsilon \ll 1$, we conclude

$$x_d \sim \frac{\pi}{2} - \frac{\sqrt{\ln(\ln\lambda)+1}}{(\ln\lambda)^{1/2}},$$

which shows that there is a singularity in the inversion layer solution, v_1 just outside the domain for $\lambda \gg 1$. As a remark, since $c_1 = c_1(\lambda)$, the inequality $c_1\eta(\ln\lambda)^{1/2} \ll 1$ further restricts the overlap region between the transition and the inversion layers. The analysis proceeds in a similar manner for $v_s \gg 1 + O(\ln(\ln\lambda)/\ln\lambda)$, and predicts $c_1^2 = (v_s - 1)\ln\lambda + 1$. Finally, the accumulation layer solution is then obtained from $w(x) = -v(x)$.

In the next section, the results from weak and strong inversion are generalized to include the more realistic case of a variable implant whose variation occurs in the depletion region of the device.

Strong and Weak Inversion (variable doping). In the case of a variable implant whose variation occurs in the depletion region of the device, the asymptotic techniques developed in the previous sections still apply, although the algebraic equations for the matching parameters become more complicated and must be solved for numerically. Even though the matching parameters must be found numerically, this asymptotic approach is still preferable to a complete numerical solution of the nonlinear Poisson equation, since for device applications, closed form expressions for the resulting device characteristics in weak and strong inversion are desired. We first generalize our results for the case of weak inversion.

In weak inversion, the depletion layer expansion holds in a region near the interface. The solution of the potential equation in this region satisfying the required boundary condition on the interface is

$$w_d = \frac{\beta}{2}x^2 + ax + w_s + (1-\beta)\int_0^x (x-\varsigma)f(\varsigma)\,d\varsigma\,. \tag{2.22}$$

Likewise, assuming that $d(x)$ is slowly varying in the bulk so that $|d''(x)d(x) - d'^2(x)| \ll d^2(x)\ln\lambda$, the bulk potential is given asymptotically by

$$w_b = -1 - \frac{\ln(d(x))}{\ln\lambda} + \cdots\,.$$

As in the previous section, the depletion layer potential is matched to the bulk by constructing a transition layer about the unknown depletion width. Using

the same scalings for the dependent and independent variables as in the previous section, and assuming that $d(x)$ is locally constant in this layer, the transition layer equation is simply

$$h'' = d(x_d) - e^{-h} \qquad \text{with} \qquad h(\infty) = -\ln(d(x_d))\,.$$

A first integral of the above equation provides the implicit relationship

$$-\sqrt{2}x_t = \int_{1-\ln d(x_d)}^{h} (e^{-y} + d(x_d)y + b_d)^{-1/2}\, dy\,,$$

where $b_d = d(x_d)(\ln(d(x_d)) - 1)$ and the lower limit of the integral has been chosen for convenience. Upon defining an intermediate variable, x_η, by

$$x_\eta = \frac{x - x_d}{\eta(\lambda)} \qquad \text{where} \qquad \frac{1}{(\ln\lambda)^{1/2}} \ll \eta(\lambda) \ll 1\,,$$

the expansion of the transition and depletion layer solutions in terms of x_η becomes

$$\begin{aligned} w_d \sim{}& \frac{\beta}{2}x_d^2 + ax_d + w_s + (1-\beta)\left(x_d I_1(x_d) - I_2(x_d)\right) \\ &+ x_\eta\eta\left(\beta x_d + a + (1-\beta)I_1(x_d)\right) + \frac{d(x_d)}{2}x_\eta^2\eta^2\,, \\ w_t \sim{}& -1 + \frac{d(x_d)}{2}x_\eta^2\eta^2 - \frac{x_\eta\eta\, c\, d(x_d)}{\sqrt{2\ln\lambda}} + \frac{1}{\ln\lambda}\left(\frac{c^2 d(x_d)}{4} + 1 - \ln(d(x_d))\right)\,, \end{aligned} \tag{2.23}$$

where we have used the abbreviations

$$\begin{aligned} c =& c(x_d) \equiv \int_{1-\ln(d(x_d))}^{\infty} \left[(d(x_d)y + b_d)^{-1/2} - (e^{-y} + d(x_d)y + b_d)^{-1/2}\right] dy\,, \\ I_1(x_d) \equiv& \int_0^{x_d} f(\varsigma)\, d\varsigma \quad \text{and} \quad I_2(x_d) \equiv \int_0^{x_d} \varsigma f(\varsigma)\, d\varsigma\,. \end{aligned} \tag{2.24}$$

Matching the $O(1)$ and $O(\eta(\lambda))$ terms in the above two expressions gives,

$$\begin{aligned} \frac{\beta}{2}x_d^2 + ax_d + w_s + (1-\beta)(x_d I_1 - I_2) &= -1 + \frac{1}{\ln\lambda}\left(\frac{c^2 d(x_d)}{4} + 1 - \ln(d(x_d))\right)\,, \\ \beta x_d + a + (1-\beta)I_1 &= -\frac{c\, d(x_d)}{\sqrt{2\ln\lambda}}\,. \end{aligned} \tag{2.25}$$

By eliminating a from the two equations, the depletion width is found to be the solution of

$$\int_0^{x_d} \varsigma d(\varsigma)\, d\varsigma = 1 + w_s - \frac{x_d\, c\, d(x_d)}{\sqrt{2 \ln \lambda}} - \frac{1}{\ln \lambda}\left(\frac{c^2 d(x_d)}{4} + 1 - \ln(d(x_d))\right), \quad (2.26)$$

which, for general implant profiles, is a transcendental equation that must be solved numerically. Notice that for constant doping, $\beta = 1$, or equivalently $d(x) \equiv 1$, the above expression for the depletion width reduces to (2.6).

Since we are mainly interested in the depletion width and the matching parameter a in weak inversion away from flatband conditions, we do not solve the full implicit equation (2.26). Instead, using $\ln \lambda \gg 1$, we solve the leading order equation

$$\int_0^{x_d} \varsigma d(\varsigma)\, d\varsigma = 1 + w_s \quad (2.27)$$

for x_d, so that the matching parameter a is then determined asymptotically by

$$a = -\beta x_d - (1-\beta) I_1(x_d). \quad (2.28)$$

This approximation is equivalent to the depletion approximation in which the details of the transition layer are neglected. As in the case of constant doping, this approximation is very good in weak inversion.

To obtain an initial guess for a Newton iteration procedure applied to (2.27), we expand the depletion width in powers of $(1-\beta)$, which corresponds to a small perturbation from the constant doping limit $\beta = 1$. The depletion width is then determined via the iteration

$$x_d^{\nu+1} = x_d^{\nu} - \frac{\int_0^{x_d^{\nu}} \varsigma d(\varsigma)\, d\varsigma - (1 + w_s)}{x_d^{\nu} d(x_d^{\nu})}.$$

Provided that w_s is away from flatband, only a few iterations are required for convergence of the Newton iterates to within a small specified tolerance.

In the case of strong inversion, the layer equations in the inversion layer are the same as in the previous section, since by assumption, the doping is locally constant in this layer. Once again, the matching of the inversion to the depletion region must occur in a neighbourhood of $w = 1$. Furthermore, as with constant

doping, a switchback term, K, must be added to the depletion layer expansion in order to match the inversion and depletion layers. Formally carrying out the matching of the depletion layer to the inversion layer as in the previous section, and retaining the same notation, we find

$$b = 1 + K(\lambda, w_s, \alpha_0) \qquad \text{and} \qquad a = -\sqrt{2}\alpha_0\,, \tag{2.29}$$

where $K(\lambda, w_s, \alpha_0)$ is given by (2.16). Now by constructing an internal layer at the depletion edge and keeping only the leading order terms as in weak inversion, we obtain two coupled equations for a and x_d

$$\frac{\beta}{2}x_d^2 + ax_d + (1-\beta)\,(x_d I_1 - I_2) = -2 - K(\lambda, w_s, \alpha_0)\,,$$
$$\beta x_d + a + (1-\beta)I_1 = 0\,.$$

The abbreviations for the integrals are defined in (2.24). As a remark, the leading order term in the constant doping limit is recovered by formally setting $\beta = 1$.

After some manipulations, the equations determining the matching constants in strong inversion can be written as

$$\frac{\beta}{2}x_d^2 + (1-\beta)I_2 = 2 + K(\lambda, w_s, \alpha_0)\,, \tag{2.30a}$$

$$\beta x_d - \sqrt{2}\alpha_0 + (1-\beta)I_1 = 0\,, \tag{2.30b}$$

which are two weakly coupled equations in x_d and α_0. The remaining matching constant, a, is then directly determined once α_0 is known. In order to obtain an initial guess to the solution of $(2.30a, b)$ we again construct a formal expansion for α_0 and x_d in powers of $(1-\beta)$. Using the initial guess generated from this procedure, we then apply a straightforward Newton's method to the coupled system $(2.30a, b)$. Once again, convergence to within a small set tolerance is very rapid.

The asymptotic potential for a variable doping profile in strong inversion is shown in Figure 2.3. As in the case of constant doping, the agreement between the numerical solution of the one-dimensional nonlinear Poisson equation and the asymptotic potential is found to be excellent.

2.2 Enhancement Mode Device – Device Applications

In this section, the surface potential is related to the input gate voltage by

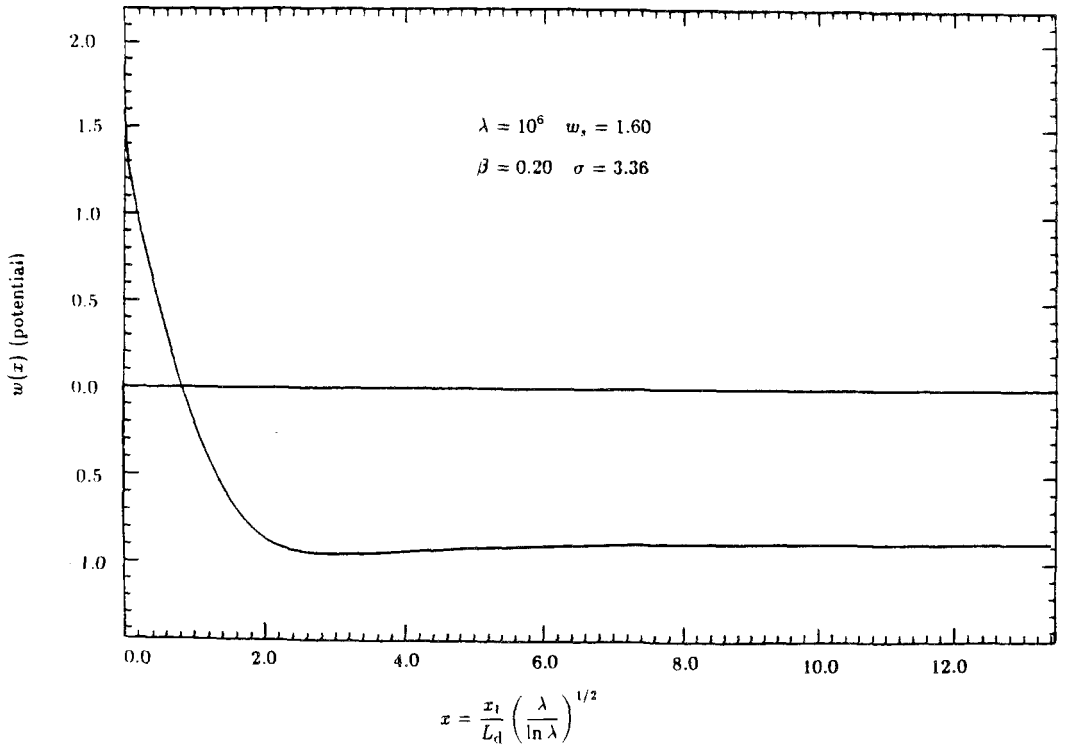

FIGURE 2.3. Equilibrium Potential with Variable Doping in Strong Inversion

studying the boundary condition that holds on the semiconductor-insulator interface,

$$-w_x + c_{ox}\left(\frac{\ln\lambda}{\lambda}\right)^{1/2}(w_s+1) = c_{ox}\left(\frac{\ln\lambda}{\lambda}\right)^{1/2}\frac{\bar{v}_{gs}}{\ln\lambda} \qquad \text{on } x=0\,.$$

In addition, we shall compute the mobile charge due to the conduction electrons as predicted by the one-dimensional theory. This calculation is necessary to derive device characteristics for the MOSFET under non-equilibrium conditions. In this section, we consider only weak and strong inversion and specialize our results to a Gaussian doping profile for which $f(x) = \exp(-(x/\sigma)^2)$. The constant doping limit is recovered by formally setting $\beta = 1$.

Relationship of the total charge to the gate voltage. The total charge, Q_s, as predicted by the one-dimensional theory, is the integral of the space charge density over the semi-infinite interval normal to the interface. In the scaled quantities, we define

$$Q_s \equiv -(\lambda\ln\lambda)^{1/2}\int_0^\infty w''(x)\,dx = (\lambda\ln\lambda)^{1/2}\,w'(0)\,.$$

Using the above definition of Q_s, the mixed boundary condition for the potential on the interface can be written as

$$F(w_s, \bar{v}_{gs}) \equiv (w_s + 1)\ \ln\lambda - \frac{Q_s(w_s)}{c_{ox}} - \bar{v}_{gs} = 0\,. \tag{2.31}$$

For a given surface potential, w_s, the total charge, and hence the required gate voltage can easily be computed. However for a specified input gate voltage, (2.31) is an implicit relationship for the surface potential that must be solved numerically. To invert this relationship, it is necessary that the total charge be calculated as a function of the surface potential in both weak and strong inversion.

From the asymptotic potential constructed for constant doping, Q_s satisfies

$$Q_s = -\sqrt{2}\begin{cases} e^{w_s \ln\lambda/2}\,(1+\alpha^2)^{1/2} & w_s \geq 1\,, \\ (\lambda\ln\lambda)^{1/2}(w_s + 1 - 1/\ln\lambda)^{1/2} & -1 + O(1/\ln\lambda) \ll w_s \leq 1\,, \end{cases} \tag{2.32}$$

where α and α_0 are given by (2.13) and (2.18), respectively. The above two expressions agree asymptotically at $w_s = 1$. The factor α is thus seen to provide a transition for the total charge between weak and strong inversion.

In the conventional GCA, the total charge is obtained from the first integral of the governing Poisson equation evaluated on the interface. The standard result using the asymptotic boundary condition for large constant doping in the bulk is

$$Q_{sc} = -\sqrt{2}\big(e^{w_s \ln\lambda} + e^{-w_s \ln\lambda} + w_s\lambda\ln\lambda + \lambda(\ln\lambda - 1)\big)^{1/2}\,.$$

The total charge for constant doping as a function of the gate voltage, $\bar{v}_{gs}$, as obtained from the first integral and the asymptotic potential is compared in Figure 2.4 where the relative error is plotted. The two expressions for the total charge are seen to agree to within .050 percent under both weak and strong inversion.

For variable doping, in which there is no first integral to the Poisson equation, a similar result for the asymptotic total charge is available using the leading term of the asymptotic equilibrium potential. In both weak and strong inversion for a Gaussian implant we find

$$Q_s \sim -\begin{cases} \sqrt{2}e^{w_s \ln\lambda/2}(1+\alpha^2)^{1/2} & w_s \geq 1, \\ (\lambda\ln\lambda)^{1/2}\left(\beta x_d + \frac{\sigma\sqrt{\pi}}{2}(1-\beta)\mathrm{erf}(x_d/\sigma)\right) & w_s \leq 1\,, \end{cases} \tag{2.33}$$

where α and α_0 are given by (2.13) and (2.30a,b), respectively. The depletion width in weak inversion is found from (2.27). The expression for $w_s < 1$ is valid away from flatband conditions.

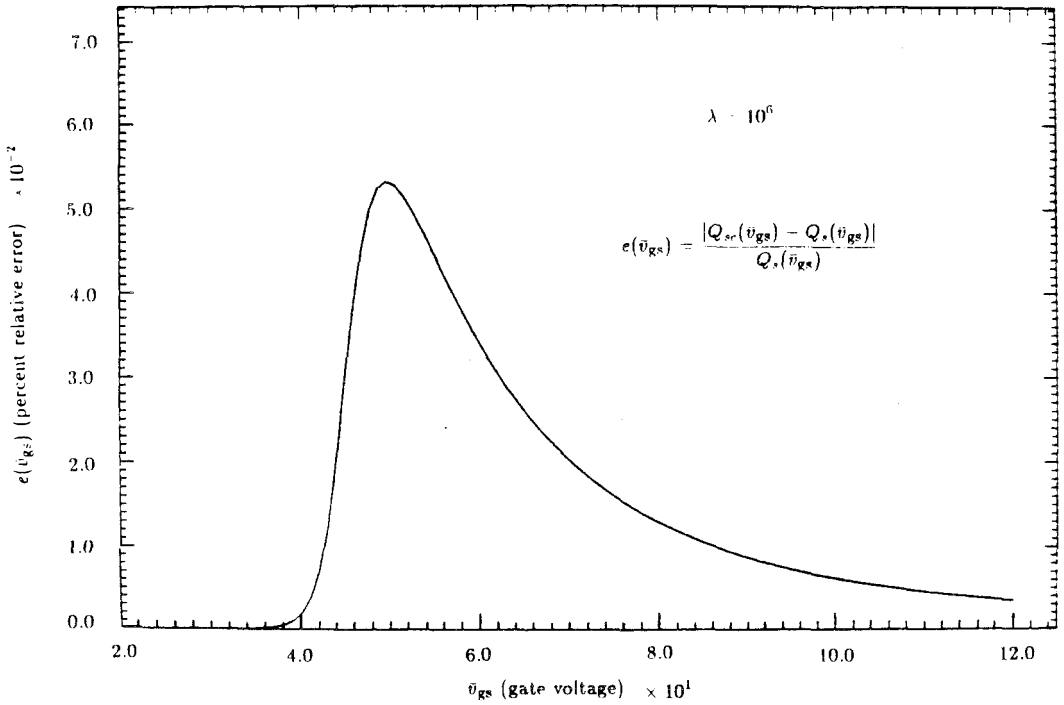

FIGURE 2.4. Comparison of the Total Charge

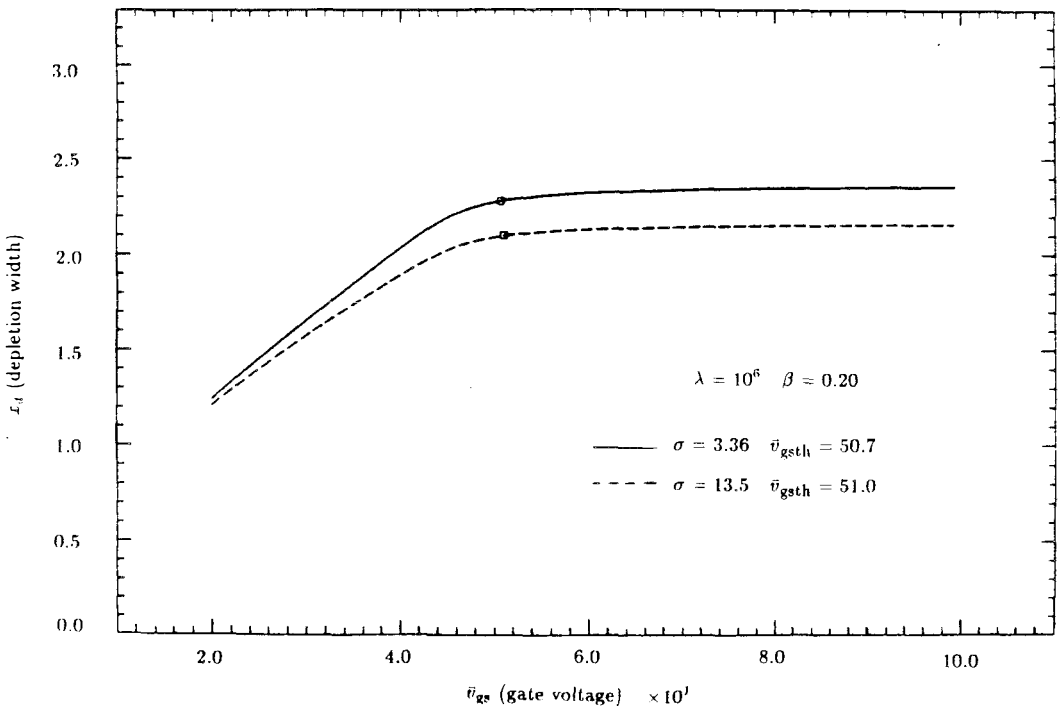

FIGURE 2.5. Depletion Width as a Function of the Gate Voltage

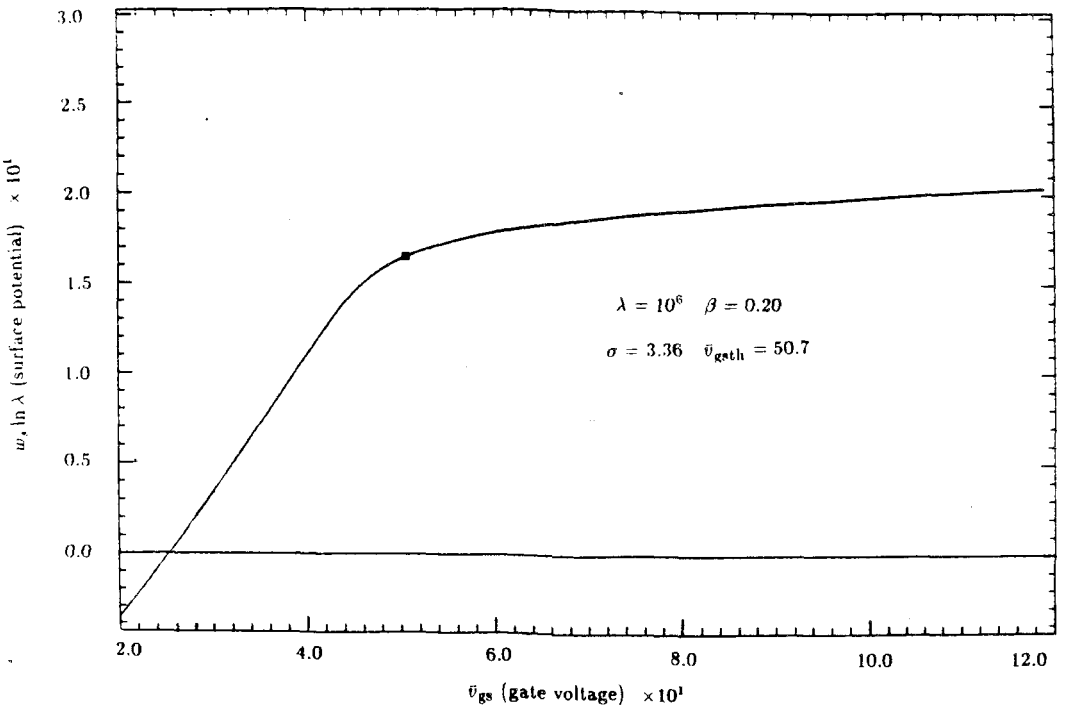

FIGURE 2.6. Surface Potential as a Function of the Gate Voltage

Since the total charge in both weak and strong inversion is expressed as a function of the surface potential, a Newton iteration procedure is used on (2.31) to solve for $w_s = w_s(\bar{v}_{gs})$. With an appropriate initial guess for the surface potential, the Newton iterates are generated by

$$w_s^{\nu+1} = w_s^{\nu} - \frac{F(w_s^{\nu}, \bar{v}_{gs})}{(\ln \lambda - Q_s'(w_s^{\nu})/c_{ox})} . \tag{2.34}$$

In the variable doping case, the total charge at the ν^{th} iterate must be found by solving numerically for the appropriate matching constants. Therefore, for variable doping an inner Newton iteration is needed to solve for the matching constants for a given surface potential.

By continuing in the gate voltage, the plots $x_d = x_d(\bar{v}_{gs})$ and $w_s = w_s(\bar{v}_{gs})$ as seen in Figures 2.5 and 2.6, respectively, are easily generated in both weak and strong inversion and for various doping parameters. The threshold gate voltage, defined as the value of $\bar{v}_{gs}$ for which $w_s = 1 + \ln(\ln \lambda)/\ln \lambda$, is labelled on the graphs.

Even though it is not possible in general to invert (2.31) analytically for all

ranges of gate voltages, the relationship can be inverted asymptotically for $\lambda \gg 1$ in very strong inversion. In very strong inversion, typically when $w_s \approx 1.2$, the total charge is linear in the gate voltage, and thus the surface potential has a logarithmic dependence on the gate voltage of the form

$$w_s \approx \frac{2}{\ln \lambda} \ln \left(\frac{c_{ox}}{\sqrt{2}} \bar{v}_{gs} \right) ,$$

independent of the implant. Therfore, the surface potential and the depletion width increase only marginally after the condition for very strong inversion has been achieved. However, the implant profile is important in determining device characteristics at the onset of strong inversion.

Computation of the mobile and fixed charge. To obtain the device characteristics, the amount of mobile charge near the interface available for current conduction must be computed. The scaled amount of mobile charge is defined by

$$Q_c = -\left(\frac{\ln \lambda}{\lambda} \right)^{1/2} \int_0^{x_d} e^{w \ln \lambda} \, dx .$$

Since the dominant contribution to this integral arises from the charges near the interface, the upper limit of the integral is not important in finding the leading order contribution. Even though this integral cannot be computed exactly, it is possible to evaluate this integral asymptotically as $\lambda \to \infty$ in both weak and strong inversion.

Similarly, the scaled amount of fixed bulk charge is defined by

$$Q_b = -(\lambda \ln \lambda)^{1/2} \int_0^{x_d} d(x) \, dx .$$

This integral can easily be computed for a Gaussian implant in terms of the error function. We shall now evaluate these integrals in both the weak and strong inversion regimes.

Using the form of the Gaussian implant, the bulk charge can be expressed in terms of the depletion width. A simple integration yields

$$Q_b \sim -(\lambda \ln \lambda)^{1/2} \left(\beta x_d + \frac{\sigma \sqrt{\pi}}{2} (1 - \beta) \mathrm{erf}(\frac{x_d}{\sigma}) \right) ,$$

where in weak inversion and strong inversion the depletion width is given by (2.27) and (2.30a, b), respectively. Notice that in weak inversion, the total charge

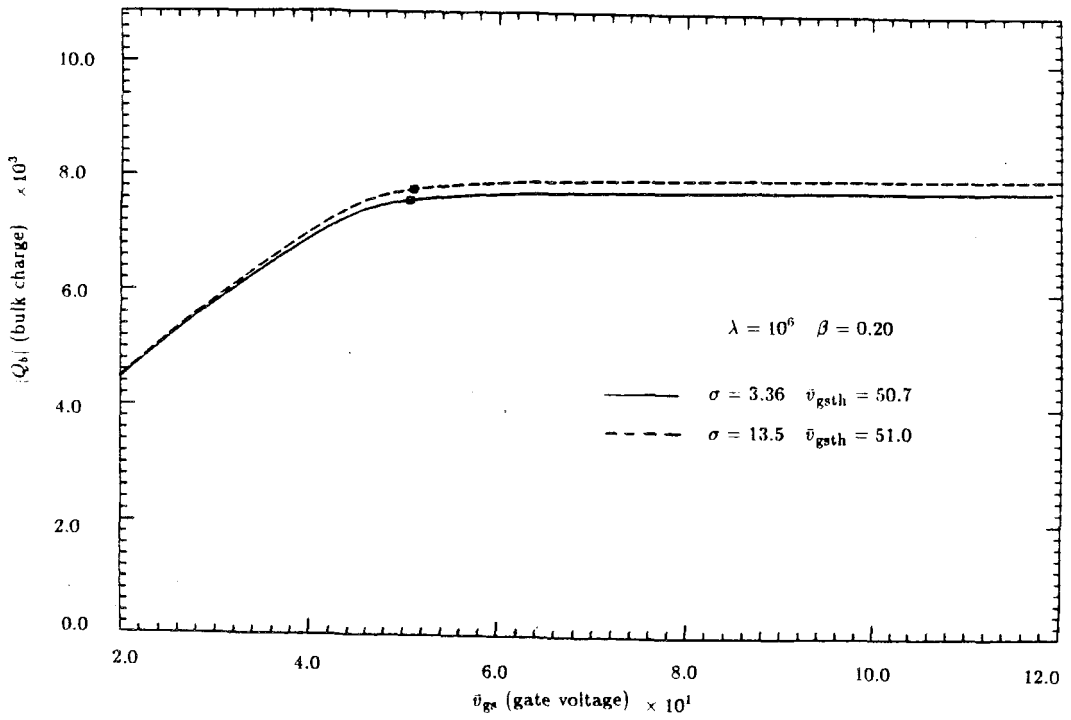

FIGURE 2.7. Bulk Charge as a Function of the Gate Voltage

is dominated by the fixed bulk charge due to the impurities. However, since the depletion width is insensitive to gate voltages above threshold, the bulk charge increases only slightly in strong inversion. The bulk charge as a function of the gate voltage in both weak and strong inversion is displayed in Figure 2.7. We now compute the mobile charge asymptotically.

Since the dominant contribution to the mobile charge arises from the interface where the total charge does not vanish, the amount of mobile charge can be computed asymptotically using integration by parts. A two term expansion using ths method yields

$$Q_c \sim \frac{e^{w_s \ln \lambda}}{(\lambda \ln \lambda)^{1/2} w'(0)} \left(1 + \frac{1}{\ln \lambda} \frac{w''(0)}{w'(0)^2}\right). \tag{2.35}$$

Using the leading order asymptotic expansion of the potential in weak inversion under variable doping gives

$$Q_c \sim \frac{e^{w_s \ln \lambda}}{(\lambda \ln \lambda)^{1/2}\, a} \left(1 + \frac{1}{a^2 \ln \lambda}\right) \tag{2.36}$$

where $a = -(\beta x_d + (1-\beta) I_1(x_d))$ and the depletion width x_d is determined from (2.27). As a remark, we recall that with constant doping the infinite order expan-

sion in $\ln\lambda$ provided $a = -\sqrt{2(1 + w_s - 1/\ln\lambda)}$. It is to be noticed that in weak inversion the amount of mobile charge is subdominant as $\lambda \to \infty$ to the amount of fixed bulk charge.

In strong inversion, the dominant contribution to the integral defining the mobile charge also arises from the interface. However, using the asymptotic potential in strong inversion, w_{i0}, we find

$$\frac{w_{i0}''(0)}{\ln\lambda w_{i0}'(0)^2} = \frac{1}{2(1+\alpha^2)} = O(1) \quad \text{for } \alpha \ll 1\,,$$

which shows that Laplace's method is not directly applicable in strong inversion. The failure of Laplace's method is a result of the strong dependence of the slope of w_{i0} on λ and the near logarithmic singularity of the inversion layer potential at $\tilde{x} = -\sqrt{2}\gamma/\alpha_0 \ll 1$ just outside the domain. To remedy this situation, we evaluate the integral directly by integrating over the inversion layer from the interface to infinity in the stretched variable $\tilde{x}$. Using the inversion layer potential and changing to the stretched variable $\tilde{x}$ in this layer, the mobile charge integral becomes

$$Q_c \sim -(\lambda\ln\lambda)^{1/2}\,\alpha_0^2 \int_0^\infty \frac{1}{\sinh^2(\alpha_0\tilde{x}/\sqrt{2}+\gamma)} d\tilde{x}\,.$$

A direct computation of this integral provides

$$Q_c \sim -\sqrt{2}\,e^{w_s\ln\lambda/2}\left(\sqrt{1+\alpha^2}-\alpha\right)\,, \tag{2.37}$$

where α and α_0 are given by (2.13) and (2.30a,b), respectively. To show that this expression reduces for constant doping to the leading order term in (2.36) as $w_s \to 1$, we notice that in this limit $\alpha \to \sqrt{2}(\ln\lambda)^{1/2}$ so that the expansion

$$(1+\alpha^2)^{1/2} - \alpha \approx 1/2\alpha \quad \text{for } \alpha \gg 1$$

applies. Using this expansion in (2.37) we find $Q_c \sim -\frac{1}{2}(\lambda/\ln\lambda)^{1/2}$ which is seen to be the leading order term of (2.36) when $w_s = 1$. A similar transition holds for the variable doping case.

In the limiting case of very strong inversion, in which α is transcendentally small, the total charge given by (2.32) and (2.33) in constant and variable doping, respectively, is seen to be dominated by the mobile charge. The asymptotic mobile charge as a function of the gate voltage for various doping parameters is shown in Figure 2.8.

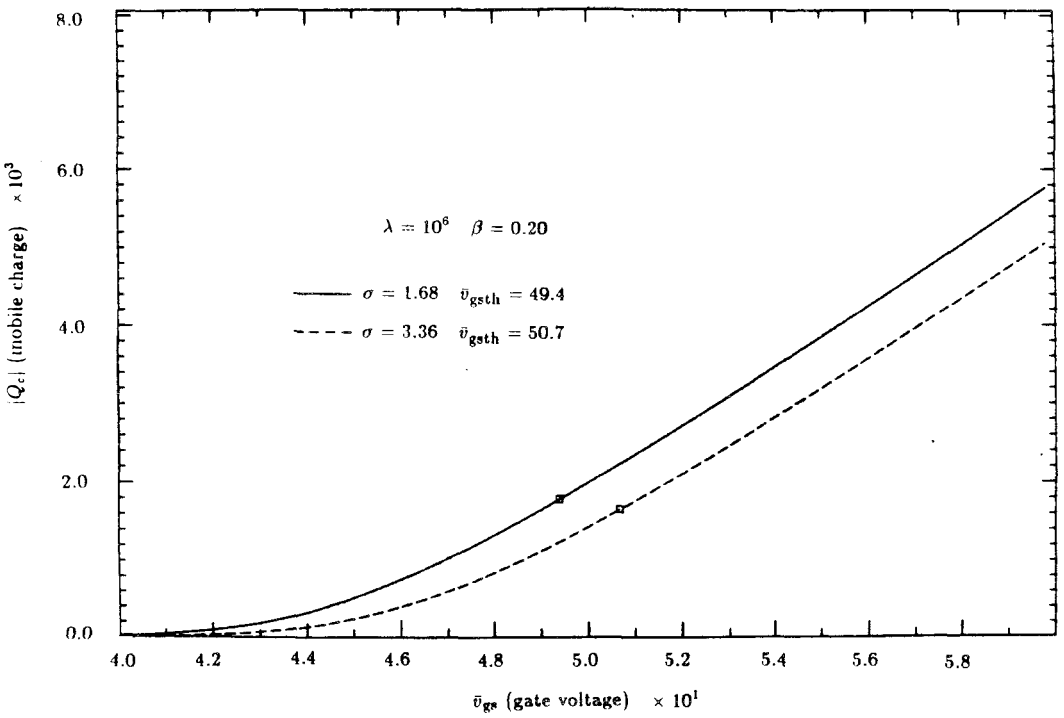

FIGURE 2.8. Mobile Charge as a Function of the Gate Voltage

CHAPTER 3

Asymptotic Theory Of The One-Dimensional Equilibrium Potential: II

The built-in channel device is formed by implanting both donors and acceptors into the substrate resulting in a channel region away from the interface in some bias regimes. The built-in channel device can be desirable since the mobility of the carriers near the interface for the enhancement device can be degraded due to surface effects that reduce the conductivity of the channel. In this chapter, we shall assume that the doping profile is discontinuous and shall neglect the normally thin transition layer between the donor and acceptor regions. The point of discontinuity in the implant profile, x_0, is termed the junction depth, as an abrupt n-p junction will be formed in the vicinity of x_0. Eventually in Chapter 4, we shall take into account the finite width of the transition layer and remark on its effect on the validity of the asymptotic expansion for the potential in the vicinity of the juncton. For simplicity, the doping profile is assumed to be anti-symmetric about the junction depth. Therefore, the scaled doping profile can be written as

$$d(x) = f(x - x_0) = \begin{cases} -1 & \text{for} \quad x < x_0 \qquad \text{donors,} \\ 1 & \text{for} \quad x > x_0 \qquad \text{acceptors.} \end{cases}$$

In this chapter, the asymptotic potential will be constructed in the entire (w_s, x_0) control plane. In addition, the mobile and total charge needed to determine the device characteristics will be computed asymptotically.

3.1 Built-In Channel Device – Asymptotic Potential

The built-in channel device is known to operate in many different bias regimes depending on the gate bias and the junction depth. The primary bias regimes are designated partial depletion, full depletion, accumulation and inversion. In the literature there appears to be no established terminology for these different gate bias regimes.

Since many of the layers for the built-in channel device are also found in the enhancement device, we shall only give a brief discussion of the derivation

of the asymptotic potential for each case. Throughout the analysis we assume that $x_0 \gg \ln(\ln\lambda)/\ln\lambda$. The asymptotic potential is first constructed for partial depletion.

Partial Depletion Mode - Symmetric Abrupt Junction. The partial depletion mode is characterized by the formation of a channel in the middle of the device with a depletion layer near the interface. A plot of the leading order asymptotic potential in this case is shown in Figure 3.1. In this regime, the asymptotic potential exhibits a depletion layer near the interface followed by a channel region and then an n-p junction. A transition layer identical to the enhancement device connects the depletion layers of the n-p junction to both the channel region and the bulk. Without further elaboration, the asymptotic potential in the various regions can easily be constructed. Referring to Figure 3.1, and using the infinite order $\ln\lambda$ expansion for the depletion layers, as in weak inversion for the enhancement device , we find

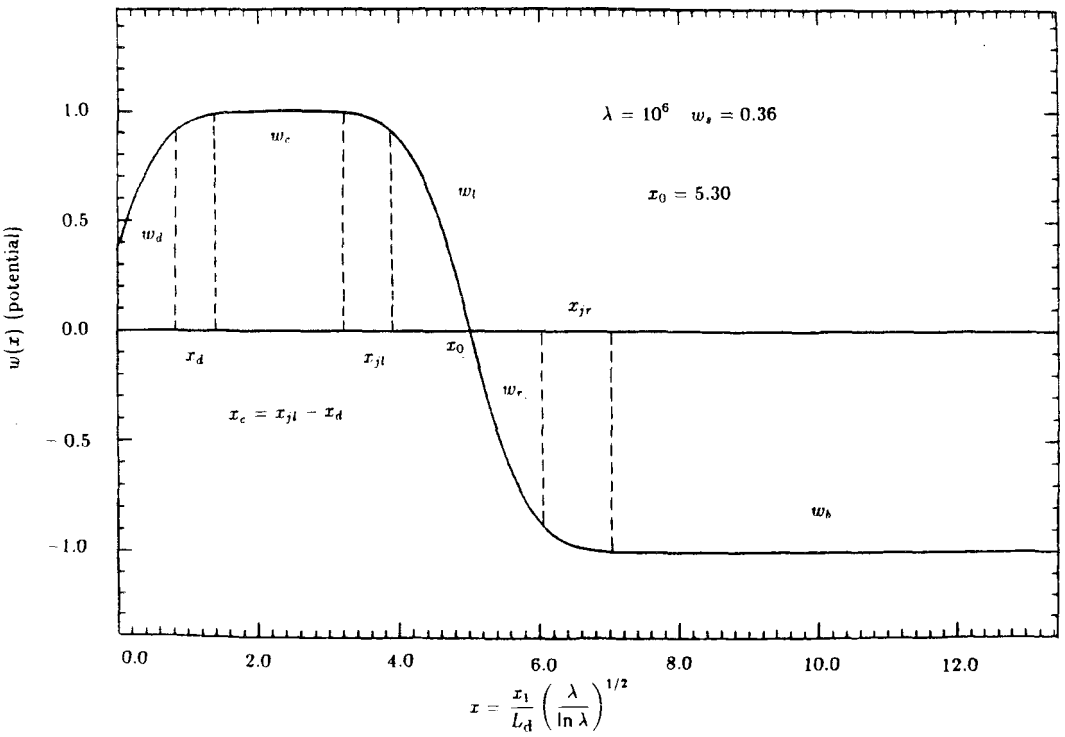

FIGURE 3.1. Asymptotic Potential in Partial Depletion Mode

$$w_d(x) = -\frac{1}{2}x^2 + \sqrt{2}(1 - w_s - 1/\ln\lambda)^{1/2}x + w_s \; ; \; 0 \le x \le x_d - O((\ln\lambda)^{-1/2}) \,,$$

$$w_c(x) = 1 \; ; \; x_d + O((\ln\lambda)^{-1/2}) \le x \le x_{jl} - O((\ln\lambda)^{-1/2}) \,,$$

$$w_l(x) = -\frac{1}{2}(x - x_0)^2 - \sqrt{2}(1 - 1/\ln\lambda)^{1/2}(x - x_0) \; ; \; x_{jl} + O((\ln\lambda)^{-1/2}) \le x \le x_0 \,,$$

$$w_r(x) = \frac{1}{2}(x - x_0)^2 - \sqrt{2}(1 - 1/\ln\lambda)^{1/2}(x - x_0) \; ; \; x_0 \le x \le x_{jr} - O((\ln\lambda)^{-1/2}) \,,$$

$$w_b(x) = -1 \; ; \; x_{jr} + O((\ln\lambda)^{-1/2}) \le x < \infty \,.$$

Between each of the depletion layers and the channel and bulk layers there is a transition layer, h, that ensures the continuity of the second derivative of the potential. As usual, the depletion widths are also found in the matching process. They are

$$x_d = \sqrt{2}(1 - w_s - 1/\ln\lambda)^{1/2} - \frac{c}{\sqrt{2}}(\ln\lambda)^{-1/2} \,,$$

$$x_{jl} = x_0 - \sqrt{2}(1 - 1/\ln\lambda)^{1/2} + \frac{c}{\sqrt{2}}(\ln\lambda)^{-1/2} \,,$$

$$x_{jr} = x_0 + \sqrt{2}(1 - 1/\ln\lambda)^{1/2} - \frac{c}{\sqrt{2}}(\ln\lambda)^{-1/2} \,,$$

where $c \approx .81785$ is the integral defined in Chapter 2.

For partial depletion, the infinite order $\ln\lambda$ expansion is essential for the depletion layer near the interface since the expansion breaks down near inversion when $w_s = 1 - O(1/\ln\lambda)$. This breakdown of the depletion layer expansion is analogous to the near flatband situation for the enhancement device.

In the analysis we have assumed that the channel width $x_c \equiv x_{jl} - x_d$ is nonnegative. Using the expression for the channel width, we notice that if $x_0 \ge 2 + \sqrt{2}$, there is a channel region for all surface potentials giving rise to a depletion layer near the interface. Alternatively, for $x_0 \le \sqrt{2}$, there is no channel region for any surface potential in the range $-1 \le w_s \le 1$. For junction depths intermediate to these two limiting cases, the surface potential must satisfy the inequality $1 - (x_0 - \sqrt{2})^2/2 \le w_s \le 1$ for there to be a channel region. It is noted that if the upper limit on the surface potential is exceeded the n-carriers cannot be neglected near the interface, and we have an inversion layer.

Furthermore, when $x_c = O((\ln\lambda)^{-1/2})$ the two transition layers merge into a new transition layer, requiring a special analysis. Before considering this case we

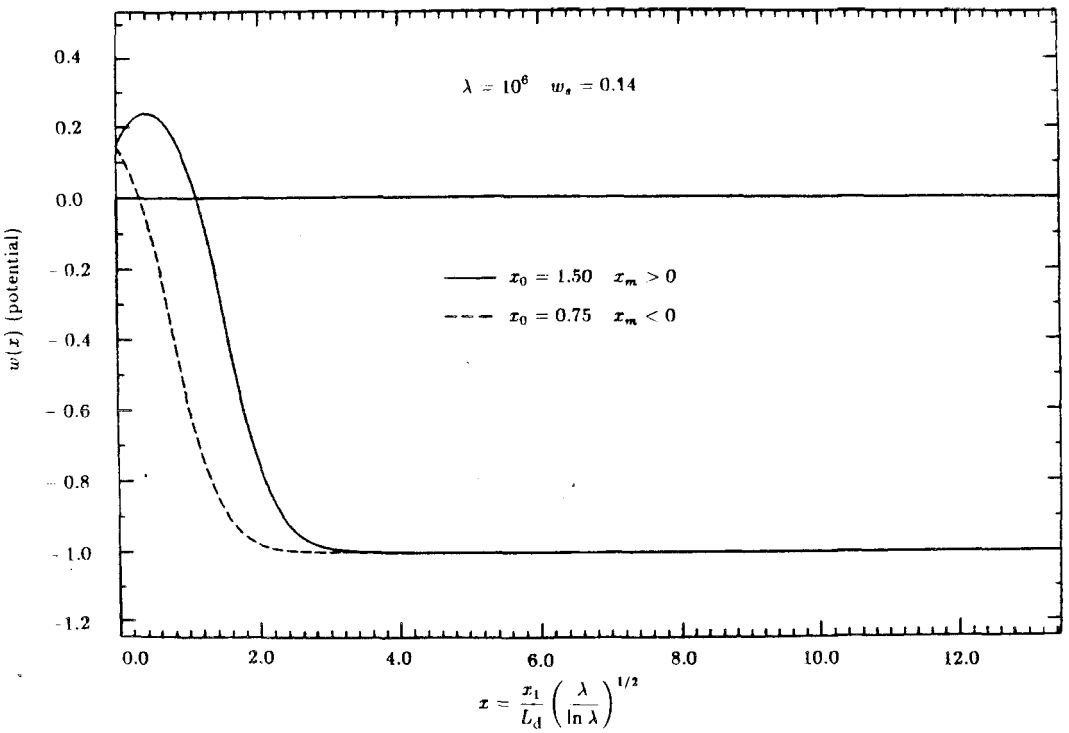

FIGURE 3.2. Asymptotic Potential in Full Depletion for Various x_0

analyze the simpler situation in which there is no channel formation.

Full Depletion Mode - Symmetric Abrupt Junction. This regime of the built-in channel device corresponds to the weak inversion case for the enhancement device since only a small leakage current will flow between the source and drain upon application of a bias.

In the full depletion mode there is no channel present, and the asymptotic expansion for the potential is constructed by patching two depletion layer solutions for C^1 continuity at the junction depth. A transition layer is needed to match the depletion layer furthest from the interface to the bulk. A plot of the leading order asymptotic potential for two particular junction depths is shown in Figure 3.2.

The leading order asymptotic potential in the depletion layers is

$$w_l(x) = -\frac{1}{2}x^2 + x_m x + w_s \qquad \text{for } x < x_0\,,$$

$$w_r(x) = \frac{1}{2}x^2 + (x_m - 2x_0)x + (w_s + x_0^2) \qquad \text{for } x_0 < x < x_j - O((\ln\lambda)^{-1/2})\,,$$

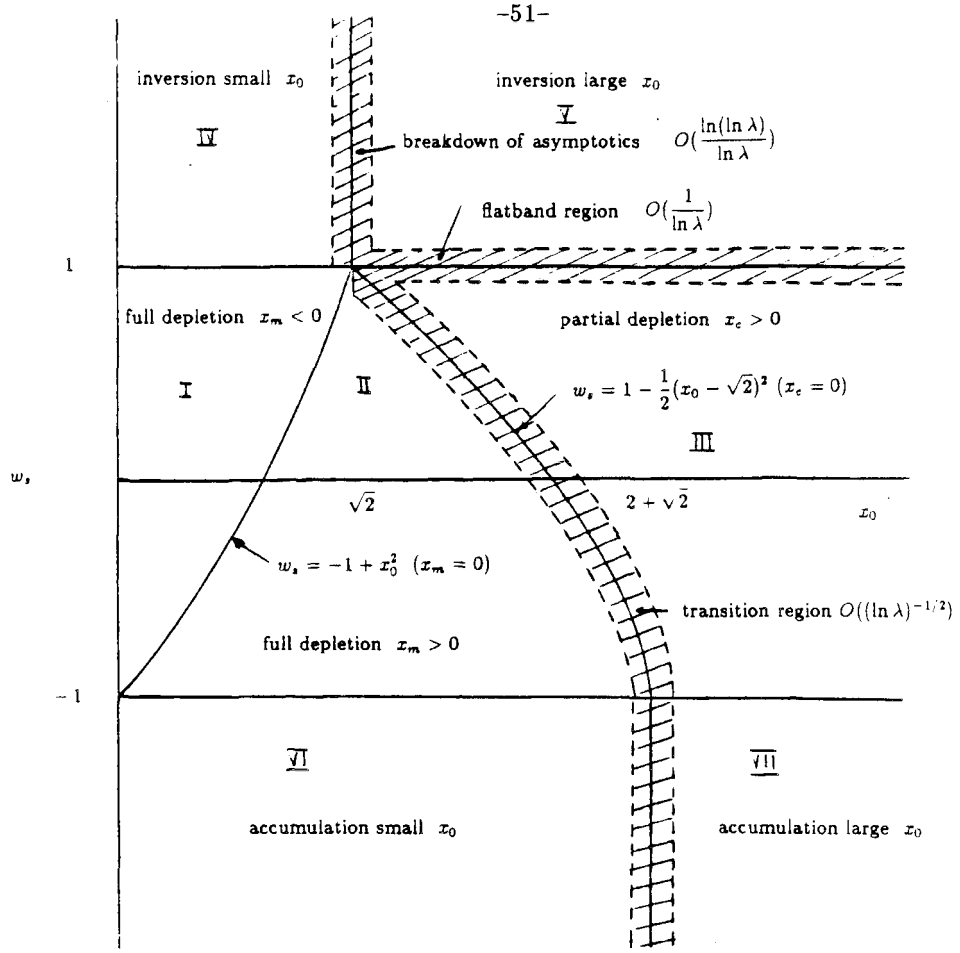

FIGURE 3.3. Surface Potential, Junction Depth Plane

where

$$x_m = -\sqrt{2}(1 + w_s + x_0^2 - 1/\ln\lambda)^{1/2} + 2x_0 \text{ and } x_j = 2x_0 - x_m - \frac{c}{\sqrt{2}}(\ln\lambda)^{-1/2}.$$

Notice that if $x_0 \leq \sqrt{2}$, the device is in full depletion for all surface potentials in the range $-1 \leq w_s \leq 1$. Alternatively, if the junction depth satisfies $x_0 \geq 2 + \sqrt{2}$ the device does not operate in the full depletion mode for any surface potential giving rise to depletion layer near the interface. It is to be noted from Figure 3.2 that the sign of x_m determines where the dominant contribution to the mobile charge arises. Before examining other regimes, we display our results graphically in Figure 3.3 in the surface potential-junction depth parameter plane. The boundaries between inversion, accumulation, full depletion, and partial depletion are labelled in the figure. In addition, for future reference, the case of full depletion is divided into two subcases depending on whether the dominant contribution to the mobile charge

arises from the interface or from some interior location. We now consider the more complicated case when $x_c = O((\ln\lambda)^{-1/2})$ where a new type of transition layer is needed to match the two depletion layers.

Transition Between Partial And Full Depletion. In this regime, we examine closely the region in the (w_s, x_0) parameter plane where the channel width x_c is small. Specifically, we define the stretching $z = G(w_s, x_0)(\ln\lambda)^{1/2}$ where $G(w_s, x_0) \equiv w_s - 1 + (x_0 - \sqrt{2})^2/2$, and $G(w_s, x_0) = 0$ represents the curve $x_c = 0$ in the (w_s, x_0) parameter plane. We will now construct the asymptotic potential for arbitrary z and x_0 where $z = O(1)$.

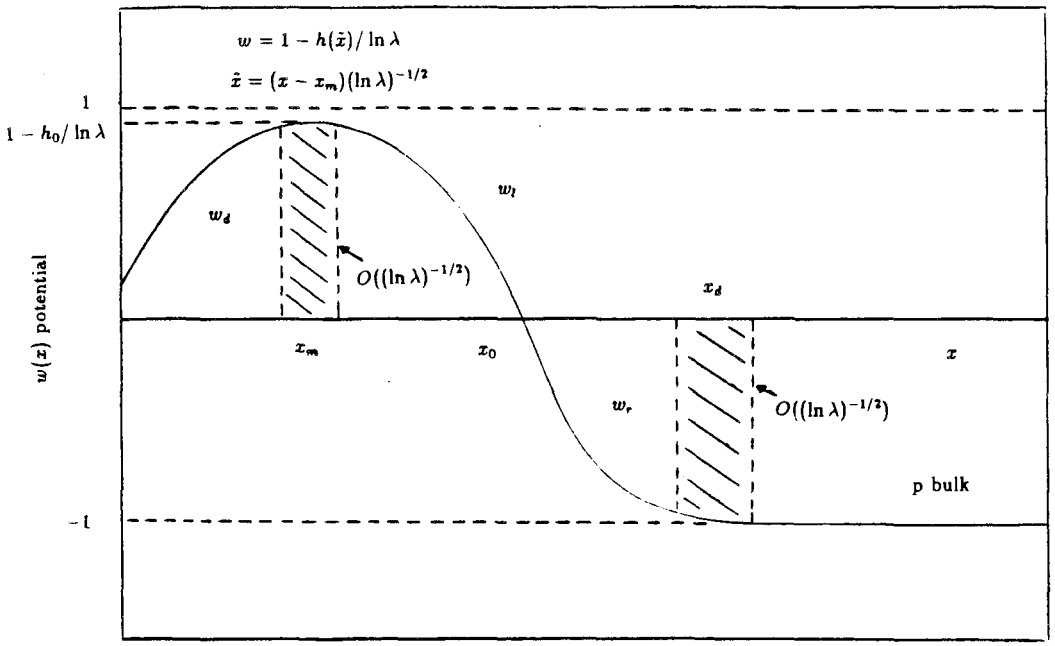

FIGURE 3.4. Asymptotic Potential for Transition Between Partial and Full Depletion

Referring to the schematic diagram in Figure 3.4, to construct the asymptotic potential in the vicinity of the curve $G(w_s, x_0) = 0$ we begin by defining the transition layer variables near the channel by

$$w_t(x) = 1 - h(\tilde{x})/\ln\lambda \quad \text{and} \quad \tilde{x} = (x - x_m)(\ln\lambda)^{-1/2},$$

resulting in the familiar transition layer equation $h'' = 1 - e^{-h}$. Instead of defining x_m to be the location where $h = 1$, as has previously been done, it is more

convenient to define x_m to be the location where $h'(0) = 0$. Then, setting $h(0) = h_0 > 0$ to be the unknown minimum value of h, we obtain

$$h' = \sqrt{2}\,\mathrm{sign}\,(\tilde{x})(h + e^{-h} - h_0 - e^{-h_0})^{1/2}.$$

Varying $h_0 > 0$ where $h_0 = O(1)$ will be seen below to be equivalent to varying $z = O(1)$ with $z > 0$ in the neighbourhood of $G(w_s, x_0) = 0$.

This transition layer solution must match to depletion layer solutions on either side of $x = x_m$. Defining as usual an intermediate variable x_η and setting $\tilde{x} = x_\eta \eta (\ln \lambda)^{1/2}$, the expansion of the transition layer equation as $|\tilde{x}| \to \infty$ becomes

$$w_t \sim 1 - (\frac{c_{h0}^2}{4} + h_0 + e^{-h_0})(\ln \lambda)^{-1} - \frac{x_\eta \eta\, c_{h0}}{\sqrt{2}}(\ln \lambda)^{-1/2}\,\mathrm{sign}(\tilde{x}) - \frac{1}{2}x_\eta^2 \eta^2,$$

where c_{h0} is given by

$$c_{h0} = -\int_{h_0}^{h_0 + e^{-h_0}} (y + e^{-y} - h_0 - e^{-h_0})^{-1/2}\, dy + \int_{h_0 + e^{-h_0}}^{\infty} \left[(y - h_0 - e^{-h_0})^{-1/2} - (y + e^{-y} - h_0 - e^{-h_0})^{-1/2}\right] dy.$$

A simple change of variables in the integrand results in the less cumbersome expression

$$c_{h0} = -e^{-h_0/2} \int_0^1 (y - 1 + \exp(-ye^{-h_0}))^{-1/2}\, dy + \int_0^{\infty} \left[y^{-1/2} - (y + \exp(-y - h_0 - e^{-h_0}))^{-1/2}\right] dy.$$

The asymptotics of this expression for $h_0 \gg 1$ and $h_0 \to 0$, which are needed later, are $c_{h0} \sim -2e^{-h_0/2}$ for $h_0 \gg 1$ and $c_{h0} \sim -2h_0^{-1/2}$ for $h_0 \to 0$.

Referring to Figure 3.4, the depletion layer potentials are given by

$$w(x) \sim \begin{cases} w_d = -\frac{1}{2}x^2 + ax + w_s & \text{for} \quad 0 < x < x_m - O((\ln \lambda)^{-1/2}), \\ w_l = -\frac{1}{2}x^2 + a_l x + b_l & \text{for} \quad x_m + O((\ln \lambda)^{-1/2}) < x < x_0, \\ w_r = \frac{1}{2}x^2 + (a_l - 2x_0)x + b_l + x_0^2 & \text{for} \quad x_0 < x < x_d - O((\ln \lambda)^{-1/2}). \end{cases}$$

Notice that the depletion layer potentials w_l and w_r have been patched for C^1 continuity at x_0. Matching w_d to w_t then gives

$$a^2/2 + w_s = 1 - (h_0 + e^{-h_0})(\ln \lambda)^{-1} \quad \text{and} \quad x_m = a - \frac{c_{h0}}{\sqrt{2}}(\ln \lambda)^{-1/2}. \qquad (3.1)$$

Similarly, matching w_l to w_t implies

$$a_l^2/2 + b_l = 1 - (h_0 + e^{-h_0})(\ln\lambda)^{-1} \quad \text{and} \quad x_m = a_l + \frac{c_{h0}}{\sqrt{2}}(\ln\lambda)^{-1/2}. \tag{3.2}$$

Finally, matching w_r to the p-type bulk gives

$$a_l - 2x_0 = -\sqrt{2}(b_l + x_0^2 + 1 - 1/\ln\lambda)^{1/2} \quad \text{and} \quad x_d = 2x_0 - a_l - \frac{c}{\sqrt{2}}(\ln\lambda)^{-1/2}, \tag{3.3}$$

where $c \approx .81785$. Equations (3.1),(3.2), and (3.3) are equations for a_l, b_l, x_m, a, and w_s as functions of x_0 and h_0 where h_0 measures the deviation from the curve $G(w_s, x_0) = 0$. Some algebraic manipulations provide

$$\begin{aligned}
a &= \sqrt{2}(1 - w_s - (h_0 + e^{-h_0})/\ln\lambda)^{1/2}, \\
a_l &= a - \frac{c_{h0}}{\sqrt{2}}(\ln\lambda)^{-1/2}, \\
b_l &= 1 - a_l^2/2 - (h_0 + e^{-h_0})(\ln\lambda)^{-1}, \\
w_s &= 1 - (x_0 - \sqrt{2})^2/2 - \sqrt{2}c_{h0}(x_0 - \sqrt{2})(\ln\lambda)^{-1/2} + O(1/\ln\lambda),
\end{aligned}$$

which are then easily solved in terms of h_0 and x_0. Defining $z = -\sqrt{2}c_{h0}(x_0 - \sqrt{2})$, and using $c_{h0} \in (-\infty, 0)$ for $h_0 > 0$, the above equation for w_s verifies that the potential has been computed in an $O((\ln\lambda)^{-1/2})$ neighbourhood of the curve $G(w_s, x_0) = 0$. The implicit expression for h_0 in terms of z shows why the asymptotic potential in the neighbourhood of $G(w_s, x_0) = 0$ is more conveniently parametrized by h_0 rather than z.

Finally, it is informative to consider the formal limits $h_0 \gg 1$ and $h_0 \to 0$ to reproduce the partial and full depletion regime results. In the limit $h_0 \gg 1$, the centre of the transition layer x_m is seen to coincide with the maximum value of the potential in the full depletion mode. In addition, we have $a_l \sim a$ and thus the two depletion layers w_d and w_l merge into a single depletion layer as in the previous bias regime. Alternatively for $h_0 \to 0$, the above expansion breaks down since $c_{h0} \to -\infty$. Therefore, in this formal limit, the partial depletion regime analysis is appropriate as the transition layer near the channel splits into two layers each of which must match to a bulk type layer.

We now consider the inversion regime characterized by a different dominant balance near the interface.

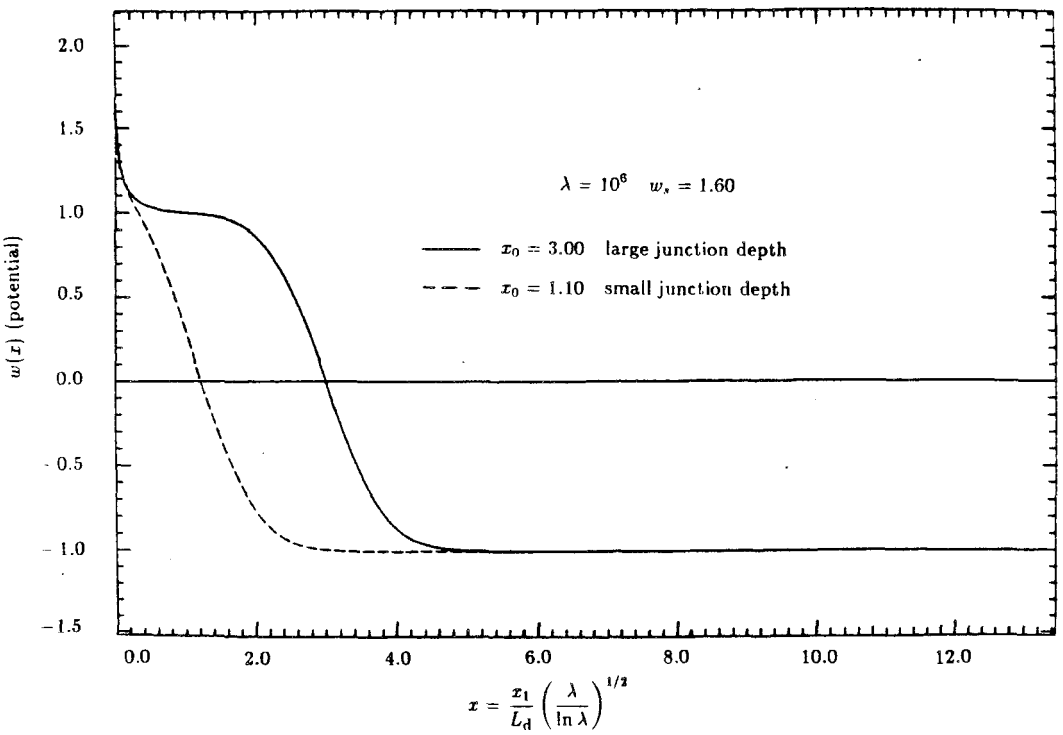

FIGURE 3.5. Asymptotic Potential in Inversion Mode for Various x_0

Inversion Mode - Symmetric Abrupt Junction. In the inversion mode, $w_s \geq 1$, there is an inversion layer present near the interface. In contrast to the enhancement device, this layer is to be matched either to a constant potential solution or a depletion layer depending on the location of the junction depth. A plot of the leading order asymptotic potential under inversion conditions is shown in Figure 3.5 for two junction depths. The critical value of the junction depth seperating the two subcases will be found in the analysis. From Figure 3.3, we anticipate that the critical junction depth is near $x_0 = \sqrt{2}$. This conjecture will be confirmed in the analysis.

We begin by assuming that x_0 is sufficiently small so that we can match the inversion layer near the interface to a depletion layer. The convexity of the depletion layer in this case is different than that considered in the enhancement device and will be seen to be the cause of the breakdown of the expansion for the potential when the junction depth approaches $\sqrt{2}$.

As in the inversion layer for the enhancement device, we consider stretched

variables defined by

$$\tilde{x} = \frac{x}{\nu(\lambda)} \qquad \text{and} \qquad w_i(\tilde{x}) = w(\tilde{x}\nu(\lambda)) = w_{i0}(\tilde{x},\lambda) + \sigma(\lambda) w_{i1}(\tilde{x},\lambda) + \cdots ,$$

where $\sigma(\lambda)$, $\nu(\lambda) \to 0$ as $\lambda \to \infty$.

Substituting this expansion into the full nonlinear Poisson equation then yields

$$\frac{1}{\nu^2(\lambda)}(w_{i0}'' + \sigma(\lambda) w_{i1}'' + \cdots) = \frac{2}{\lambda}\sinh\left((w_{i0} + \sigma(\lambda) w_{i1} + \cdots)\ln\lambda\right) - 1 .$$

From the study of the enhancement device, the appropriate boundary layer scalings in the inversion layer are $\sigma(\lambda) = 1/(\ln\lambda)^2$ and $\nu(\lambda) = 1/\ln\lambda$.

The solution of the leading order equation is then simply

$$w_{i0} = w_s - \frac{2}{\ln\lambda}\ln\left(\frac{1}{\alpha}\sinh(\alpha\sqrt{\frac{A}{2}}\tilde{x} + \gamma)\right), \tag{3.4}$$

where

$$A(\lambda) = \lambda^{w_s - 1}/\ln\lambda \qquad \text{and} \qquad \gamma = \sinh^{-1}(\alpha) .$$

The unknown constant, α, is to be found by matching.

Expanding the inversion layer potential in terms of an intermediate variable $\tilde{x} = x_\eta \eta \ln\lambda$ and using the asymptotics of w_{i1} as $\tilde{x} \to \infty$ gives

$$w \sim w_s + \frac{2}{\ln\lambda}\ln\left(\frac{2\alpha}{\alpha + \sqrt{\alpha^2+1}}\right) - \sqrt{\frac{2}{\ln\lambda}}\,\alpha\lambda^{(w_s-1)/2} x_\eta \eta - \frac{1}{2}x_\eta^2\eta^2 + \cdots . \tag{3.5}$$

In the depletion layer, the leading order asymptotic potential is given by patching two depletion layer solutions for C^1 continuity at the junction depth. We recall that the depletion layer solution furthest from the interface is matched to the bulk by a transition layer. In addition, from the study of the enhancement device, we must insert a switchback term K in the depletion layer expansion in order to match to the inversion layer. Therefore, the depletion layer expansion is assumed to have the form

$$w_l = -\frac{1}{2}x^2 + ax + 1 + K(\lambda, w_s, \alpha_0) \quad \text{for} \quad 0 \le x \le x_0 ,$$

$$w_r = \frac{1}{2}x^2 - x_j x + b \quad \text{for} \quad x_0 \le x \le x_d - O((\ln\lambda)^{-1/2}) .$$

Patching for C^1 continuity at x_0 and matching to the bulk to an infinite order in $\ln\lambda$ then determines the unknown matching parameters

$$\begin{aligned} x_j &= \sqrt{2}\left(2 + x_0^2 + K(\lambda, w_s, \alpha_0) - 1/\ln\lambda\right)^{1/2}, \\ b &= 1 + x_0^2 + K(\lambda, w_s, \alpha_0), \\ a &= 2x_0 - \sqrt{2}\left(2 + x_0^2 + K(\lambda, w_s, \alpha_0) - 1/\ln\lambda\right)^{1/2}, \\ x_d &= x_j - \frac{c}{\sqrt{2}}(\ln\lambda)^{-1/2}. \end{aligned}$$

It is to be noted that the above solution is indeed C^1 continuous at the junction depth.

Expanding the depletion layer potential w_l in terms of an intermediate variable x_η gives

$$w_l \sim 1 + K(\lambda, w_s, \alpha_0) + a x_\eta \eta - \frac{1}{2} x_\eta^2 \eta^2 . \tag{3.6}$$

Comparing the $O(\eta)$ terms in (3.6) and (3.5) we notice that to match we require

$$\alpha = \lambda^{(1-w_s)/2}\sqrt{\ln\lambda}\,\alpha_0 , \tag{3.7}$$

where $\alpha_0 = O(1)$ as $\lambda \to \infty$. Substituting the expression for α into the inversion layer expansion (3.5), we then find

$$w \sim 1 + \frac{\ln(\ln\lambda)}{\ln\lambda} + \frac{2}{\ln\lambda}\ln\left(\frac{2\alpha_0}{\alpha + \sqrt{\alpha^2+1}}\right) - \sqrt{2}\alpha_0 x_\eta \eta - \frac{1}{2}x_\eta^2\eta^2 + \cdots . \tag{3.8}$$

Finally, matching the inversion layer potential to the depletion layer determines $K(\lambda, w_s, \alpha_0)$ and α_0. We obtain

$$\alpha_0 = \left(2 + x_0^2 + K(\lambda, w_s, \alpha_0) - 1/\ln\lambda\right)^{1/2} - \sqrt{2}x_0 , \tag{3.9a}$$

$$K(\lambda, w_s, \alpha_0) = \frac{\ln(\ln\lambda)}{\ln\lambda} + \frac{2}{\ln\lambda}\left[\ln(2\alpha_0) - \sinh^{-1}(\alpha)\right] , \tag{3.9b}$$

which is a weakly nonlinear equation in the unknown matching parameter α_0. Once α_0 is known, the other matching parameters x_j, x_d, a and b are determined. We now determine the range of validity of this expansion and show how the expansion breaks down.

With the matching parameters now determined, the inversion layer potential becomes

$$w_{i0} = w_s - \frac{2}{\ln \lambda} \ln \left(\frac{1}{\alpha} \sinh(\frac{\alpha_0}{\sqrt{2}} \tilde{x} + \gamma) \right),$$

and thus we notice that the expansion will break down if α_0 approaches zero. Specifically, from considering the assumption needed for the large argument expansion of the inversion layer potential, the expansion is no longer valid when $\alpha_0 \ln \lambda \ll 1$, which from (3.9$a$) implies $x_0 = \sqrt{2} - O(\ln(\ln \lambda)/\ln \lambda)$. This vertical line is shown in the surface potential-junction depth plane. The expansion is valid for junction depths less than this critical value.

For $x_0 \geq \sqrt{2}$, the construction of the inversion layer potential must be modified. In this case, the inversion layer solution must be matched to a constant bulk potential. The analysis of the matching for this case is similar to the enhancement device in the accumulation regime using the ln(sec) solution for the inversion layer potential. Therefore, the analysis is not repeated here.

We remark that if both $x_0 > \sqrt{2}$ and the surface potential can be expanded in the series $w_s = 1 + w_{s1}/\ln \lambda$, the depletion approximation in the partial depletion mode is not strictly valid since the contribution to the space charge density of the mobile n-carriers cannot be neglected. In this case, a transition layer is valid all the way up to the interface.

Accumulation Mode - Symmetric Abrupt Junction. In the accumulation mode, $w_s \leq -1$, the space charge density is dominated by the p-carriers near the interface. As anticipated from Figure 3.3, the structure of the asymptotic potential is different on either side of the critical value of $x_0 = 2 + \sqrt{2}$.

For $x_0 > 2 + \sqrt{2}$, the structure of the asymptotic potential for $x < 2$ is an inversion layer for holes followed by a depletion layer that matches onto an n-type bulk solution. The layers needed are identical to the inversion regime for the enhancement device (simply using $w \rightarrow -w$) and can easily be constructed. The remaining layers for $x \geq 2$ are similar to the partial depletion regime.

For $x_0 = 2 + \sqrt{2} + O((\ln \lambda)^{-1/2})$, the two depletion layers near the channel merge into a layer similar to that needed to bridge the full and partial depletion regimes. The analysis for this case will also not be repeated.

We shall only briefy describe the construction of the asymptotic potential for the case $x_0 < 2+\sqrt{2}$ where the layer structure is slightly more complicated.

With the same scalings as in the previous section, the leading order solution in the p-type inversion layer is simply

$$w_{i0}(\tilde{x}) = -1 - \frac{1}{\ln\lambda}\left[\ln(\ln\lambda) + 2\ln(\alpha_0)\right] + \frac{2}{\ln\lambda}\ln\left(\sinh(\frac{\alpha_0}{\sqrt{2}}\tilde{x}+\gamma)\right),$$

where $\sinh(\gamma) = \alpha \equiv \alpha_0(\ln\lambda)^{1/2}\lambda^{(1+w_s)/2}$. Expanding out of the inversion layer and going to second order gives as usual

$$w_i \sim -1 - K + \sqrt{2}\alpha_0 x_\eta \eta - \frac{1}{2}x_\eta^2\eta^2 + \cdots,$$

where K is defined by (3.9*b*).

In the depletion layers, we have

$$w_d(x) = \begin{cases} -\frac{1}{2}x^2 + a_l x - 1 - K & \text{for} \quad O((\ln\lambda)^{-1}) < x < x_0, \\ \frac{1}{2}x^2 + a_r x + b_r & \text{for} \quad x_0 < x < x_d + O((\ln\lambda)^{-1/2}). \end{cases}$$

The equations for the matching constants are derived by patching the depletion layers for C^1 continuity at x_0 and by matching to the p-type bulk. Some algebra provides

$$\begin{aligned} a_r &= -\sqrt{2}(x_0^2 - K - 1/\ln\lambda)^{1/2}, \\ a_l &= 2x_0 - \sqrt{2}(x_0^2 - K - 1/\ln\lambda)^{1/2}, \\ b_r &= -1 - K + x_0^2, \\ x_d &= \sqrt{2}(x_0^2 - K - 1/\ln\lambda)^{1/2} - \frac{c}{\sqrt{2}}(\ln\lambda)^{-1/2}. \end{aligned}$$

Finally, matching the inversion layer potential to the depletion layer determines α_0, $K(\lambda, w_s, \alpha_0)$ and thus the other matching parameters. The equation for α_0 is

$$\alpha_0 = \sqrt{2}x_0 - (x_0^2 - K - 1/\ln\lambda)^{1/2}.$$

Unlike the inversion mode solution in the previous section, this equation for α_0 always has a solution as x_0 is varied, provided that $x_0 \gg \ln(\ln\lambda)/\ln\lambda$.

Finally, we remark that the region near $x_0 = \sqrt{2}$ and $w_s = 1$, where several of the boundaries between the various regimes intersect, appears to require a higher

order boundary layer approximation to fully resolve. This analysis seems to be quite difficult and is not presented here.

We now invert the relationship for $w_s = w_s(\bar{v}_{gs})$ and construct the asymptotic mobile charge in the entire (w_s, x_0) control plane.

3.2 Computation Of The Total And Mobile Charge

Using the definition of the total charge as predicted by the one-dimensional theory, the mixed boundary condition on the interface becomes

$$F(w_s, \bar{v}_{gs}) \equiv (w_s + 1)\,\ln\lambda - \frac{Q_s(w_s)}{c_{ox}} - \bar{v}_{gs} = 0\,. \tag{3.10}$$

Once again, for a specified input gate voltage, (3.10) is an implicit relationship, for the surface potential that must be solved numerically. To invert this relationship it is necessary that the total charge be calculated as a function of the surface potential in all the bias regimes. In all the calculations, the asymptotic potential constructed in the various regimes is used.

Evaluating the derivative of the asymptotic potential at the origin, we obtain the following expressions for the total charge in the various regions of the (w_s, x_0) plane:

$$Q_s = (2\lambda\,\ln\lambda)^{1/2}(1 - w_s - 1/\ln\lambda)^{1/2} \quad \text{in region III},$$

$$Q_s = (\lambda\,\ln\lambda)^{1/2}(2x_0 - \sqrt{2}(1 + w_s + x_0^2 - 1/\ln\lambda)^{1/2}) \quad \text{in regions I and II},$$

$$Q_s = -(2\lambda\,\ln\lambda)^{1/2}\left(\frac{1}{\lambda\ln\lambda}e^{w_s\ln\lambda} - w_s + (1 - \frac{1}{\ln\lambda})\right)^{1/2} \quad \text{in region V},$$

$$Q_s = -\sqrt{2}(1+\alpha^2)^{1/2}\,e^{w_s\ln\lambda/2} \quad \text{in region IV},$$

where α and α_0 are given by by (3.7) and (3.9a), respectively. A similar calculation can be done for the two accumulation regimes. In all cases, the total charge agrees at least asymptotically across the boundaries between the various regimes.

Using these expressions for Q_s, the surface potential is then computed for given input gate voltage by applying Newton's method to (3.10). A plot of the gate voltage as a function of the surface potential for several x_0 is shown in Figure 3.6. By solving numerically for the surface potential in terms of the gate voltage, the (w_s, x_0) plane can easily be mapped to the $(\bar{v}_{gs}, x_0)$ plane for device design purposes.

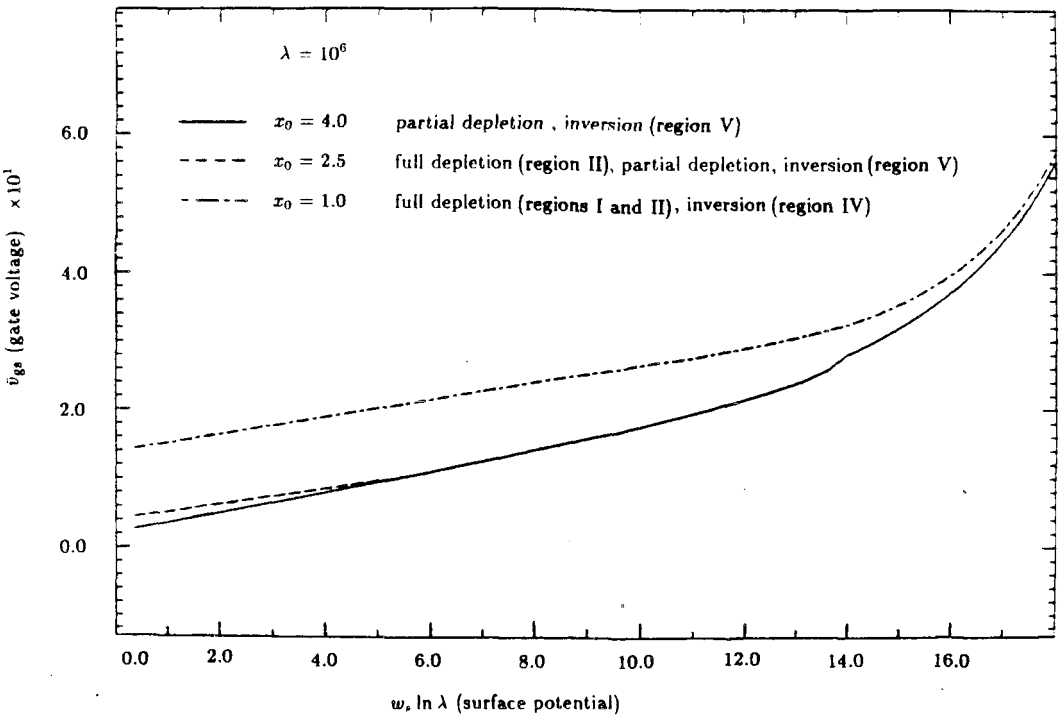

FIGURE 3.6. Surface Potential Versus Gate Voltage for Several x_0

As in the case of the enhancement device, we now compute asymptotically the amount of mobile charge available for current conduction. This computation is needed to derive device characteristics under non-equilibrium conditions. This calculation requires some care since the dominant contribution to the integral defining the mobile charge may arise from the interface or from some interior location depending on the gate bias regime.

We recall that the amount of mobile charge available for current conduction is given by

$$Q_c = -\left(\frac{\ln \lambda}{\lambda}\right)^{1/2} \int_0^{x_k} e^{w \ln \lambda}\, dx\,,$$

where x_k denotes the position where the depletion layer furthest from the interface is matched to the p-bulk. We now compute this integral asymptotically as $\lambda \to \infty$ by using the leading order asymptotic potential in the various gate bias regimes. We begin with full depletion.

In full depletion, the dominant contribution arises from $\max\{0, x_m\}$ where $x_m = 2x_0 - \sqrt{2}(1 + w_s + x_0^2 - 1 \ln \lambda)^{1/2}$. In region I, the dominant contribution arises from the interface; whereas in region II, the dominant contribution arises

from the interior maximum. To obtain device characteristics that behave uniformly as $\bar{v}_{gs}$ and $\bar{v}_{ds}$ are varied, the asymptotic expression for the mobile charge must be made uniformly valid across the boundary between regions I and II in the (w_s, x_0) parameter plane.

Using the leading order asymptotic potential w_l and w_r in full depletion, the uniform expression for the mobile charge in regions I and II is simply

$$Q_c \sim -\left(\frac{\pi}{2\lambda}\right)^{1/2} e^{(w_s + x_m^2/2)\ln\lambda} \left[1 + \mathrm{erf}(x_m(\ln\lambda/2)^{1/2})\right] . \tag{3.11}$$

It is informative to further simplify this expression in the two full depletion regimes in the (w_s, x_0) plane. In region II, the large positive argument expansion of the error function applies, and the mobile charge reduces to

$$Q_c \sim -\left(\frac{2\pi}{\lambda}\right)^{1/2} e^{(w_s + x_m^2/2)\ln\lambda} . \tag{3.12}$$

Similarly, in region I, the large negative argument expansion of the error function applies, and we obtain

$$Q_c \sim -\frac{1}{\sqrt{\lambda \ln\lambda}} \frac{e^{w_s \ln\lambda}}{|x_m|} \left(1 - \frac{1}{x_m^2 \ln\lambda}\right) .$$

This is the result that would have been obtained using a two term expansion from integrating by parts. The error function in the expression for the mobile charge is needed in the thin region near $x_m = 0$ of order $O((\ln\lambda)^{-1/2})$ and ensures a smooth transition between the behaviors on either side of the boundary.

In the accumulation mode for small x_0 (region VI), the asymptotic mobile charge for $|w_s| \gg 1 + \ln(\ln\lambda)/\ln\lambda$ with $w_s < 0$ is simply

$$Q_c \sim -\left(\frac{\pi}{2\lambda}\right)^{1/2} (\lambda \ln\lambda)^{-1} e^{a_l^2/2 \ln\lambda} \left[1 + \mathrm{erf}(a_l(\ln\lambda/2)^{1/2})\right] , \tag{3.13}$$

where $a_l \sim 2x_0 - \sqrt{2}(x_0^2 - \ln(\ln\lambda)/\ln\lambda - 1 \ln\lambda)^{1/2}$. This expression agrees with the full depletion expression (3.11) at $w_s = -1 - \ln(\ln\lambda)/\ln\lambda$.

In partial depletion, the dominant contribution to the mobile charge integral arises from the channel region. Referring to the notation of Figure 3.1 and splitting

the range of the integrand, we have

$$Q_c = -\left(\frac{\ln\lambda}{\lambda}\right)^{1/2}\left[\int_0^{x_d} e^{w\ln\lambda}\,dx + \int_{x_d}^{x_{jl}} e^{w\ln\lambda}\,dx + \int_{x_{jl}}^{x_k} e^{w\ln\lambda}\,dx\right].$$

Each of these integrals can now be evaluated asymptotically using the asymptotic potential in partial depletion. The integrals I_1 and I_3 below are evaluated using the depletion layer potentials. A routine application of Laplace's method provides:

$$I_1 \equiv \int_0^{x_d} e^{w\ln\lambda}\,dx \sim \lambda(\ln\lambda)^{-1/2}(\pi/2)^{1/2}\,\mathrm{erf}(x_d(\ln\lambda/2)^{1/2}),$$

$$I_2 \equiv \int_{x_d}^{x_{jl}} e^{w\ln\lambda}\,dx \sim \lambda(x_{jl}-x_d),$$

$$I_3 \equiv \int_{x_{jl}}^{x_k} e^{w\ln\lambda}\,dx \sim \lambda(\ln\lambda)^{-1/2}(\pi/2)^{1/2},$$

so that

$$Q_c \sim -(\lambda\ln\lambda)^{1/2}(x_{jl}-x_d) - (\frac{\pi\lambda}{2})^{1/2}\left[1+\mathrm{erf}(x_d(\ln\lambda/2)^{1/2})\right], \qquad (3.14)$$

where

$$x_{jl} \sim x_0 - \sqrt{2}(1-1/\ln\lambda)^{1/2} \quad \text{and} \quad x_d \sim \sqrt{2}(1-w_s-1/\ln\lambda)^{1/2}.$$

In the accumulation regime for large x_0 (region VII), the asymptotic mobile charge is found by replacing w_s in the above expression by $-1-\ln(\ln\lambda)/\ln\lambda$.

Notice also that the above expression breaks down when $x_d = O(\ln\lambda^{-1/2})$, or, equivalently, when $w_s = 1 - O(1/\ln\lambda)$, since there is no depletion layer near the interface. This occurs at the boundary between the partial depletion regime and the inversion regime for large x_0 (region V). In this case, Q_c is decomposed into

$$Q_c = -\left(\frac{\ln\lambda}{\lambda}\right)^{1/2}\left[\int_0^{x_{jl}} e^{w\ln\lambda}\,dx + \int_{x_{jl}}^{x_k} e^{w\ln\lambda}\,dx\right]$$

Using the asymptotic potential constructed in the inversion regime for large x_0, we find

$$I_1 \equiv \int_{x_{jl}}^{x_k} e^{w\ln\lambda}\,dx \sim \lambda(\ln\lambda)^{-1/2}(\pi/2)^{1/2},$$

$$I_2 \equiv \int_0^{x_{jl}} e^{w\ln\lambda}\,dx \sim \lambda(x_{jl}+w'(0)),$$

where $w'(0) = \sqrt{2}\,\mathrm{sign}\,(w_s - 1)(1 - w_s + e^{(w_s-1)\ln\lambda}/\ln\lambda - 1/\ln\lambda)^{1/2}$. Therefore, the asymptotic mobile charge in region V is

$$Q_c = -(\lambda \ln \lambda)^{-1/2}(x_{jl} + w'(0)) - (\pi\lambda/2)^{1/2}\,, \tag{3.15}$$

which agrees asymptotically with (3.14) in the formal limit $w_s \ll 1$.

The amount of mobile charge in inversion for small x_0 (region IV) can be evaluated as in the strong inversion case for the enhancement device. A similar argument to that presented there provides

$$Q_c \sim -\sqrt{2}e^{w_s \ln\lambda/2}\left(\sqrt{1+\alpha^2} - \alpha\right)\,, \tag{3.16}$$

where α and α_0 are given by (3.7) and (3.9), respectively. This expression also agrees to leading order in $\ln\lambda$ at the boundary between full depletion and inversion for small x_0.

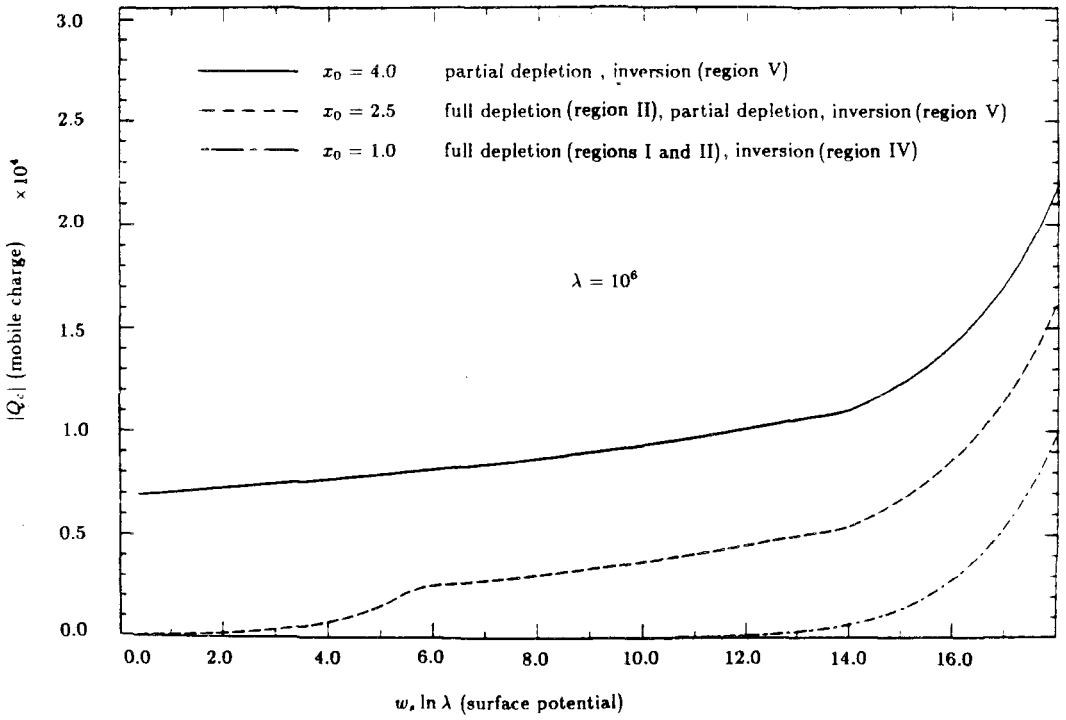

FIGURE 3.7. Mobile Charge Versus the Surface Potential for Several x_0

Plots of the asymptotic mobile charge for various x_0 as a function of the surface potential are shown in Figure 3.7. It is to be noted from this figure that

the mobile charge agrees only asymptotically and not exactly across the boundaries between the various regimes. Furthermore, the derivative of the asymptotic mobile charge with respect to the surface potential does not agree asymptotically across the boundary between full and partial depletion. Removing the asymptotic discontinuity in the derivative of the mobile charge across this boundary is quite difficult, as the details of the transition layer solution in the vicinity of the curve $G(w_s, x_0) = 0$ are needed. Since the details of the calculation become very involved, this problem is simply noted but is not discussed further.

Finally, using the mixed boundary condition on the interface, the surface potential and hence the asymptotic mobile charge can be computed for given $\bar{v}_{gs}$ and x_0.

CHAPTER 4

Some Miscellaneous Equilibrium Potential Problems

In this Chapter, we study some more equilbrium potential problems that exhibit boundary layer structure somewhat different than that already examined in Chapters 2 and 3. Some of the problems to be considered are relevant to the MOSFET away from the corner regions near the source and drain (see Figure 4.1). In these problems, we will show how to construct the asymptotic potential in equilibrium for an n^+-p junction for both planar and radial geometries.

In regard to the built-in channel device, we will make some remarks on the construction of the equilbrium potential for a graded junction where we do not neglect the thin region in which the doping profile changes rapidly. In addition, we will also examine the potential for a shallow implant on an intrinsic bulk and the potential for an asymmetrically doped junction.

Finally, for amusement, we construct the asymptotic equilibrium potential for an n^+-n-n^+ structure with a short n-region.

4.1 Strongly One-Sided Planar Junctions

For an asymmetric abrupt junction, the asymptotic theory of the potential constructed for the partial depletion mode still applies provided that the junction is not too strongly one-sided. For a strongly one-sided n^+-p junction, the depletion approximation in the p-region is no longer valid since the electrons on the p-side in the vicinity of the junction cannot be neglected in the space charge density. Furthermore, the potential drop in the heavily doped n-region decreases as the doping in that region increases.

For a planar n^+-p junction the potential, ψ, normalized by the thermal voltage, satisfies

$$\psi'' = e^{\psi} - e^{-\psi} + \begin{cases} -\lambda_n & \text{for} \quad x < 0 \qquad \text{donors,} \\ \lambda_p & \text{for} \quad x > 0 \qquad \text{acceptors .} \end{cases}$$

The length has been scaled by the intrinsic Debye length, L_d. Typical values of the doping levels near the source and drain are $\lambda_n \approx 10^8$ and $\lambda_p \approx 10^6$. We are

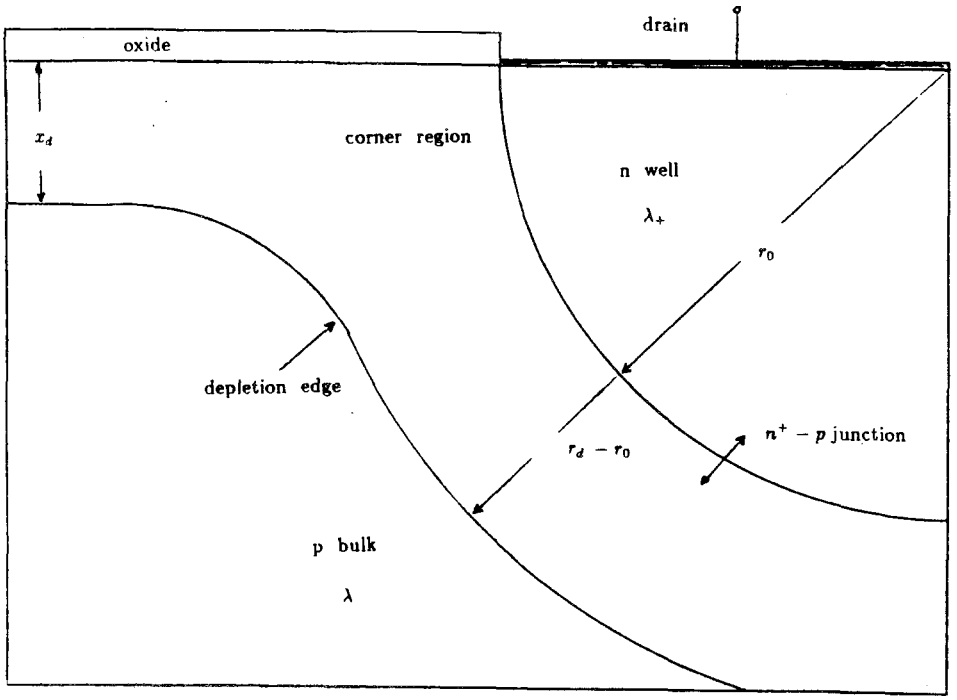

FIGURE 4.1. Equilibrium Potential near the n^+-p Junction of the n-Well

interested in determining the structure of the asymptotic potential for $\lambda_n \gg 1$, $\lambda_p \gg 1$, and λ_n/λ_p large. The potential computed numerically for $\lambda_p = 10^6$ and for various λ_n is shown in Figure 4.2.

Referring to this figure, we notice that as λ_n/λ_p increases an inversion layer forms on the p-side near the junction. Therefore, the structure of the asymptotic potential on the p-side consists of an inversion layer followed by a depletion layer and finally a transition layer that allows a smooth decay onto the p-bulk. All of these layers have previously been considered in the strong inversion case of the enhancement device, and it is possible to match these layers without difficulty for $\lambda_p \gg 1$. The new feature of this problem is that the potential is not specified *a priori* on $x = 0$ but is determined from the condition that the potential be C^1 continuous at the junction. To find the condition that determines the potential at the junction the potential in the heavily doped n-region must be resolved.

In the heavily doped n-region, the depletion approximation is not valid since the potential drop in this layer is minimal. Instead, in this region a transition layer solution, which balances the contribution to the space charge density of the n-carriers and the donors, is needed. By forming this transition layer in the

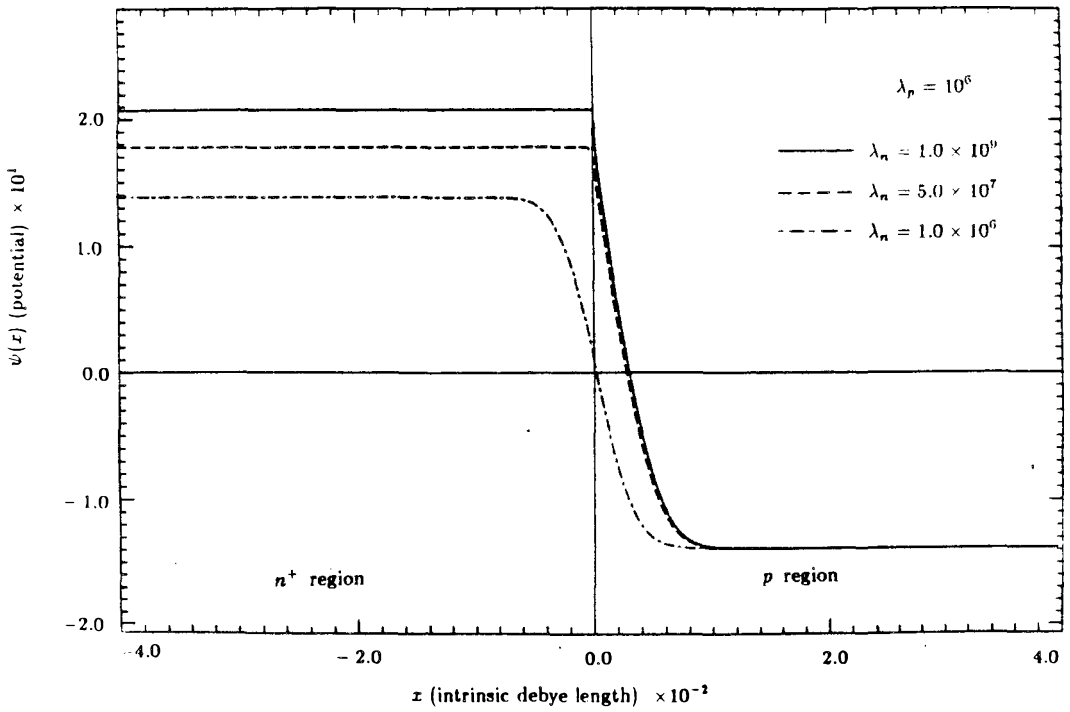

FIGURE 4.2. Numerical Potential for Strongly One-Sided Junctions

heavily doped n-region and by ensuring that the potential is C^1 continuous at the junction, a trancendental equation for the junction potential, which can be solved asymptotically, can be obtained. Once the junction potential is calculated, the details of the structure of the potential on the p-side, including the depletion width, is known. The explicit illustration of the matching is shown only for the more detailed case of the radial n^+-p junction, which we now consider.

4.2 The Radial n^+-p Junction

The asymptotic potential for the radial n^+-p junction in equilibrium that is relevant to the MOSFET away from the corner is given by

$$\psi''(R) + \frac{1}{R}\psi'(R) = 2\sinh(\psi) + \lambda N(R) \qquad \text{on } R > 0 \qquad \text{with } \lambda \gg 1 .$$

The strongly asymmetric doping profile satisfies $N(R) = 1$ for $R > R_0$ and $N(R) = -\lambda_+/\lambda \gg 1$ for $R < R_0$. We also assume that the depth of the n-well, R_0, is on the order of a depletion width $O((\ln\lambda/\lambda)^{1/2})$ based on the doping level of the p-region. Formally, we write $R_0 = r_0(\ln\lambda/\lambda)^{1/2}$, where r_0 is taken as an $O(1)$ parameter.

A schematic plot of the layer structure of the equilibrium potential is shown in Figure 4.3.

On the p-side of the junction, we scale the potential equation by $\psi = w \ln \lambda$, $r = R(\lambda/\ln\lambda)^{1/2}$ giving

$$w''(r) + \frac{1}{r}w'(r) = \frac{2}{\lambda}\sinh(w \ln \lambda) + 1 \qquad \text{on } r \geq r_0 \qquad \text{with } \lambda \gg 1 .$$

Now, in the depletion layer, the radial potential for $\lambda \gg 1$ is found by neglecting the nonlinearity in the Poisson equation

$$w \sim w_d = a + b\ln(r) + \frac{r^2}{4},$$

where $a = a(\lambda)$, $b = b(\lambda)$ are to be found by matching. Constructing an internal layer as usual near the unknown depletion edge and assuming the asymptotic sequence

$$w_t = -1 + \frac{h_0}{\ln\lambda} + \frac{h_1}{(\ln\lambda)^{3/2}} + \cdots \qquad \text{with } \tilde{r} = (r - r_d)(\ln\lambda)^{1/2}$$

for the potential, the first few internal layer equations in the hierarchy are

$$h_0'' = 1 - e^{-h_0} \qquad \text{with} \qquad h_0(\infty) = 0,$$
$$h_1'' - e^{-h_0}h_1 = -h_0'/r_d \qquad \text{with} \qquad h_1(\infty) = 0.$$

Expanding towards the depletion layer in an intermediate variable r_η with $\tilde{r} = r_\eta\eta(\ln\lambda)^{1/2}$ gives

$$\begin{aligned} w_t \sim -1 - \frac{c}{\sqrt{2}}(\ln\lambda)^{-1/2}r_\eta\eta + (1 + c^2/4)(\ln\lambda)^{-1} \\ + \frac{1}{2}r_\eta^2\eta^2(1 + \frac{c}{\sqrt{2}r_d}(\ln\lambda)^{-1/2}) - \frac{r_\eta^3\eta^3}{6r_d}(1 + \frac{\sqrt{2}\,c}{r_d}(\ln\lambda)^{-1/2}) + \cdots, \end{aligned} \tag{4.1}$$

where $c \approx .81785$ is the integral defined by (2.5) in Chapter 2. We remark that since $h_0(\tilde{r}) \sim \tilde{r}^2/2$ as $\tilde{r} \to -\infty$, the term $e^{-h_0}h_1$ can be neglected out of the transition layer.

Similarly, expanding the depletion layer solution in terms of an intermediate variable $r = r_d + r_\eta\eta$ by expanding the logarithm near the depletion edge, we find

$$w_d \sim a + b\ln(r_d) + \frac{r_d^2}{4} + r_\eta\eta(\frac{r_d}{2} + \frac{b}{r_d}) + r_\eta^2\eta^2(\frac{1}{4} - \frac{b}{2r_d^2}) + \frac{br_\eta^3\eta^3}{3r_d^3} + \cdots . \tag{4.2}$$

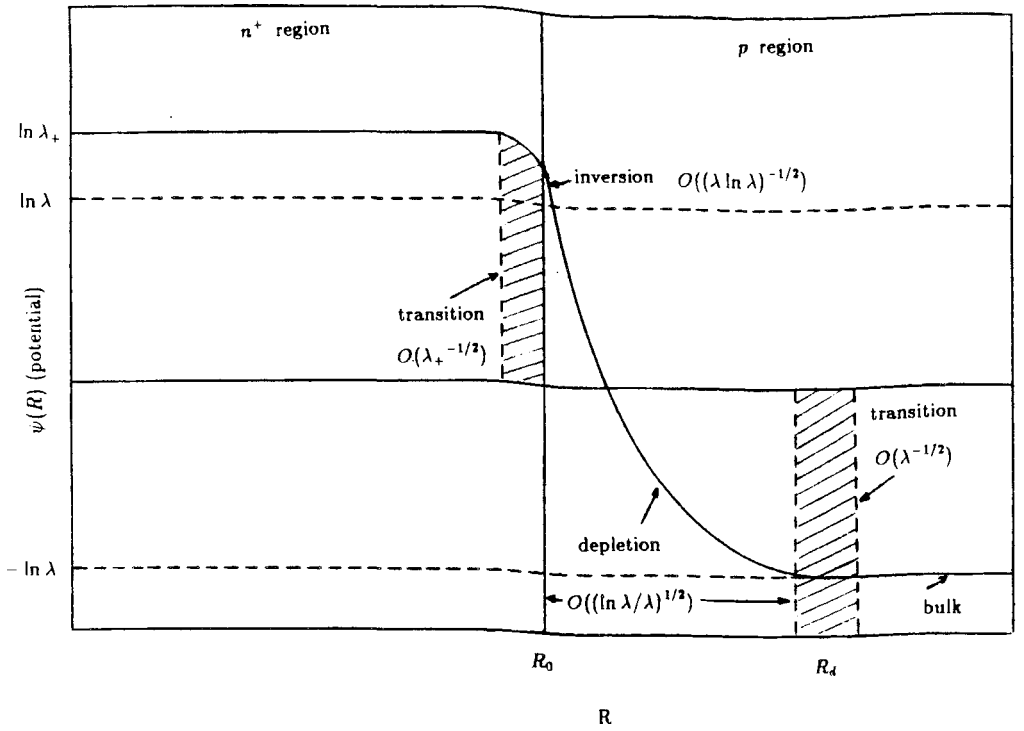

FIGURE 4.3. Schematic Plot of Equilibrium Potential for n^+-p Radial Structure

Comparing (4.1) and (4.2), we notice that to match the $O(1), O(\eta)$ terms we require

$$\begin{aligned} a + b\ln(r_d) + \frac{r_d^2}{4} &= -1 + (1 + c^2/4)(\ln\lambda)^{-1}, \\ \frac{r_d}{2} + \frac{b}{r_d} &= -\frac{c}{\sqrt{2}}(\ln\lambda)^{-1/2}, \end{aligned} \tag{4.3}$$

which are two equations in the three unknowns a, b, and r_d. The $O(\eta^2), O(\eta^3)$ terms are then seen to match identically.

In contrast to a symmetric n-p junction, there is a thin inversion layer of mobile n-carriers near the junction for $r > r_0$. In this inversion layer, formed by carriers spilling over from the n^+ region, we take the scalings

$$w_i(\tilde{r}) = w_{i0}(\tilde{r}) + \frac{w_{i1}(\tilde{r})}{\ln\lambda} + \frac{w_{i2}(\tilde{r})}{(\ln\lambda)^2} + \cdots \qquad \text{where} \qquad \tilde{r} = (r - r_0)\ln\lambda\,,$$

to obtain the layer equations

$$w_{i0}'' - \frac{1}{\lambda(\ln\lambda)^2} e^{w_{i0}\ln\lambda} = 0\,,$$
$$w_{i1}'' + \frac{1}{\lambda\ln\lambda}\, e^{w_{i0}\ln\lambda + w_{i1}} = -\frac{1}{r_0} w_{i0}'\,,$$
$$w_{i2}'' + \frac{1}{\lambda\ln\lambda}\, e^{w_{i0}\ln\lambda + w_{i1}} w_{i2} = -\frac{1}{r_0} w_{i1}' + 1 + \frac{\tilde{r}}{r_0^2} w_{i0}'\,.$$

The boundary condition $w_{i0}(0) = w_s$ will be found by patching the potential for C^1 continuity to the n^+ region. The solution of the leading order layer equation has appeared several times and is simply

$$w_{i0}(\tilde{r}) = 1 + \frac{\ln(\ln\lambda)}{\ln\lambda} + 2\frac{\ln(\alpha_0)}{\ln\lambda} - \frac{2}{\ln\lambda}\ln\left(\sinh(\frac{\alpha_0}{\sqrt{2}}\tilde{r} + \gamma)\right)\,,$$

where $\sinh(\gamma) = \alpha_0(\ln\lambda)^{1/2}\lambda^{(1-w_s)/2} \equiv \alpha$. Expanding w_{i0}, w_{i1}, w_{i2}, $\cdots$ as $\tilde{r} \to \infty$, we obtain

$$w_{i0} \sim 1 + K(\lambda, w_s, \alpha_0) - \sqrt{2}\alpha_0\frac{\tilde{r}}{\ln\lambda}\,,$$
$$w_{i1} \sim \frac{\sqrt{2}\alpha_0\tilde{r}^2}{2r_0\ln\lambda} + A_1\tilde{r} + B_1\,,$$
$$w_{i2} \sim \frac{\tilde{r}^2}{2} - \frac{A_1\tilde{r}^2}{2r_0} - \frac{\sqrt{2}\alpha_0\tilde{r}^3}{3r_0^2\ln\lambda} + A_2\tilde{r} + B_2\,,$$
$$w_{i3} \sim -\frac{\tilde{r}^3}{6r_0} + A_3\tilde{r} + B_3 + \text{ higher order terms}\,,$$

where $K(\lambda, w_s, \alpha_0)$ is defined in (2.16). As in the case of the planar inversion layer, matching to the depletion layer forces $A_i, B_i = 0$. Expressing these expansions in terms of an intermediate variable $r_\eta = (r - r_0)/\eta$ then gives

$$w_i \sim 1 + K - \sqrt{2}\alpha_0 r_\eta\eta + \frac{r_\eta^2\eta^2}{2}(\frac{\sqrt{2}\alpha_0}{r_0} + 1) - \frac{r_\eta^3\eta^3}{3}(\frac{\sqrt{2}\alpha_0}{r_0^2} + \frac{1}{2r_0}) + \cdots\,.$$

Similarly, the expansion of the depletion layer solution in terms of an intermediate variable is

$$w_d \sim a + b\ln(r_0) + \frac{r_0^2}{4} + r_\eta\eta(\frac{r_0}{2} + \frac{b}{r_0}) + r_\eta^2\eta^2(\frac{1}{4} - \frac{b}{2r_0^2}) + b\frac{r_\eta^3\eta^3}{3r_0^3} + \cdots\,.$$

Matching the two expansions w_i and w_d then enforces

$$\begin{aligned} \frac{r_0}{2} + \frac{b}{r_0} &= -\sqrt{2}\alpha_0 \,, \\ a + b\ln(r_0) + \frac{r_0^2}{4} &= 1 + K \,. \end{aligned} \tag{4.4}$$

The remaining terms match identically. Before solving the equations for the matching constants, the potential at the interface, w_s, must be found.

Near the junction on the n^+-side, a thin boundary layer exists that allows for the C^1 continuity of the potential. The appropriate scalings for this boundary layer are $\psi = \ln(\lambda_+) - u$, $\tilde{r} = (R - R_0)\lambda_+^{1/2}$ so that the Poisson equation becomes

$$u''(\tilde{r}) = 1 - e^{-u} \qquad \text{with } u_{\tilde{r}} > 0 \qquad \text{and } u(-\infty) = 0 \,.$$

Integrating once and evaluating at the junction $\tilde{r} = 0$ and defining $u(0) = u_0$ gives

$$\frac{1}{2}u_{\tilde{r}}^2 = u_0 + e^{-u_0} - 1 \qquad \text{on } \tilde{r} = 0 \,.$$

Once u_0 has been found, the potential in this layer is given implicitly by

$$\sqrt{2}\tilde{r} = \int_{u_0}^{u} (y + e^{-y} - 1)^{-1/2}\, dy \,.$$

Patching u for C^1 continuity to the inversion layer potential, w_{i0}, and using $\lambda_+/\lambda \gg 1$, gives $(u_0 + e^{-u_0} - 1)^{1/2} \sim e^{-u_0/2}$, which thus implies $u_0 \sim 1$. Noticing that $w_s = \ln\lambda_+/\ln\lambda - u_0/\ln\lambda$ then gives the boundary condition at the junction for the inversion layer: $w_s = \ln\lambda_+/\ln\lambda - 1/\ln\lambda$. Therefore, for a strongly one-sided junction, we observe that the potential drop on the n^+-side is minimal.

The four equations for the matching parameters r_d, b, α_0, and a defined from (4.3) and (4.4) can be manipulated into the form

$$\begin{aligned} b &= -\frac{r_0^2}{2} - \sqrt{2}\alpha_0 r_0 \,, \\ a &= -b\ln r_0 - \frac{r_0^2}{4} + 1 + K \,, \\ \alpha_0 &= \frac{1}{\sqrt{2}r_0}\left(\frac{r_d^2 - r_0^2}{2} + \frac{c\, r_d}{\sqrt{2}}(\ln\lambda)^{-1/2}\right) \,, \end{aligned}$$

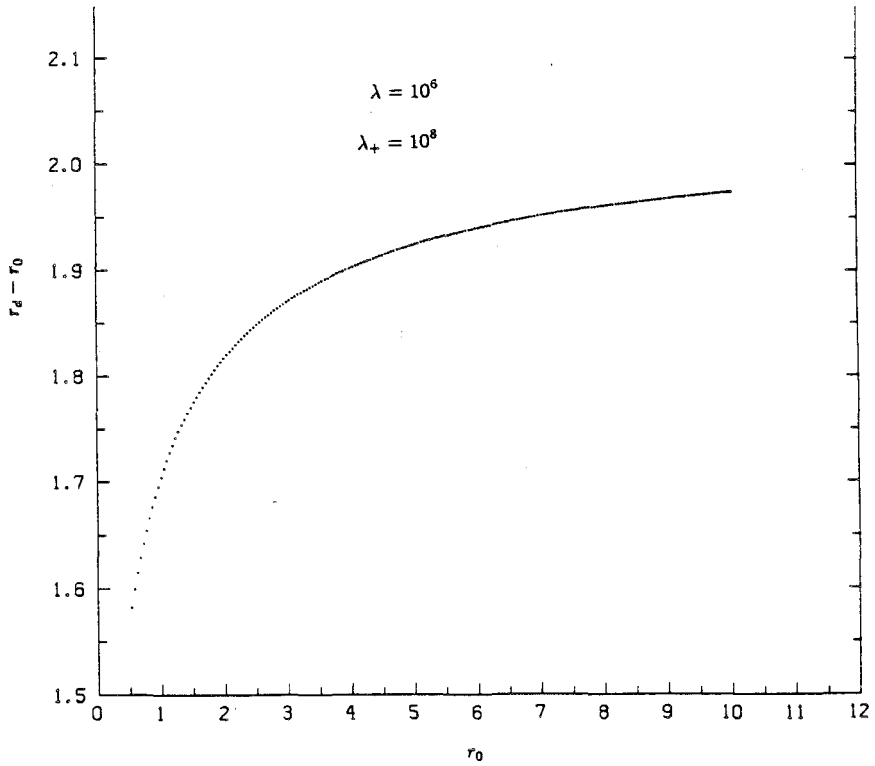

FIGURE 4.4. The Radial Depletion Width as a Function of the Depth of the n-Well

where the depletion width r_d satisfies

$$\left(\frac{r_d^2}{2} + \frac{c\, r_d}{\sqrt{2}}(\ln\lambda)^{-1/2}\right)\ln(r_d/r_0) - \frac{(r_d^2 - r_0^2)}{4} = 2 + K - (\frac{c^2}{4} + 1)(\ln\lambda)^{-1}. \quad (4.5)$$

With $K = K(\lambda, \ln\lambda_+/\ln\lambda - 1/\ln\lambda, \alpha_0)$ and since K depends weakly on α_0, the equations for r_d and α_0 are virtually uncoupled. As a remark, the formal limit $r_0 \to \infty$ reproduces the planar solutions for α_0 and the depletion width $r_d - r_0$. A plot of the numerical solution to (4.5) for $r_d - r_0 = r_d(r_0) - r_0$ is shown in Figure 4.4. From this figure, we notice that the depletion width for a radial geometry is smaller than for a planar geometry.

As a remark, the mobile charge in $r > r_0$ in an angular section from $\theta = 0$ to $\theta = \theta_1$ defined by

$$Q_c \sim -\theta_1\,(\ln\lambda/\lambda)^{1/2}\int_{r_0}^{r_d} r\, e^{w\,\ln\lambda}\, dr$$

can be evaluated asymptotically for $\ln\lambda \gg 1$ using the inversion layer potential already constructed. Since the dominant contribution to the integral arises from the inversion layer, we have

$$Q_c \sim -\alpha_0^2\theta_1(\lambda\ln\lambda)^{1/2}\int_0^{\infty} \frac{(r_0 + \tilde{r}/\ln\lambda)}{\sinh^2(\alpha_0\tilde{r}/\sqrt{2} + \gamma)}\, d\tilde{r}\,.$$

Evaluating the required integrals gives

$$Q_c \sim -\sqrt{2}\theta_1 r_0 \lambda^{w_s/2}\left((1+\alpha^2)^{1/2}-\alpha\right)$$
$$-\theta_1(\lambda \ln\lambda)^{1/2}\left(w_s - 1 - \ln(\ln\lambda)/\ln\lambda - 2(\ln(\alpha_0)-\gamma)/\ln\lambda\right) ,$$

where $w_s = \ln\lambda_+/\ln\lambda - 1/\ln\lambda$.

4.3 Potential For A Graded Planar Junction

Doping profiles for a built-in channel device are normally not abrupt but are rapidly varying functions near the junction. The grade or steepness of the junction is determined by the implant process and generally does not depend on the doping level.

For junctions with a steep grade, the depletion approximation is still valid near the junction, and the grade of the doping profile simply introduces an internal layer for the potential in the vicinity of the junction. However, for slowly varying doping profiles, the depletion approximation can no longer be justified as the contribution to the space charge density of the mobile carriers becomes significant near the junction. For these slowly varying profiles, numerical methods must be employed to compute the potential.

To illustrate the effect of a graded junction on the validity of the depletion layer expansion, we consider the BVP

$$w'' = \frac{1}{\lambda}(e^{w\ln\lambda} - e^{-w\ln\lambda}) + d(x)$$

on an infinite interval in x where the anti-symmetric doping profile, $d(x)$, satisfies either

$$d(x) = \begin{cases} x/(|x|+\sigma) & \text{algebraic decay at infinity,} \\ \text{sign}(x)(1-e^{-|x|/\sigma}) & \text{exponential decay at infinity .} \end{cases}$$

Both doping profiles satisfy $d(x) \to \pm 1$ as $x \to \pm\infty$ but differ in their approach to these values. In both cases, $0 < \sigma \ll 1$ corresponds to a steeply graded junction. By considering the width of the transition layer at the depletion edge, we anticipate that the depletion approximation should be valid provided $\sigma(\ln\lambda)^{1/2} \ll 1$.

Applying the depletion approximation, in which the nonlinearity is neglected and the potential is patched for C^1 continuity to the bulk, a transcendental equa-

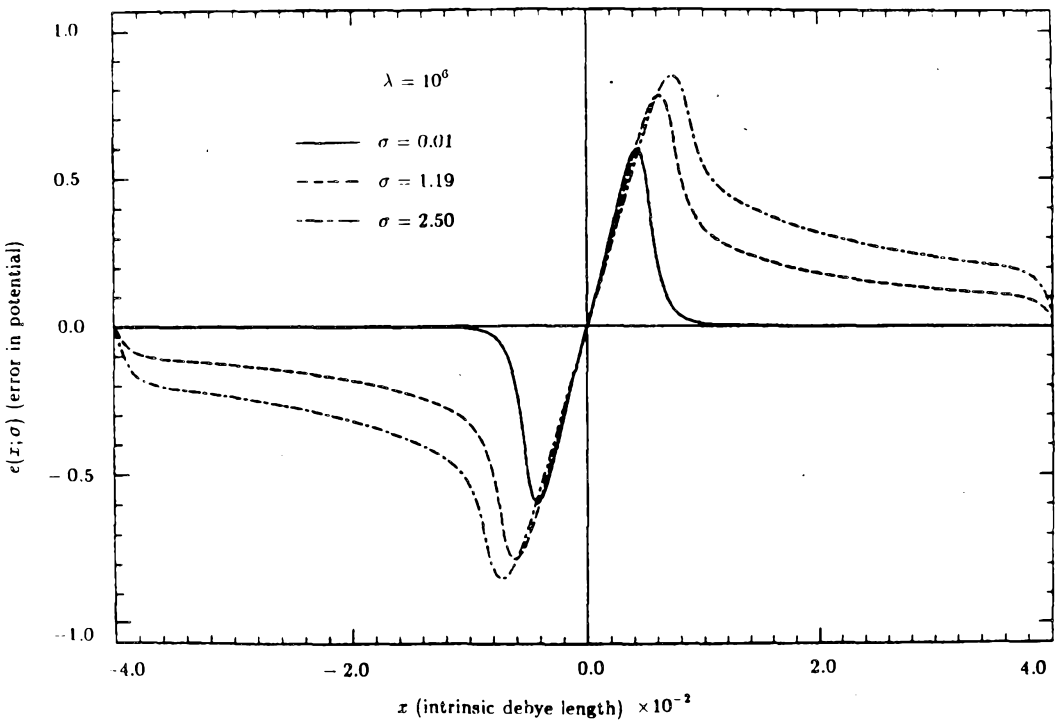

FIGURE 4.5. Error in the Potential for a Graded Junction with Algebraic Decay

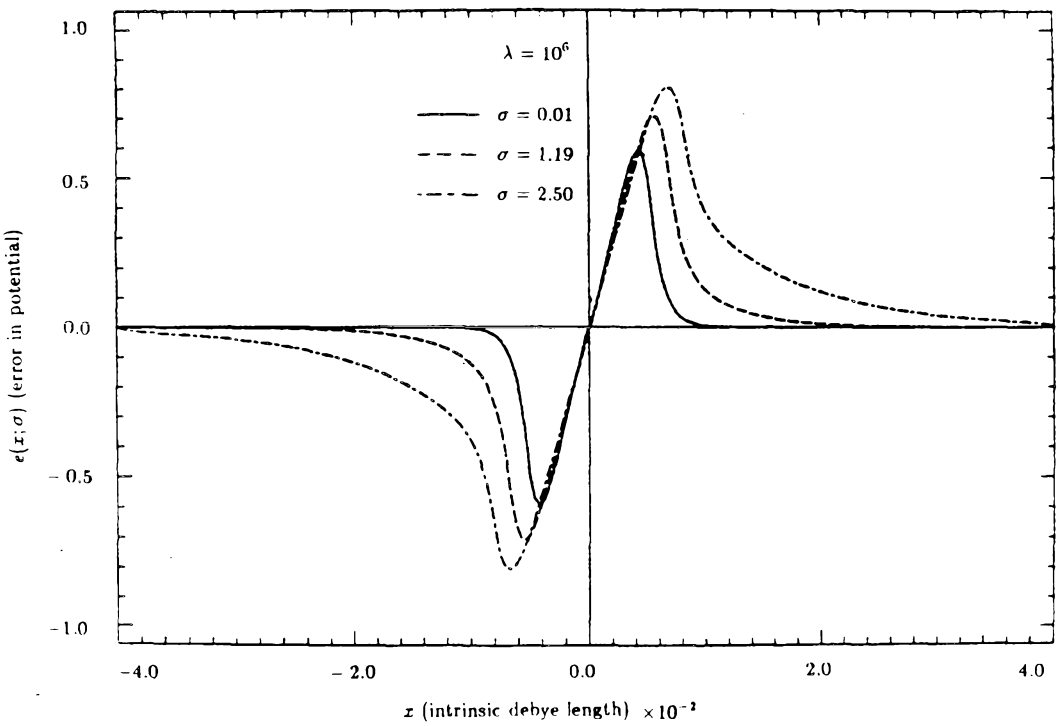

FIGURE 4.6. Error in the Potential for a Graded Junction with Exponential Decay

tion of the form $F(x_d\,;\sigma) = 0$ for the depletion width is obtained for both cases

$$F(x_d,\sigma) \equiv \begin{cases} x_d^2/2 + \sigma^2 \ln\left((x_d+\sigma)/\sigma\right) - \sigma x_d - 1 & \text{algebraic,} \\ x_d^2/2 + \sigma(x_d+\sigma)\, e^{-x_d/\sigma} - (\sigma^2+1) & \text{exponential .} \end{cases}$$

Graphical considerations imply that there is exactly one root $x_d = x_d(\sigma) > 0$ in both cases. These equations are easily solved by straightforward Newton iterations. Once x_d has been computed, the depletion layer potential is known for both profiles. For the profile with algebraic decay onto the uniform doping levels, we find

$$w_d(x) = \frac{x^2}{2} - x(x_d - \sigma) - \sigma^2 \ln\left(\frac{x+\sigma}{\sigma}\right) + \sigma x \ln\left(\frac{x_d+\sigma}{x+\sigma}\right).$$

Similarly, for the profile with exponential decay, we have

$$w_d(x) = \frac{x^2}{2} + \sigma^2(1 - e^{-x/\sigma}) - x(x_d + \sigma e^{-x_d/\sigma}).$$

The difference between the numerical potential generated from finite differences and the potential obtained from the depletion approximation for the case of algebraic decay is displayed in Figure 4.5. The error for the doping profile with exponential decay is shown in Figure 4.6. From these figures, we notice that the maximum error occurs near the depletion edge and is amplified as σ increases. In addition, the error in the bulk potential is due to the residual electric field in these regions that is not resolved by the depletion approximation. This bulk electric field is less pronounced for doping profiles decaying exponentially rather than algebraically as $x \to \pm\infty$.

A comparison of the L_2 error as σ is varied is shown in Figure 4.7, for both cases. The error for the profile with exponential decay is seen to be significantly smaller than the error for the profile with algebraic decay. Although as σ increases the depletion approximation becomes more difficult to justify, the approximation to the numerical potential provided by this method is still suprisingly good.

4.4 Shallow Implant On An Intrinsic Bulk

We now construct the asymptotic potential for the partial depletion mode of a built-in channel device with a large donor concentration implanted into an intrinsic material. The transition between the donor implant and the intrinsic

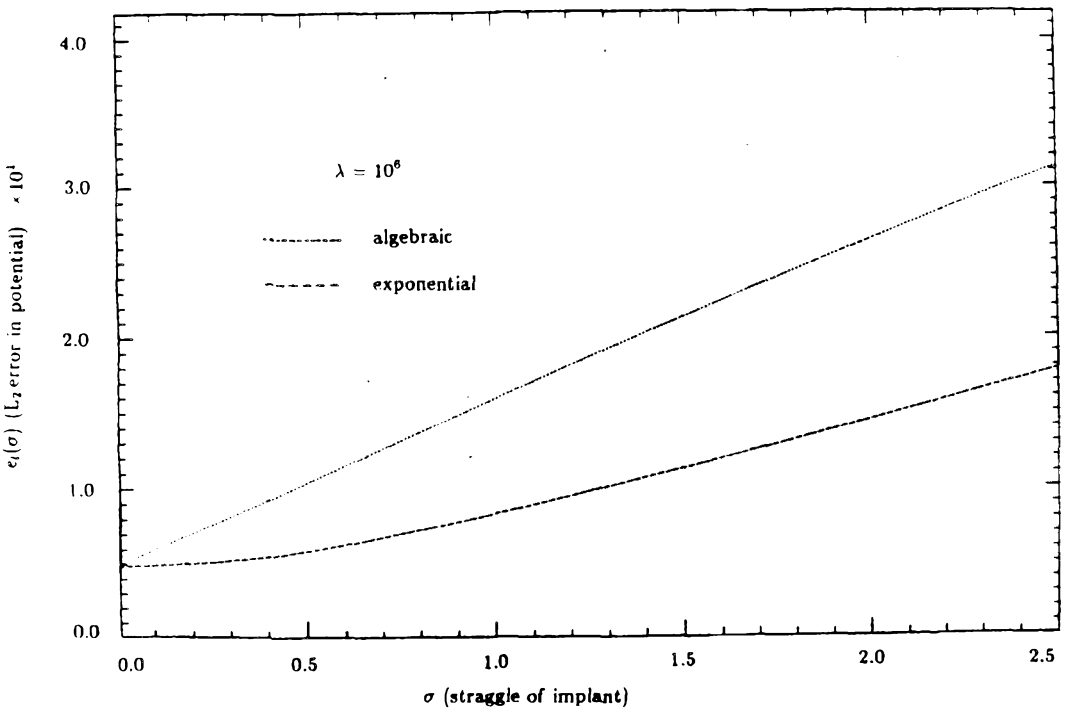

FIGURE 4.7. L_2 Error Comparison for Algebraic and Exponential Decay

bulk is assumed to have negligible width. The potential, ψ, therefore satisfies

$$\psi'' = e^{\psi} - e^{-\psi} + \begin{cases} -\lambda & \text{for} \quad x < x_0 \quad \text{donors,} \\ 0 & \text{for} \quad x > x_0 \quad \text{intrinsic ,} \end{cases}$$

where $\lambda \gg 1$. A plot of the numerical potential for this case when $x_0 > 2 + \sqrt{2}$, is shown in Figure 4.8, where it is seen that the length scale in the intrinsic bulk is much larger than near the interface. The new feature of this problem is to match the intrinsic bulk to the channel region. This matching is accomplished using the exact solution of the nonlinear Poisson equation for an intrinsic material.

For $x > x_0$, the exact solution to the nonlinear Poisson equation satisfying $w_i \to 0$ as $x \to \infty$ is

$$\psi_i = 4 \tanh^{-1}\left(e^{-\sqrt{2}(x-x_0)} \tanh(\psi_0/4)\right)$$

where ψ_0 is an arbitrary constant to be determined. As in the strongly one-sided junction, the potential in the intrinsic region is to be patched for C^1 continuity at x_0 to a transition layer potential valid near the channel region. Constructing a transition layer in the channel region and patching the potential for C^1 continuity

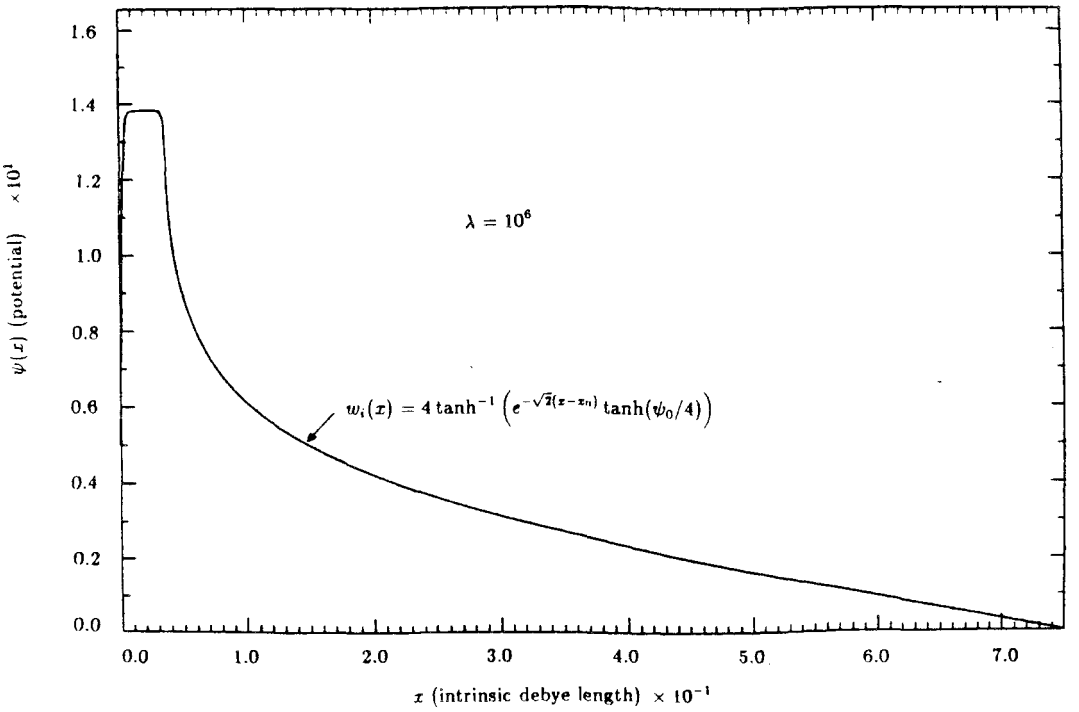

FIGURE 4.8. Numerical Potential for an Implant on an Intrinsic Bulk

at x_0 gives a transcendental equation for ψ_0

$$\psi_0 = \ln\lambda - v\,,$$

where

$$2\sinh((\ln\lambda - v)/2) = \sqrt{\lambda}(e^{-v} + v - 1)^{1/2}\,.$$

Using $\lambda \gg 1$, we find $\psi_0 = \ln\lambda - 1 + O(1/\lambda^2)$. With the junction potential known, the asymptotic potential for an implant on an intrinsic material can then easily be determined.

4.5 Asymmetric Step Profile

We now compute the asymptotic potential in equilibrium for an asymmetric step profile where ψ satisfies

$$\psi'' = \exp(\psi) - \exp(-\psi) + \lambda d(x) \tag{4.6}$$

with

$$d(x) = \begin{cases} d_1 & \text{for} \quad x < 0 \qquad \text{p-side,} \\ -d_2 & \text{for} \quad x > 0 \qquad \text{n-side.} \end{cases}$$

It is assumed that the ratio of the two doping levels is near unity so that the depletion approximation holds.

In the depletion layer, we consider the scalings $\psi = w \ln \lambda$, $\bar{x} = x(\ln \lambda/\lambda)^{-1/2}$ so that the depletion layer potential is given by

$$w_d(x) = \begin{cases} d_1\bar{x}^2/2 + a\bar{x} + b & \text{for} \quad \bar{x} < 0 \qquad \text{p-side,} \\ -d_2\bar{x}^2/2 + a\bar{x} + b & \text{for} \quad \bar{x} > 0 \qquad \text{n-side,} \end{cases}$$

where a and b are to be found by matching.

On the n-side, we take the scalings $\psi = \ln \lambda - \psi_n$ and $\hat{x} = (\bar{x} - \bar{x}_r)(\ln \lambda)^{1/2}$ where $\bar{x}_r$ is the unknown depletion width on the n-side. Substituting into (4.6), we obtain the layer equation

$$\psi_n'' = d_2 - \exp(-\psi_n) \quad \text{with} \quad \psi_n' < 0 \quad \text{and} \quad \psi_n \to -\ln d_2 \ \text{ as } \ \hat{x} \to \infty .$$

Integrating the equation once and expanding in terms of an intermediate variable as $\hat{x} \to -\infty$, we obtain

$$\psi \sim \ln \lambda + \ln d_2 - 1 - \frac{d_2 c^2(d_2)}{4} + \frac{d_2 c(d_2)}{\sqrt{2}} x_\eta \eta (\ln \lambda)^{1/2} - \ln \lambda d_2 \frac{x_\eta^2 \eta^2}{2} ,$$

where $c(d_2) \approx .81785\, d_2^{-1/2}$.

Similarly on the p-side, we take the scalings $\psi = -\ln \lambda + \psi_p$ and $\hat{x} = (\bar{x} - \bar{x}_l)(\ln \lambda)^{1/2}$ so that substituting into (4.6), we obtain the layer equation

$$\psi_p'' = d_1 - \exp(-\psi_p) \quad \text{with} \quad \psi_p' > 0 \quad \text{and} \quad \psi_p \to -\ln d_1 \ \text{ as } \ \hat{x} \to \infty .$$

Integrating the equation once and expanding in terms of an intermediate variable as $\hat{x} \to +\infty$, we obtain

$$\psi \sim -\ln \lambda - \ln d_1 + 1 + \frac{d_1 c^2(d_1)}{4} + \frac{d_1 c(d_1)}{\sqrt{2}} x_\eta \eta (\ln \lambda)^{1/2} + \ln \lambda d_1 \frac{x_{eta}^2 \eta^2}{2} ,$$

where $c(d_1) \approx .81785\, d_1^{-1/2}$.

Matching the transition layers to the depletion layers gives four equations for a, b, $\bar{x}_r$ and $\bar{x}_l$:

$$a - d_2\bar{x}_r = \frac{d_2 c(d_2)}{\sqrt{2}} (\ln \lambda)^{-1/2} \quad \text{and} \quad a + d_1\bar{x}_l = \frac{d_1 c(d_1)}{\sqrt{2}} (\ln \lambda)^{-1/2} ,$$

$$\frac{a^2}{2d_2} + b = 1 + \frac{(\ln d_2 - 1)}{\ln \lambda} \quad \text{and} \quad \frac{a^2}{2d_1} - b = 1 + \frac{(\ln d_1 - 1)}{\ln \lambda} .$$

Solving for the matching parameters then gives

$$a = \left(\frac{4d_1d_2}{d_1+d_2}\right)^{1/2}\left(1-\frac{1}{\ln\lambda}(1-\frac{\ln(d_1d_2)}{2})\right)^{1/2},$$

$$b = \frac{d_2-d_1}{d_2+d_1}+\frac{d_1(1-\ln d_1)-d_2(1-\ln d_2)}{(d_1+d_2)\ln\lambda},$$

$$\bar{x}_r = \left(\frac{4d_1}{d_2(d_1+d_2)}\right)^{1/2}\left(1-\frac{1}{\ln\lambda}(1-\frac{\ln(d_1d_2)}{2})\right)^{1/2}+\frac{c(d_1)}{\sqrt{2}}(\ln\lambda)^{-1/2},$$

$$\bar{x}_l = -\left(\frac{4d_2}{d_1(d_1+d_2)}\right)^{1/2}\left(1-\frac{1}{\ln\lambda}(1-\frac{\ln(d_1d_2)}{2})\right)^{1/2}-\frac{c(d_2)}{\sqrt{2}}(\ln\lambda)^{-1/2}.$$

From this infinite order expansion in powers of $O(1/\ln\lambda)$, the depletion layer expansion is valid provided that

$$\frac{\max(d_1,d_2)}{\min(d_1,d_2)} \ll \ln\lambda\,.$$

If this condition is not met, then the assumption of depletion layers in the potential on both the n and p-sides is invalid, and the junction is thus strongly one-sided. For realistic doping levels of $\lambda \approx 10^5$, the above criterion implies that the ratio of the maximum to minimum doping level not exceed roughly 10 for the depletion approximation to be valid.

4.6 The n^+-n-n^+ Structure

We now determine the asymptotic potential of the n^+-n-n^+ structure as a function of the length, L, and doping level, λ, of the middle n-region. The asymptotic potential for this case relies on the following exact solution shown below.

Consider the boundary value problem

$$\phi''(x) = \alpha^2 e^{\phi} \qquad \text{with} \qquad \phi(0)=0\,,\ \phi(1)=0\,.$$

The unique solution is

$$\phi(x) = -\ln 2 + 2\ln\left(a\sec(\alpha a(x-1/2)/2)\right)\,,$$

where $\phi'' > 0$ and $\phi < 0$, and a satisfies the transcendental equation $a\sec(|\alpha|a/4) = \sqrt{2}$. Defining $\beta = |\alpha|\,a/4$, we have $4\beta = \sqrt{2}|\alpha|\cos(\beta)$, which always has a root in

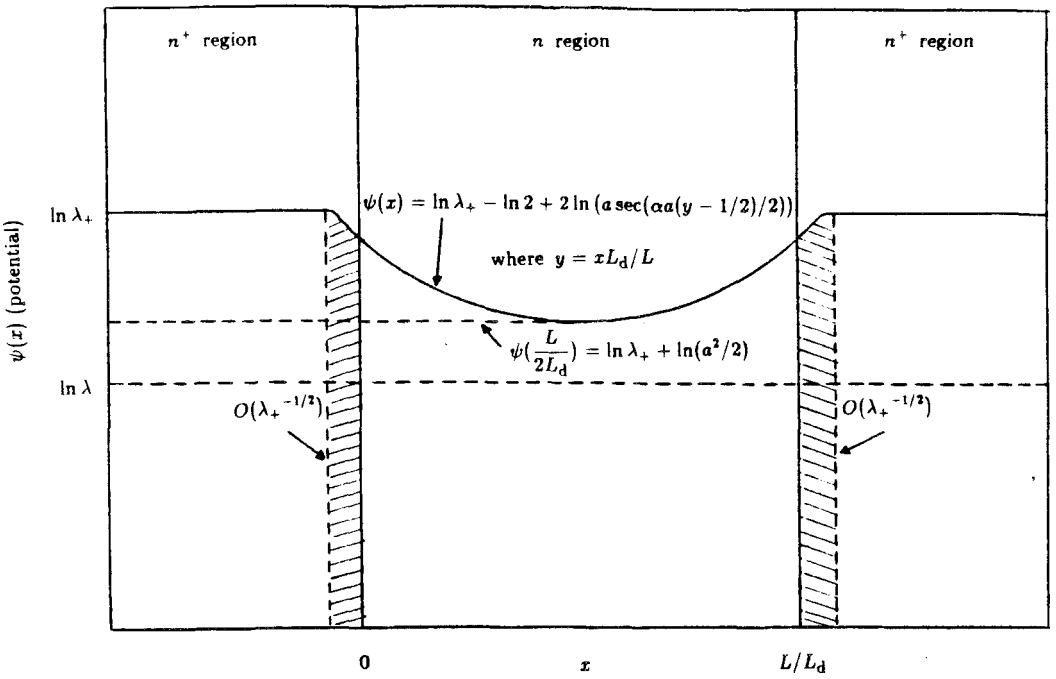

FIGURE 4.9. Schematic Plot of Equilibrium Potential for n^+-n-n^+ Structure

$\beta \in (0, \pi/2)\ \forall|\alpha|$. In the two limiting cases $|\alpha| \gg 1$ and $|\alpha| \ll 1$, we have

$$\beta = \begin{cases} \sqrt{2}|\alpha|/4 - \sqrt{2}\alpha^3/64 + \cdots & \text{for } \alpha \ll 1\,, \\ \pi/2 - \sqrt{2}\pi/|\alpha| + \cdots & \text{for } \alpha \gg 1\,. \end{cases} \tag{4.7}$$

Now consider an n^+-n-n^+ structure with $L/L_d \ll \lambda^{-1/2}$ and where the potential in equilibrium satisfies

$$\psi''(x) = e^{\psi} - \lambda N(x)\,,$$

with

$$N(x) = \begin{cases} \lambda_+/\lambda & \text{for } x < 0\,, \\ 1 & \text{for } x \in (0, L/L_d)\,, \\ \lambda_+/\lambda & \text{for } x > L/L_d\,. \end{cases}$$

We also assume that $\lambda_+/\lambda \gg 1$. A schematic plot of the equilibrium potential is shown in Figure 4.9. In the middle n-region, we scale by $\psi = \ln(\lambda_+) + w$ and $y = xL_d/L$ so that

$$w_{yy} = \lambda_+(L/L_d)^2\, e^w - \lambda(L/L_d)^2\,.$$

Now assuming $w \gg \ln(\lambda/\lambda_+)$ and $L/L_d \ll \lambda^{-1/2}$, the leading order asymptotic

potential in the middle n-region is simply

$$w_{0yy} = \kappa^2 e^{w_0} \qquad \text{with} \qquad \kappa^2 = \lambda_+ (L/L_d)^2$$

with boundary conditions $w_0(0) = w_0(1) = w_{s0}$, where w_{s0} will be found by matching to the n^+-regions. Using the exact solution mentioned above, we then have

$$w_0(y) = -\ln(2) + 2\ln\left(a \sec(\alpha a(y - 1/2)/2)\right) \tag{4.8}$$

$$\text{where} \quad a \sec(a|\alpha|/4) = \sqrt{2} \qquad \text{and} \qquad \alpha = \kappa e^{w_{s0}/2} .$$

To determine an extra relation between for the matching constants w_{s0} and a, we now consider the n^+-region. By symmetry, we need only analyze the region $x < 0$.

To match the potential smoothly across the n^+-n junction, we require a thin layer near the junction on the n^+-side. Setting $\tilde{x} = x\lambda_+^{1/2}$ and $\psi = \ln \lambda_+ - w_t$ and using the boundary condition $w_t(-\infty) = 0$, we obtain

$$w_t'(\tilde{x}) = \sqrt{2}\left(e^{-w_t} - 1 + w_t\right)^{1/2} . \tag{4.9}$$

Forcing the potential defined by (4.9) for $x < 0$ and (4.8) for $x > 0$ to be C^1 continuous at $x = 0$ gives an additional relationship between a and w_{s0}. The two equations for a and w_{s0} then are

$$a^2/2 = (1 + w_{s0})e^{-w_{s0}} ,$$
$$a \sec(a|\alpha|/4) = \sqrt{2} \qquad \text{where} \qquad \alpha = \kappa e^{w_{s0}/2} .$$

These two equations can be solved approximately when either $\kappa \gg 1$ or $\kappa \ll 1$. The solutions in these two limiting cases are

$$a \sim 2\pi e^{1/2}/\kappa \qquad \text{and} \qquad w_{s0} \sim -1 + 2\pi^2/\kappa^2 \qquad \text{for } \kappa \gg 1 ,$$
$$a \sim \sqrt{2}(1 - \kappa^2/16) \qquad \text{and} \qquad w_{s0} = -\kappa/2\sqrt{2} \qquad \text{for } \kappa \ll 1 .$$

For $\kappa = O(1)$ these coupled equations must be solved numerically.

Qualitatively, the limit $\kappa \ll 1$ implies that the middle n-region is sufficiently short so that the difference in the potential between the n^+ and the n-regions is very small. Consequently, a linearization of the potential about $\ln(\lambda_+)$ would have been sufficient to describe the potential in the middle n-region. As a remark, since

$w_0(1/2) = \ln(a^2/2) \gg \ln(\lambda/\lambda_+)$, the assumption $L/L_d \ll \lambda^{-1/2}$ ensures that there cannot be an n-type bulk layer in the middle n-region even when $\kappa \gg 1$. In the other limiting case, $L/L_d \gg \lambda^{-1/2}$ the potential can be constructed by matching local inversion layers near the junctions to a bulk potential in the middle n-region using techniques similar to those to Chapters 2 and 3.

Although the layer structure for this device in equilibrium shows some new asymptotic features, the main interest for the engineer is the construction of the $J = J(V)$ curve when the device is under some external bias. However, the equilibrium problem is not without some relevance since in the study of the p-n junction by Please [23] the layer structure of the potential under external bias generally remains the same as in equilibrium. Therefore, the analysis presented in this section could be a good starting point for the asymptotic derivation of the $J = J(V)$ curve for this device.

CHAPTER 5

The Non-Equilibrium Problem

In this chapter, we shall investigate the flow of electron current tangential to the interface driven by a non-zero source-drain bias $v_{\rm ds}$. As in all analytical modeling of the MOSFET under moderate source-drain biases, we ignore recombination and the current flow due to holes. Using these assumptions in the scaled governing equations (1.5) presented in Chapter 1, we obtain

$$\tilde{\nabla}^2 w = \frac{1}{\lambda}(e^{(w-\phi_n)\ln\lambda} - e^{-w\ln\lambda}) + d(x)\,, \tag{5.1a}$$

$$\tilde{\nabla}^2\phi_n + \tilde{\nabla}\phi_n \cdot \left(\frac{\tilde{\nabla}\mu_n}{\mu_n} + \ln\lambda\,\tilde{\nabla}(w-\phi_n)\right) = 0\,, \tag{5.1b}$$

$$\mathbf{J}_n = -\frac{kTn_i\mu_{nc}}{L_{\rm d}}(\lambda\ln\lambda)^{1/2}\mu_n\, e^{(w-\phi_n)\ln\lambda}\,\tilde{\nabla}\phi_n\,. \tag{5.1c}$$

The scaling factor for the current density vector $\mathbf{J}_n = (J_{n_{x_1}}, J_{n_{x_2}})$ is expressed in the original variables. The boundary conditions on the quasi-Fermi electron potential in the rectangular region BCGH are

$$\phi_n = 0 \;\text{ on } y = 0 \quad\text{and}\quad \phi_n = \frac{\bar{v}_{\rm ds}}{\ln\lambda} \;\text{ on } y = 1\,, \tag{5.2a}$$

$$\frac{\partial\phi_n}{\partial x} = 0 \;\text{ on } x = 0 \quad\text{and}\quad \frac{\partial\phi_n}{\partial x} = 0 \;\text{ on } x = x^*\,, \tag{5.2b}$$

where x^* is the scaled depth of the n-well reservoirs of the source and drain and $\bar{v}_{\rm ds} = v_{\rm ds}/v_{\rm th}$.

The effect of recombination and its associated length scale depending on the carrier lifetimes normally allows an equilibrium boundary condition of $\phi_n = 0$ as $x \to \infty$ to be satisfied. However, since we are ignoring recombination, an equilibrium boundary condition at infinity for the quasi-Fermi potential is not appropriate. Instead, we impose that the current flux normal to the interface vanishes at the depth of the n-well reservoir x^*, which is typically larger than the depletion width normal to the interface. This boundary condition is reasonable

since for large doping the electric field is neglibible for distances normal to the interface larger than the depletion width.

The device behavior observed under normal operating conditions is a consequence of the interaction of the internal electric field on the electron transport equation. However with these model assumptions complicated physical effects such as impact ionization, which require the solution of both transport equations with various recombination mechanisms, are not covered here. Our main interest is focused on the coupling of the electron transport equation with the electric field established by the Poisson equation. The one-dimensional asymptotic equilibrium potential constructed in Chapters 2 and 3 is essential to the success of the analysis. Before beginning the analysis, a definition of the source-drain current is given.

By integrating the current density parallel to the interface over the active channel cross section and averaging over the channel length, we arrive at the definition of the source-drain current

$$I_{\rm ds} = -\int_0^1 \left(\int_0^{x_1^*} J_{n_{x_2}}\, dx_1 \right) dy\,. \tag{5.3}$$

This is the standard definition found in the literature. In the above expression, we have assumed a unit width perpendicular to the plane of the MOSFET. Using the current density given by (5.1c) and changing to (x, y) variables, (5.3) becomes

$$I_{\rm ds} = I_{\rm c} \int_0^1 \left(\int_0^{x^*} \ln\lambda \frac{\partial \phi_n}{\partial y} \mu_n \left(\frac{\ln\lambda}{\lambda} \right)^{1/2} e^{(w-\phi_n)\ln\lambda}\, dx \right) dy\,, \tag{5.4}$$

where $I_{\rm c} = kTn_i\mu_{nc}L_{\rm d}/L$.

We begin the analysis by seeking a regular perturbation expansion of the potential and the electron quasi-Fermi potential in the middle of the channel in the form

$$\begin{aligned} w(x,y) &= w^0(x,y) + \varepsilon^2 w^1(x,y) + \cdots\,, \\ \phi_n(x,y) &= \phi_n^0(x,y) + \varepsilon^2 \phi_n^1(x,y) + \cdots\,. \end{aligned}$$

In addition, we assume that the mobility model is a known function of both x and the partial derivative in the channel-wise direction of the electron quasi-Fermi

potential:

$$\mu_n = \mu_n(x, \frac{\partial \phi_n^0}{\partial y}) > 0 .$$

Substitutng the regular perturbation expansion into $(5.1a, b)$ and equating powers of ε yields to leading order

$$\frac{\partial^2 w^0}{\partial x^2} = \frac{1}{\lambda}(e^{(w^0 - \phi_n^0)\ln\lambda} - e^{-w^0 \ln\lambda}) + d(x) , \tag{5.5a}$$

$$\frac{\partial^2 \phi_n^0}{\partial x^2} + \left(\frac{1}{\mu_n^0}\frac{\partial \mu_n^0}{\partial x} + \ln\lambda(\frac{\partial w^0}{\partial x} - \frac{\partial \phi_n^0}{\partial x}) \right) \frac{\partial \phi_n^0}{\partial x} = 0 , \tag{5.5b}$$

where μ_n^0 is the leading order term in the expansion of the mobility. At first sight, these leading order ordinary nonlinear differential equations appear formidably coupled. However, the boundary conditions on the electron quasi-Fermi potential $(5.2b)$ effectively uncouples this system. In fact, these boundary conditions imply that the leading order electron quasi-Fermi potential depends only on y, i.e.,

$$\phi_n^0 \equiv \phi_n^0(y) \quad \text{only} .$$

Thus most of the electron current flow is tangential to the interface regardless of the leading order electric field established by the Poisson equation. Using the form of the leading order electron quasi-Fermi potential, the second order equation in the expansion of the electron transport equation becomes

$$\begin{aligned} \frac{\partial^2 \phi_n^1}{\partial x^2} + \left(\frac{1}{\mu_n^0}\frac{\partial \mu_n^0}{\partial x} + \ln\lambda \frac{\partial w^0}{\partial x} \right) \frac{\partial \phi_n^1}{\partial x} = B(x, \phi_n^0) \equiv \\ - \left[\phi_n^{''0} + \left(\frac{1}{\mu_n^0}\frac{\partial \mu_n^0}{\partial y} + \ln\lambda\,(\frac{\partial w^0}{\partial y} - \phi_n^{'0}) \right) \phi_n^{'0} \right] , \end{aligned} \tag{5.6}$$

where the primes on the leading order electron quasi-Fermi potential denote total derivatives with respect to y.

Notice that the second order equation for the electron quasi-Fermi potential requires knowledge of only the leading order potential. Therefore, this perturbation expansion in ε can be interpreted as a one step analytical implementation of Gummel's iterative algorithm [16] that is commonly used in numerical device simulation. Briefly, in Gummel's algorithm, an initial guess of the electron quasi-Fermi potential is made, and then the potential is computed from the Poisson

the equation for the leading order potential, we can easily construct asymptotic expansions for the potential as $\lambda \to \infty$ for various ranges of gate bias. This is accomplished by extending the results obtained in the study of the equilibrium potential in Chapters 2 and 3. These asymptotic expansions of w^0 as $\lambda \to \infty$ for various gate bias ranges and doping profiles will be used in (5.9) to determine the BVP for ϕ_n^0 to be solved in many special cases.

The boundary conditions associated with (5.9) on the outer solution ϕ_n^0 used in this chapter are

$$\phi_n^0(0) = 0 \quad \text{and} \quad \phi_n^0(1) = \frac{\bar{v}_{\rm ds}}{\ln \lambda}. \tag{5.15}$$

In contrast to the potential, boundary layers in ϕ_n are not anticipated near the source and drain. However, the use of (5.15) necessitates computing the potential in the inner regions in order to determine both the differential equation for ϕ_n^0, given by (5.9), and the amount of source-drain current. Since the potential is not known analytically near the source and drain, a different approach is required in these regions to solve for ϕ_n^0. This problem is examined in Chapter 6.

In conventional GCA modeling to determine device characteristics, the boundary conditions (5.15) are employed and the inner regions near the source and drain are neglected. It has been noted by Brews[5] that, with this approach, the source-drain bias $\bar{v}_{\rm ds}$ is not the bias applied on the drain contact, but rather should be interpreted as the bias a few depletion widths away from the drain. In adhering to this interpretation in this chapter, we shall determine ϕ_n^0 and closed form expressions for the device characteristics in many bias regimes.

5.1 Subthreshold Current Flow

In the subthreshold case there is a small leakage current upon application of a source-drain bias. The subthreshold case for the enhancement device corresponds to a device operating in the weak inversion regime. Likewise, for a built-in channel device the subthreshold case corresponds to a device operating in the full depletion mode. In both of these cases the gate voltage is below threshold near the source. Since $\phi_n^0 \approx 0$ near the source and $\phi_n'^0(y) > 0$, the contribution to the space charge density of the mobile carriers as $\lambda \to \infty$ in (5.5a) can be neglected throughout the middle of the channel. This implies that w^0 and, hence, the surface potential is independent of ϕ_n^0 as $\lambda \to \infty$ in the middle of the channel. Therefore, for a device

operating under subthreshold conditions, the potential for non-zero source-drain bias is given by the equilbrium potential. In addition, the surface potential in the middle of the channel remains constant and can be determined numerically as a function of the gate voltage as in Chapters 2 and 3. We now determine ϕ_n^0 and the device characteristics in both subthreshold cases.

Enhancement device - weak inversion. Since w^0 is independent of ϕ_n^0 in the middle of the channel, the BVP for ϕ_n^0 from (5.9) for constant mobility reduces asymptotically for $\ln\lambda \gg 1$ to

$$\phi_n^{''0} - \ln\lambda\,(\phi_n^{'0})^2 = 0\,. \tag{5.16}$$

The solution to (5.16) satisfying (5.15) is simply

$$\phi_n^0(y) = -\frac{1}{\ln\lambda}\ln\left(1-(1-e^{-\bar{v}_{\rm ds}})y\right). \tag{5.17}$$

To determine the device characteristics for constant mobility, $\mu_n^0 \equiv 1$, we notice

$$\ln\lambda\, e^{-\phi_n^0\ln\lambda}\phi_n^{'0} = (1-e^{-\bar{v}_{\rm ds}})\,,$$

so that substituting this expression in (5.12), the source-drain current then becomes

$$I_{\rm ds} \sim I_{\rm c}\,(1-e^{-\bar{v}_{\rm ds}})\int_0^{x^*}\left(\frac{\ln\lambda}{\lambda}\right)^{1/2} e^{w^0\ln\lambda}\,dx \quad \text{as } \varepsilon\to 0\,. \tag{5.18}$$

Finally, we recall this integral was evaluated asymptotically in weak inversion for variable doping in Chapter 2. Using (2.36), we conclude,

$$I_{\rm ds} \sim I_{\rm c}\,\frac{(1-e^{-\bar{v}_{\rm ds}})e^{w_s\ln\lambda}}{(\lambda\ln\lambda)^{1/2}\,|a|}\left(1+\frac{1}{a^2\,\ln\lambda}\right) \quad \text{as } \lambda\to\infty,\ \varepsilon\to 0\,,$$

where $a = a(\bar{v}_{\rm gs})$ and $w_s = w_s(\bar{v}_{\rm gs})$ were determined in Chapter 2.

We notice that for small source-drain biases $I_{\rm ds}$ is linear in $\bar{v}_{\rm ds}$ (ohmic behavior), whereas $I_{\rm ds}$ saturates for large biases (non-ohmic behavior). The effect of channel length modulation where the current has a more complicated dependence on the source-drain bias is not discussed in this thesis. A plot of $I_{\rm ds}$ versus $\bar{v}_{\rm ds}$ for various subthreshold gate biases are shown in Figure 5.1. The transfer characteristics, $I_{\rm ds}$ versus $\bar{v}_{\rm gs}$, is shown in Figure 5.2for several source-drain biases.

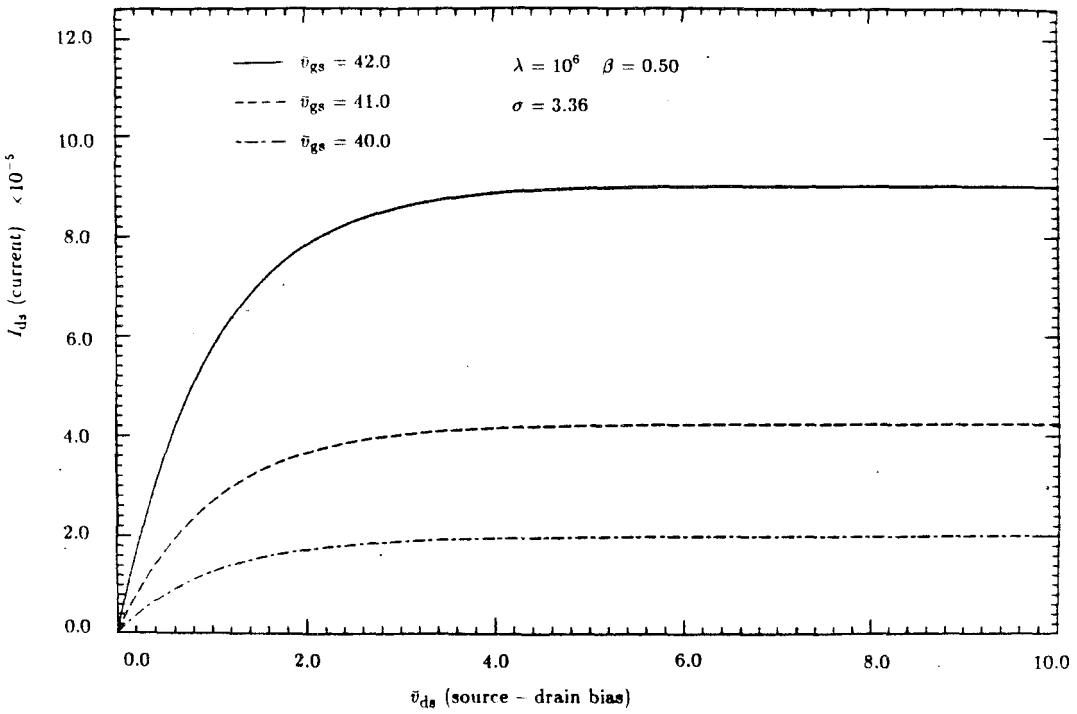

FIGURE 5.1. Current Versus Drain Bias in Weak Inversion for Various Gate Biases

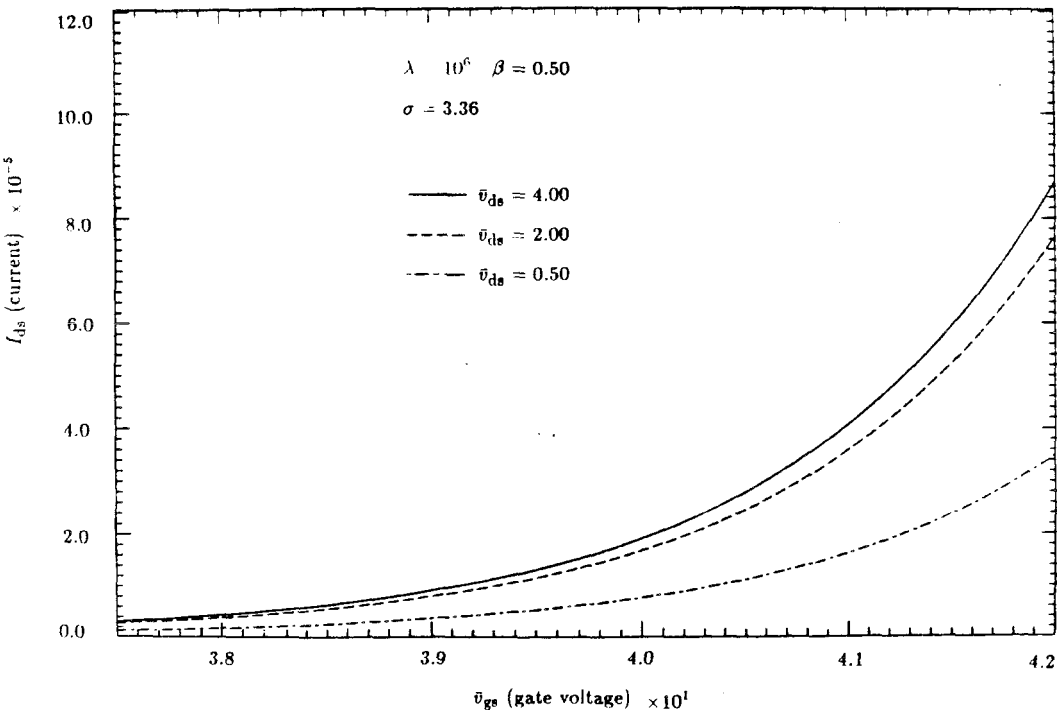

FIGURE 5.2. Current Versus Gate Bias in Weak Inversion for Various Drain Biases

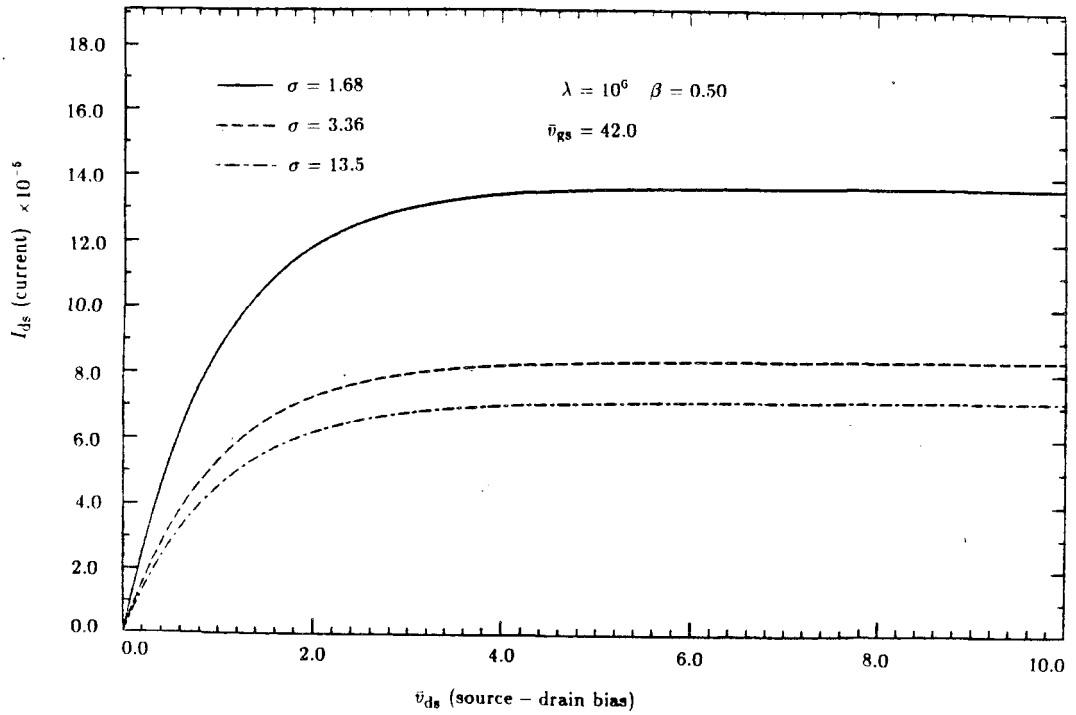

FIGURE 5.3. Current Versus Drain Bias in Weak Inversion for Various Straggles

Finally, a plot of $I_{\rm ds}$ versus $\bar{v}_{\rm ds}$ for fixed gate voltage but for various straggles σ of the implant is shown in Figure 5.3. Since from Figure 2.8, the electron concentration near the interface is smaller for larger σ, the leakage current for given source-drain bias under subthreshold conditions is also smaller for larger σ. In addition, numerical evidence suggests that the subthreshold leakage current is a concave function of the straggle. Finally, we remark that our results can also be generalized for doping profiles with non-zero projected range.

With constant doping the asymptotic expansion of the integral as $\lambda \to \infty$ of the integral in (5.18) takes a simpler form. In constant doping, we recall from Chapter 2 that $a = -(2(1 + w_s - 1/\ln\lambda))^{1/2}$, and therefore using the one term expansion for the mobile charge, we find

$$I_{\rm ds} \sim I_{\rm c} \frac{(1 - e^{-v_{\rm ds}})e^{w_s \ln\lambda}}{(2(w_s + 1 - 1/\ln\lambda)\lambda \ln\lambda)^{1/2}} \quad \text{as } \lambda \to \infty,\ \varepsilon \to 0\,.$$

This constant doping subthreshold current is in agreement with the result based on the conventional GCA derived by Barron [4].

Since the potential for $\lambda \gg 1$ does not depend on y in the channel, the flow of current in the subthreshold case is due to diffusion and not drift. Finally,

substituting (5.16) into (5.14) and assuming constant mobility, we notice that there is no current flow normal to the interface in the middle of the channel in the subthreshold case.

Built-in channel device - full depletion. The leakage current associated with an abrupt junction built-in channel device operating in the full depletion mode is obtained in a similar manner. Recalling the expression for the source-drain current with constant mobility under subthreshold conditions (5.18), and using the asymptotic evaluation of the mobile charge (3.11) derived in Chapter 3, we find

$$I_{\rm ds} \sim I_{\rm c}\,(1 - e^{-v_{\rm ds}}) e^{(w_s + x_m^2/2)\ln\lambda} \left(\frac{\pi}{2\lambda}\right)^{1/2} \left[1 + \mathrm{erf}(x_m (\ln\lambda/2)^{1/2})\right]$$

as $\lambda \to \infty$, $\varepsilon \to 0$, where $x_m = 2x_0 - 2(1 + w_s + x_0^2 - 1/\ln\lambda)^{1/2}$. From the total charge the surface potential can be computed numerically for given gate voltage and junction depth x_0 as discussed earlier.

Since we have neglected the potential in the inner regions, the source-drain current in the full depletion mode has a similar exponential dependence on the source-drain bias as does the enhancement device in weak inversion. The device characteristics $I_{\rm ds} = I_{\rm ds}(\bar{v}_{\rm ds}, \bar{v}_{\rm gs})$, in the full depletion mode can also be computed as in the weak inversion case.

Extensions to a class of mobility models: A Non-existence Result. For mobility models of the form

$$\mu_n^0 = \mu_n^0(\phi_n'^0)\,, \tag{5.19}$$

the equation for ϕ_n^0 from (5.9) reduces asymptotically for $\ln\lambda \gg 1$ to

$$\phi_n''^0 - \ln\lambda\,(\phi_n'^0)^2 + \phi_n'^0 \frac{\partial}{\partial y} \ln\mu_n^0 = 0\,, \tag{5.20}$$

with boundary conditions (5.15). In this subthreshold case, a first integral of (5.20) is

$$\mu_n^0\, e^{-\phi_n^0 \ln\lambda} \phi_n'^0 = c\,, \tag{5.21}$$

where c is some constant proportional to the source-drain current that is determined by the boundary conditions.

A class of models for silicon that semi-empirically predicts the dependence of the mobility on the field is

$$\mu_n^0 = \frac{1}{(1+\theta(\phi_n'^0)^m)^{1/m}}\,. \tag{5.22}$$

From this expression, we notice that for high fields the mobility decreases and becomes strongly field dependent. This decrease in mobility leads to saturation of the drift velocity and consequently a smaller source-drain current. Typically, m ranges between 1 and 3, and the positive scaled constant θ is less than unity in various investigations. This mobility model is widely used in numerical device simulation [29] for modeling the saturation of drift induced current.

However, in most numerical simulations, the operating regime of the device for given biases is not known *a priori*. It may happen that the mobility model (5.22) is used in regions of the device where the current flow is dominated by diffusion and not drift. For instance, this can occur in strong inversion after pinchoff is attained in the channel. Even though under subthreshold conditions the current flow is due almost entirely to diffusion, we shall investigate the implications of using such mobility models in numerical simulations in regions dominated by diffusion current. In particular, we will show that for fixed $\bar{v}_{ds} > 0$ and for positive integers m, there is no solution to (5.20) for θ sufficiently large. We begin by examining some qualitative properties of the solution to (5.20) with boundary conditions (5.15) under the mobility model (5.22).

With this class of mobility models, (5.20) becomes

$$\phi_n''^0 - \ln\lambda\left((\phi_n'^0)^2 + \theta\,(\phi_n'^0)^{m+2}\right) = 0\,. \tag{5.23}$$

Using the maximum principle of Protter and Weinberger [26], we note that if a solution to (5.23) exists, then

$$\phi_n^0(y,\theta \geq 0) \leq \phi_n^0(y,\theta = 0)\,.$$

The proof of this result follows from using the solution to (5.23) with $\theta = 0$ as a comparison function. Furthermore, the maximum principle guarantees that if a solution to (5.23) exists, it must be unique. In addition, we note that the electron concentration in the channel is larger when saturation effects become important.

However, as we shall now see, this does not imply that the source-drain current increases with θ.

In order to determine ϕ_n^0 and the device characteristics when saturation effects begin to become important, we use the first integral (5.21). We begin by assuming a small θ expansion in the form

$$\phi_n^0 \equiv v(y) = v_0(y) + \theta\, v_1(y) + \cdots ,$$

$$c = c_0 + \theta\, c_1 + \cdots .$$

The range of validity of the expansion will also be determined. For illustrative purposes we shall assume $m = 2$. The case for other m values is similar. Substituting this expansion into (5.21) and linearizing the exponential by assuming $\theta \ln \lambda \ll 1$ and equating powers of θ, gives the hierarchy of equations:

$$v_0' = c_0\, e^{v_0 \ln \lambda} , \tag{5.24a}$$

$$v_1' = e^{v_0 \ln \lambda} \left(c_1 + \frac{c_0}{2}(v_0')^2 + c_0\, v_1 \ln \lambda \right) . \tag{5.24b}$$

The solution to the leading order equation subject to (5.15) is given by (5.17). The leading order constant c_0 is simply $c_0 = (1 - e^{-\eta_{ds}})/\ln \lambda$. The second order equation in θ can be written in the form

$$v_1' - (v_0' \ln \lambda)\, v_1 = K(c_1, y) ,$$

where

$$K(c_1, y) = v_0' \left(\frac{c_1}{c_0} + \frac{(v_0')^2}{2} \right) .$$

This equation is to be solved subject to $v_1(0) = 0$ and $v_1(1) = 0$. The solution to this problem satisfying $v_1(0) = 0$ is

$$v_1(y) = e^{v_0(\eta) \ln \lambda} \int_0^y K(c_1, \eta)\, e^{-v_0(\eta) \ln \lambda}\, d\eta .$$

The boundary condition at $y = 1$ then implies

$$\int_0^1 K(c_1, \eta)\, e^{-v_0(\eta) \ln \lambda}\, d\eta = 0 ,$$

which determines the unknown constant c_1

$$c_1 = -\frac{c_0}{2} \int_0^1 (v_0')^2\, d\eta .$$

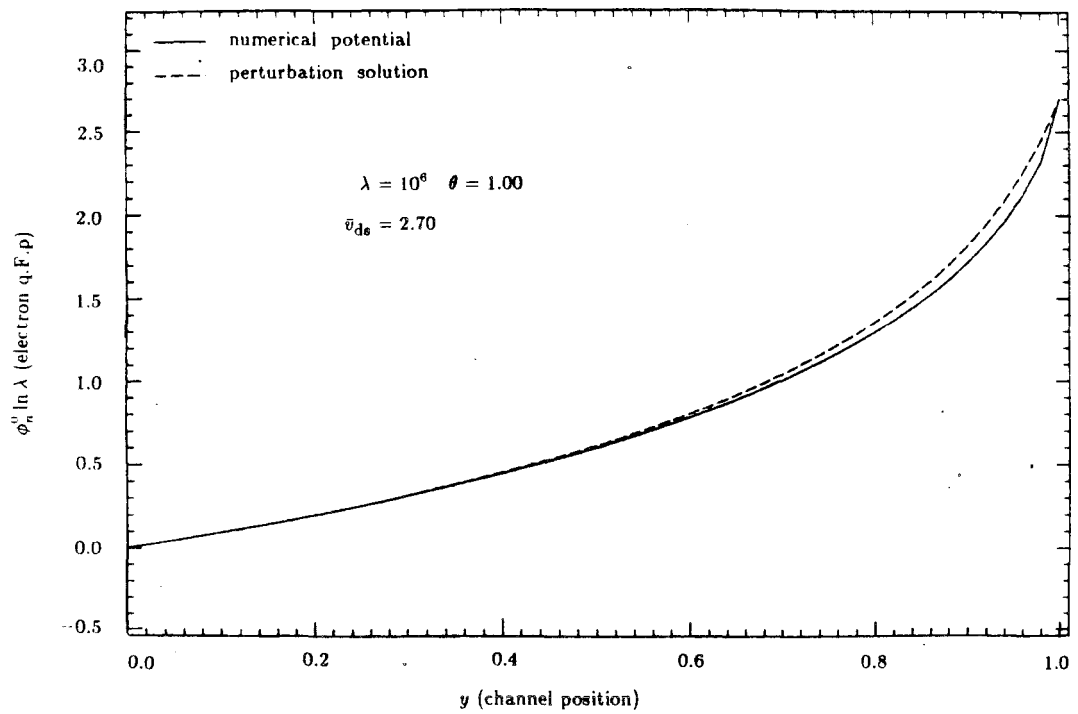

FIGURE 5.4. Electron Quasi-Fermi Potential $\phi_n^0 \ln \lambda$ Comparison

The integrals for c_1 and v_1 can be evaluated explicitly, and after some algebra, we conclude

$$\phi_n^0 \sim -\frac{1}{\ln \lambda} \ln\left(1 - (1 - e^{-\bar{v}_{ds}})y\right) - \frac{\theta\, c_0^3}{2(1-\alpha y)^2} y(1-y)(e^{\bar{v}_{ds}} - 1) \quad (5.25a)$$

$$c \sim c_0\left(1 - \frac{1}{2}\theta\, c_0^2\, e^{\bar{v}_{ds}}\right) \quad \text{as } \theta \to 0\,, \quad (5.25b)$$

where $\alpha = 1 - e^{-\bar{v}_{ds}}$. This expansion is seen to be valid provided that $\theta \ll e^{-\bar{v}_{ds}}/c_0^2$.

Notice that the expansion for $\theta \ll 1$ has a singular point just outside the domain at $y = 1/(1 - e^{-\bar{v}_{ds}}) \approx 1 + e^{-\bar{v}_{ds}}$ for $\bar{v}_{ds} \gg 1$. Therefore, in order to compare our perturbation expansion for $\theta \ll 1$ with the numerical solution to (5.23) with $m = 2$, care must be taken in the numerical scheme to solve the BVP. To avoid numerical difficulties, the exact transformation

$$\phi_n^0 = -\frac{1}{\ln \lambda} \ln\left(1 - (1 - e^{-\bar{v}_{ds}}) f(y)\right)$$

is made in (5.23) to subtract out the near singularity. The resulting BVP for $f(y)$ is then solved by COLSYS [1], and the small θ solution is then obtained by simple continuation from the $\theta = 0$ solution.

A comparison of the numerical and perturbation solutions is shown in Figure 5.4. The agreement between the perturbation solution and the numerical solution is found to be excellent. Using the small θ expansion (5.25*b*) for the first integral of (5.23) with $m = 2$, the source-drain current can easily be obtained. Since $c < c_0$ for $\theta > 0$, we notice that the source-drain current is smaller when saturation effects become important.

We now investigate the existence of solutions to (5.23) for arbitrary $\theta > 0$ and for various exponents m. In particular, it will be shown that for $\lambda > 1$, $\bar{v}_{\rm ds} > 0$ and $m > 0$ there is no solution to (5.23) for θ sufficiently large. The result is established chiefly from graphical considerations. An intuitive argument that illustrates the possible non-existence of solutions for θ large is based on (5.21). Assuming $\theta \gg 1$ and using

$$\mu_n^0 = \frac{1}{(1+\theta(\phi_n'^0)^m)^{1/m}} \sim \frac{1}{\theta}(\phi_n'^0)^{-1}\,,$$

(5.21) implies $e^{-\phi_n^0 \ln\lambda} \sim c\theta$ on the interval $y \in [0,1]$, which is clearly incompatible with the boundary conditions on ϕ_n^0.

To obtain some detailed quantitative information, we examine the first integral (5.21) more closely. Assuming $\theta\, c^m\, e^{m\bar{v}_{\rm ds}} < 1$, so that we can solve for $\phi_n'^0$, an equation for $c = c(\theta)$ is readily obtained

$$\int_1^\beta \frac{1}{w^2}(1-\theta c^m w^m)^{1/m}\,dw = c\ln\lambda\,, \quad \text{where} \quad \beta = e^{\bar{v}_{\rm ds}}\,.$$

Setting $w\,\theta^{1/m}\,c = (\sin y)^{2/m}$ and defining $\eta = (\theta c^m)^{1/2}$ then leads to an implicit equation for η on the interval $(0, e^{-m\bar{v}_{\rm ds}/2})$

$$H(\eta) \equiv \eta^{2/m}\int_{y_l}^{y_u}(\cot y)^{1+2/m}\,dy = F(\eta) \equiv \frac{m\,\ln\lambda}{2\,\theta^{1/m}}\eta^{2/m}\,, \tag{5.26}$$

where

$$y_l(\eta) = \sin^{-1}(\eta) \quad \text{and} \quad y_u(\eta) = \sin^{-1}(\eta e^{m\bar{v}_{\rm ds}/2})\,.$$

The factor $\eta^{2/m}$ on both sides of (5.26) is used to ensure that the integral remains bounded as $\eta \to 0$. The question of existence of solutions to the BVP can now be addressed by examining the existence of a root n^* to (5.26) as θ is varied. There can be at most one root as the maximum principle guaranteed that (5.23) has

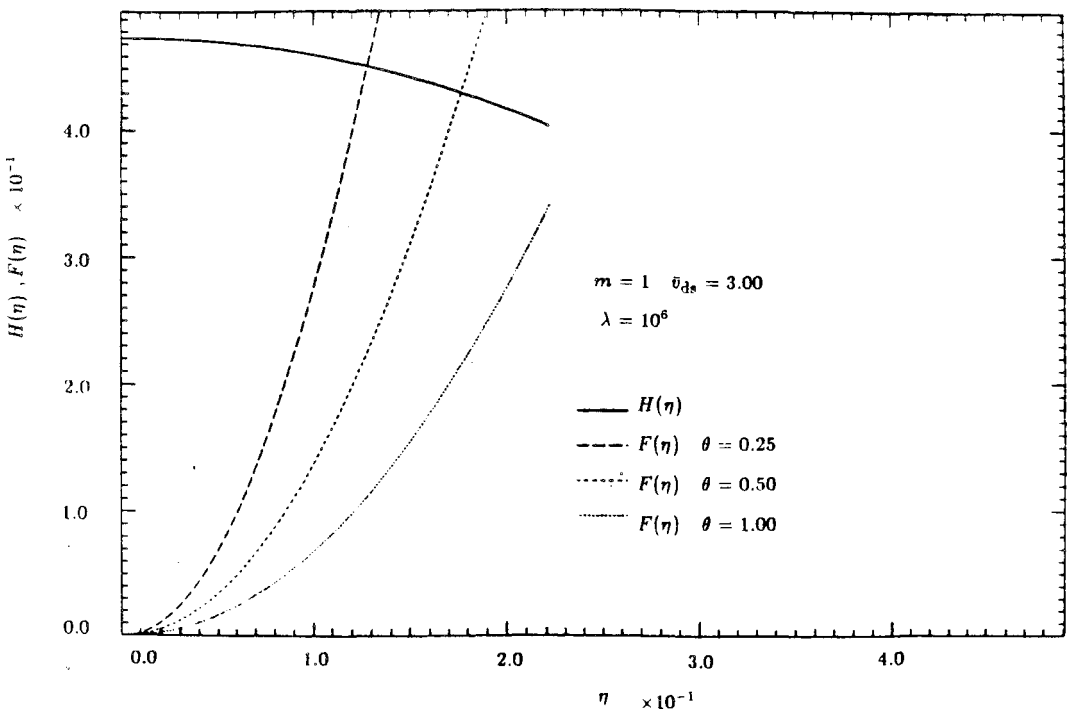

FIGURE 5.5. Plot of Graphical Determination of the Root as θ is Varied

at most one solution. We now determine the root by using both graphical and numerical procedures.

Notice that the integral in $H(\eta)$ can only be evaluated in closed form for $m = 1$ and $m = 2$. The results are

$$H(\eta) = \frac{1}{2}\left((1 - e^{-\bar{v}_{ds}}) - \eta^2 \bar{v}_{ds}\right) , \tag{5.27a}$$

$$H(\eta) = \sqrt{1-\eta^2} - \frac{\sqrt{1 - \eta^2 e^{2\bar{v}_{ds}}}}{e^{\bar{v}_{ds}}} - \eta\left(\sin^{-1}(\eta e^{\bar{v}_{ds}}) - \sin^{-1}(\eta)\right) , \tag{5.27b}$$

for $m = 1$ and $m = 2$, respectively. For general m values, we can evaluate the singular limit in the integral to conclude that as $\eta \to 0$, $H(\eta) \to \frac{m}{2}(1 - e^{-\bar{v}_{ds}})$. The curve $H(\eta)$ versus η must then be determined numerically. We also notice that $H(\eta) > 0$ on its interval of definition for all values of m. This implies that for θ sufficiently large there is no root to (5.26). For illustration, a plot of $H(\eta)$, $F(\eta)$ for $m = 1$ and for various θ values is shown in Figure 5.5.

In addition, some messy algebra shows that $H(\eta)$ is a monotone function of η. Furthermore, the two curves $H(\eta)$ and $F(\eta)$ cannot intersect at a point of tangency in the interior of the interval $(0, e^{-m\bar{v}_{ds}/2})$, as uniqueness would be

violated for nearby θ values. Therefore, the maximum value of θ such that (5.26) has a root is determined from the upper endpoint of the η interval. Specifically, if

$$\theta > \theta_c = \left(\frac{m \ln \lambda \, e^{-\bar{v}_{ds}}}{2 H(e^{-m\bar{v}_{ds}/2})} \right)^m \quad \text{for } \bar{v}_{ds} > 0 , \tag{5.28}$$

there is no solution to the BVP. Using (5.27), the existence boundary in the $(\theta, \bar{v}_{ds})$ plane becomes

$$\theta_c = \begin{cases} \ln \lambda \, \left(e^{\bar{v}_{ds}} - 1 - \bar{v}_{ds} \right)^{-1} & \text{for} \quad m = 1 , \\ (\ln \lambda)^2 \left(e^{\bar{v}_{ds}} \sqrt{1 - e^{-2\bar{v}_{ds}}} + \sin^{-1}(e^{-\bar{v}_{ds}}) - \pi/2 \right)^{-2} & \text{for} \quad m = 2 . \end{cases}$$

Using asymptotics for small and large $\bar{v}_{ds}$ for $m = 1$, we find

$$\theta_c \sim \begin{cases} e^{-\bar{v}_{ds}} \ln \lambda & \text{for} \quad \bar{v}_{ds} \gg 1 , \\ 2 \ln \lambda / \bar{v}_{ds}^2 & \text{for} \quad \bar{v}_{ds} \ll 1 . \end{cases}$$

Similarly, for $m = 2$, we conclude

$$\theta_c \sim \begin{cases} (e^{-\bar{v}_{ds}} \ln \lambda)^2 & \text{for } \bar{v}_{ds} \gg 1 , \\ 9(\ln \lambda)^2 / 8(\bar{v}_{ds})^3 & \text{for } \bar{v}_{ds} \ll 1 . \end{cases}$$

A plot of the existence boundary for $m = 1$ and for $m = 2$ is shown in Figure 5.6. Referring to the graph, the existence boundaries for $m = 1$ and $m = 2$ intersect at some bias value. Therefore, there appears to be no monotonicity result for the existence boundary as a function of m.

In order to determine the device characteristics for fixed large λ, fixed m, and for various fixed θ values, we solve (5.26) for $\eta = \eta(\bar{v}_{ds}, \theta)$ by Newton's method and then use simple continuation in $\bar{v}_{ds}$ from $\bar{v}_{ds} = 0$. The continuation procedure is successful provided that $\bar{v}_{ds}$ remains small enough to ensure $\theta < \theta_c(\bar{v}_{ds})$. Recalling the definition of the current (5.11) and using $c = (\eta^2/\theta)^{1/m}$, the device characteristics can easily be computed for various θ values. In the subthreshold case for $\theta < \theta_c$, we find for variable doping

$$I_{ds} \sim I_c \frac{\ln \lambda \, c(\bar{v}_{ds}, \theta) \, e^{w_* \ln \lambda}}{(\lambda \ln \lambda)^{1/2} |a|} \left(1 + \frac{1}{a^2 \ln \lambda} \right) \quad \text{as } \lambda \to \infty, \ \varepsilon \to 0 .$$

As a remark, the small θ asymptotics of (5.26) with $m = 2$ reproduces the small θ expansion (5.25*b*) derived directly from the differential equation. A plot of the

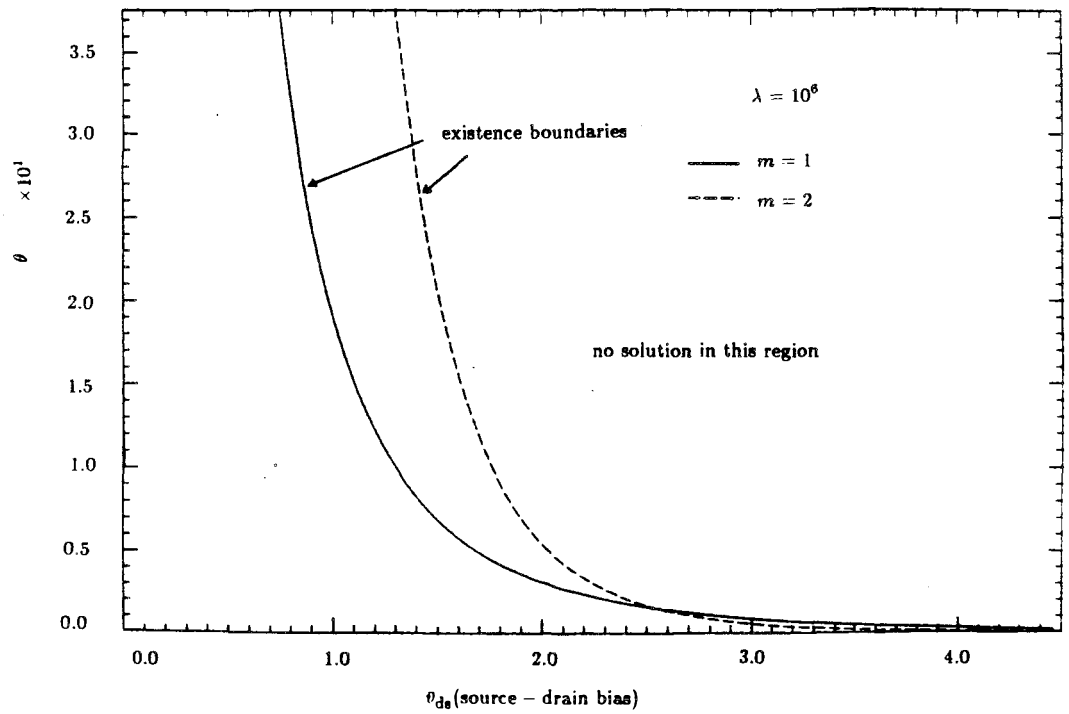

FIGURE 5.6. Existence Boundary in the $(\bar{v}_{ds}, \theta)$ Plane for $m = 1, 2$

device characteristics for $m = 1$ and for various θ values is shown in Figure 5.7. As anticipated, the source-drain current decreases as θ increases, and the degradation becomes more pronounced at higher source-drain biases.

The non-existence of solutions to (5.23) with fixed θ, m and for sufficiently large source-drain biases suggests that the class of mobility models (5.22) should not be used in regions dominated by diffusion current. It is conjectured that the non-existence of solutions to (5.23) is not an artifact of the perturbation expansion for small ε but instead reflects a similar non-existence of solutions to the full two-dimensional semiconductor equations with arbitrary aspect ratio. Many positive existence results concerning solutions to the full semiconductor equations with various assumptions on the mobility models and recombination processes is provided in Markovich [19]. The assumptions required for his existence theorems exclude mobility models that depend on the quasi-Fermi potentials. Therefore, the non-existence conjecture of solutions to the full semiconductor equations under particular bias ranges for mobility models depending on the quasi-Fermi potential apparently does not contradict any known existence theorems.

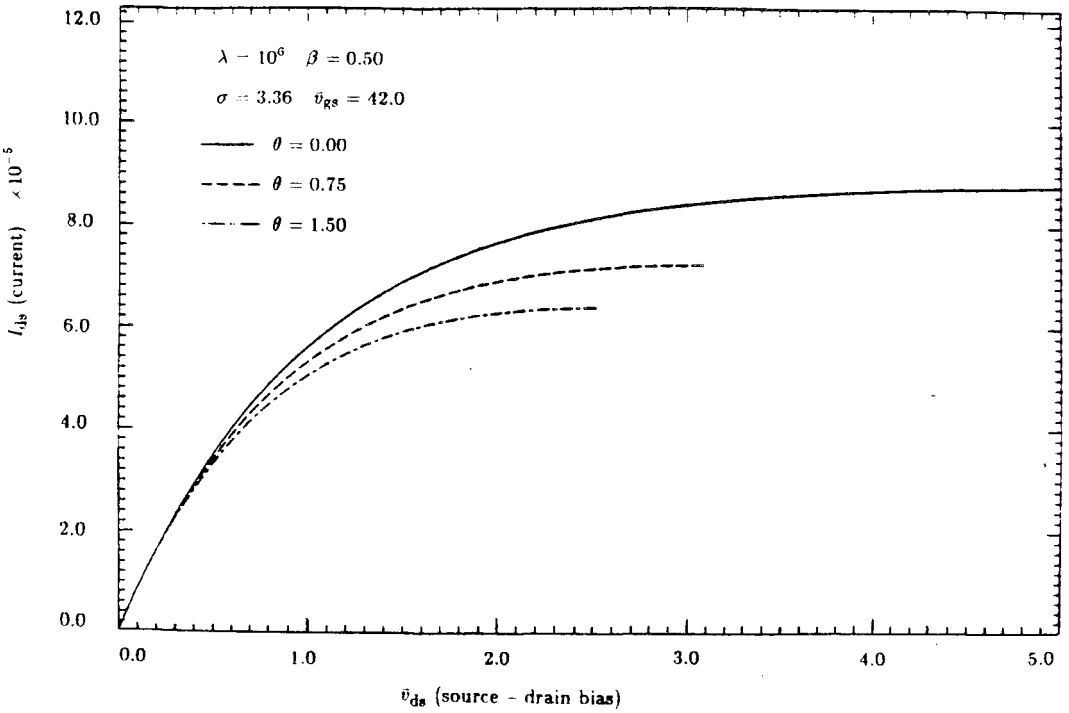

FIGURE 5.7. Device Characteristics for $m = 1$ and for Various θ Values

Since, in numerical simulations, it is not possible, in general, to determine the operating regime *a priori*, the use of a related class of mobility models dependent on the electric field component in the tangential direction, E_y, given by

$$\mu_n^0 = \frac{1}{(1 + \theta(|E_y^0|)^m)^{1/m}} \tag{5.29}$$

is preferable. This class of mobility models is also widely used in numerical simulations. The use of (5.29) guarantees that there is no mobility degradation in regions dominated by diffusion currents since, in those regions, the Poisson equation for large doping in the middle of the channel implies $E_y \approx 0$. As a remark, the electric field component, E_y, reduces to $E_y \sim -\phi_n'^0$ for $\lambda \gg 1$ in the channel region of the built-in channel device operating in the partial depletion mode. However, the use of (5.29) is not without drawbacks, as the mobility variation normal to the insulator for the enhancement mode device in strong inversion is not correctly accounted for.

5.2 Enhancement Device – Linear, Saturation Regimes and Pinchoff

In this section, the enhancement device is analyzed when the dominant con-

tribution for $\lambda \gg 1$ to the space charge density arises from the mobile n-carriers in some region of the channel. It is assumed that at an $O(\varepsilon)$ distance away from the source where $\phi_n^0 = 0$, the gate voltage exceeds threshold. Therefore, for some region of the channel an inversion layer exists, and the mobile electrons drift under the influence of the transverse electric field toward the drain. Depending on the relative magnitude of the gate voltage and the source-drain bias, the inversion layer may extend throughout the channel up to an $O(\varepsilon)$ distance away from the drain. This range of gate voltage and source-drain bias constitutes the linear regime. For other ranges of gate voltage and source-drain bias, the dominant balance for $\lambda \gg 1$ near the interface in the Poisson equation changes at some position y^* along the channel referred to as the pinchoff position. For $y > y^*$, the dominant contribution to the space charge density arises from the fixed impurity ions as the mobile n-carriers are now subdominant for $\lambda \gg 1$ near the interface. In this post-pinchoff region, which is typically quite narrow, the flow of current will be seen to be primarily due to diffusion. This range of gate voltage and source-drain bias constitutes the saturation regime. In this section, we shall determine the electron concentration and the potential throughout the channel in both the linear and saturation regimes under constant mobility but allowing for variable doping. The device characteristics associated with these regimes will also be determined. The extension of these results to a class of variable mobility and recombination models is remarked upon in §5.4.

Before discussing pinchoff in detail, the potential in the inversion layer from (5.5a) for $\lambda \gg 1$ with ϕ_n^0 as parameter can easily be constructed using the asymptotic theory of the potential presented in Chapter 2. Assuming $w_s - \phi_n^0 > 1$ near the source, so that a local inversion layer exists, the potential in this layer for $\lambda \gg 1$ is

$$w_{i0} = 1 + \phi_n^0 + \frac{\ln(\ln\lambda)}{\ln\lambda} + \frac{2}{\ln\lambda}\ln(\alpha_0) - \frac{2}{\ln\lambda}\ln\left(\sinh(\frac{\alpha_0\tilde{x}}{\sqrt{2}} + \gamma)\right) . \qquad (5.30)$$

We have dropped the superscript (0) for the potential, since only the leading order term in the ε expansion will be considered. Matching to the depletion layer in the usual way determines both α_0 and the depletion width x_d. Retaining the same notation as in Chapter 2, we find for constant doping

$$x_d = \sqrt{2}(2 + \phi_n^0 + K(\lambda, w_s, \alpha_0, \phi_n^0) - 1/\ln\lambda)^{1/2} , \qquad (5.31a)$$

$$\alpha_0 = \left(2 + \phi_n^0 + K(\lambda, w_s, \alpha_0, \phi_n^0) - 1/\ln\lambda\right)^{1/2}, \tag{5.31b}$$

where

$$K(\lambda, w_s, \alpha_0, \phi_n^0) = \frac{\ln(\ln\lambda)}{\ln\lambda} + \frac{2}{\ln\lambda}\ln\left(\frac{2\alpha_0}{\alpha + \sqrt{\alpha^2+1}}\right), \tag{5.32a}$$

$$\alpha = \alpha_0 (\ln\lambda)^{1/2} \lambda^{(1-w_s+\phi_n^0)/2} \quad \text{and} \quad \gamma = \sinh^{-1}\alpha. \tag{5.32b}$$

For variable doping, the leading order coupled system of algebraic equations for x_d and α_0 are analogous to those in (2.30a,b) in Chapter 2. These coupled equations are

$$\frac{\beta}{2}x_d^2 + (1-\beta)I_2 = 2 + \phi_n^0 + K(\lambda, w_s, \alpha_0, \phi_n^0), \tag{5.33a}$$

$$\beta x_d - \sqrt{2}\alpha_0 + (1-\beta)I_1 = 0, \tag{5.33b}$$

where the integrals I_1 and I_2 are defined in (2.24). Once the variation of ϕ_n^0 with y has been determined from the differential equation resulting from the Fredholm alternative condition, (5.13), the asymptotic potential in the middle of the channel is known explicitly in terms of x and y.

A significant complication in the analysis arises from the non-negligible transverse electric field established in the oxide as a result of the bias applied on the drain contact. This field implies that the surface potential along the interface varies significantly with the position y along the channel in the linear regime. This transverse electric field results in a drift component to the current density parallel to the interface. To determine the variation of w_s with y along the channel, we must first examine the mixed boundary condition for the potential that holds along the interface. For constant doping, we compare our $\lambda \gg 1$ results with those predicted by the conventional GCA based on the first integral of (5.5a) with ϕ_n^0 as parameter. The mixed boundary condition (2.31) from Chapter 2 for fixed $\bar{v}_{gs}$ is

$$F(w_s, \phi_n^0) \equiv (w_s+1)\ln\lambda - \frac{Q_s(w_s, \phi_n^0)}{c_{ox}} - \bar{v}_{gs} = 0, \tag{5.34}$$

where the total charge $Q_s = Q_s(w_s, \phi_n^0)$ satisfies

$$Q_s = -\sqrt{2}\begin{cases} e^{(w_s-\phi_n^0)\ln\lambda/2}\left(1+\alpha^2\right)^{1/2} & \text{asymptotic,} \\ \left(e^{(w_s-\phi_n^0)\ln\lambda} + e^{-w_s\ln\lambda} + w_s\lambda\ln\lambda + \lambda(\ln\lambda - 1)\right)^{1/2} & \text{GCA,} \end{cases}$$

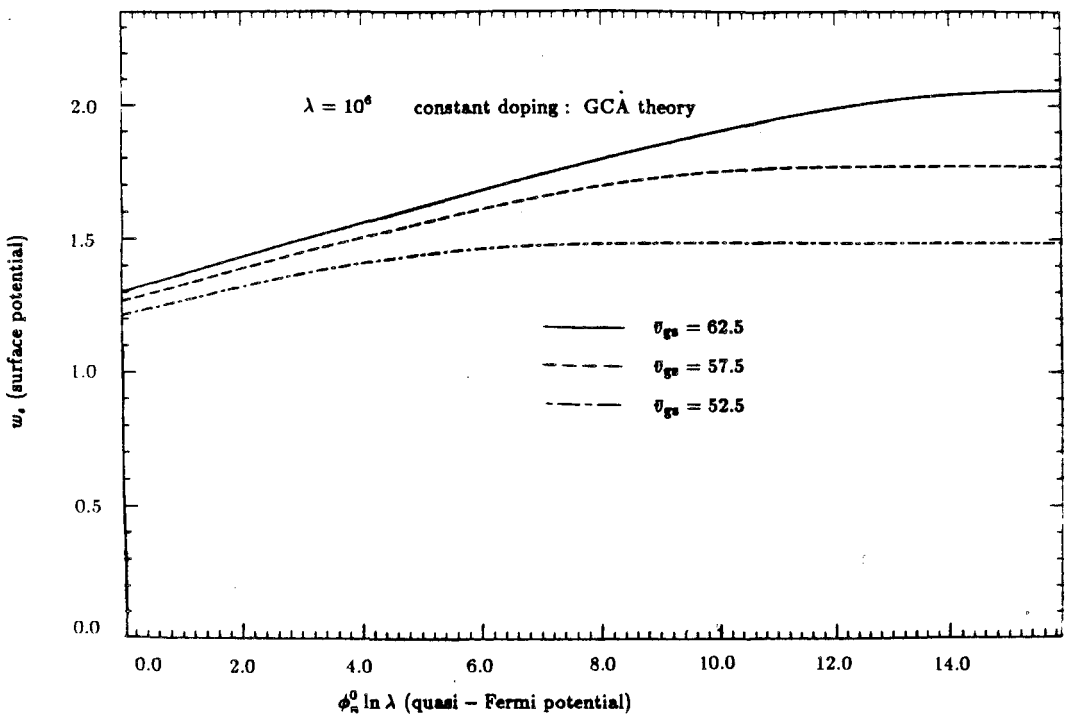

FIGURE 5.8. Surface Potential as a Function of $\phi_n^0 \ln \lambda$ for Constant Doping

and α is given by (5.32*b*). The asymptotic total charge is valid provided that an inversion layer exists, i.e., $w_s - \phi_n^0 > 1$. Once the pinchoff condition $w_s - \phi_n^0 = 1$ for some $y = y^*$ has been attained, the expression for the total charge in weak inversion is used in (5.34).

For fixed gate voltage, (5.34) is solved numerically by Newton's method for $w_s = w_s(\phi_n^0 \ln \lambda)$ using both expressions for the total charge. The results for constant doping using the GCA theory for various gate voltages are displayed in Figure 5.8. The percent error between between the asymptotic and the GCA theories shown in Figure 5.9 is less than .08 for the chosen values of the gate voltage shown on the graph.

To analyze the equation for $w_s = w_s(\phi_n^0 \ln \lambda)$ in both the saturation and linear regimes, we first observe from the conventional GCA result that

$$\frac{\partial w_s}{\partial \phi_n^0} = \frac{e^{(w_s - \phi_n^0) \ln \lambda}}{w_{xx}\,|_{x=0} - c_{ox} Q_s} < 1 \quad \forall \phi_n^0 > 0\,,$$

$$\text{where} \qquad w_{xx}\,|_{x=0} = e^{(w_s - \phi_n^0) \ln \lambda} - e^{-w_s \ln \lambda} + \lambda\,.$$

In particular, deep in the linear regime, defined by $w_s - \phi_n^0 \gg 1 + \ln(\ln \lambda)/\ln \lambda$, the

above expression reduces asymptotically to $w_s' = 1 + O(1/\ln\lambda)$, where the prime denotes a derivative with respect to ϕ_n^0. Therefore, in this limit, w_s varies linearly with ϕ_n^0. Alternatively, for $w_s - \phi_n^0 \ll 1$, we have $w_s' \sim e^{(w_s - \phi_n^0 - 1)\ln\lambda}$, which shows that there is only a transcendentally small increase in w_s with increasing ϕ_n^0 in this limit. This transcendentaly small increase in w_s in the post-pinchoff regime is neglected in the asymptotic theory. Once the variation of ϕ_n^0 with y is known, the surface potential is known throughout the channel. Furthermore, since both $w_s' < 1$ for all $\phi_n^0 > 0$ and $w_s > 1$ near the source, a unique root w_{sp} to $w_s - \phi_n^0 = 1$ is attained for some sufficiently large ϕ_n^0. We now discuss the applicability of the assumption of a one-dimensional potential drop in the insulator.

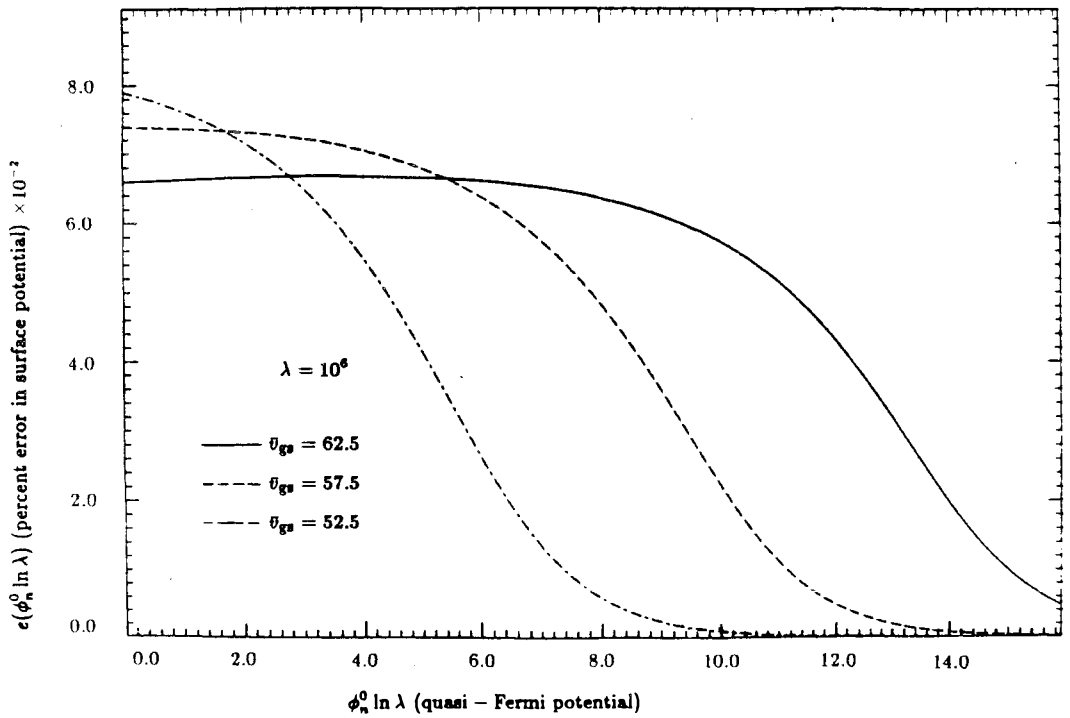

FIGURE 5.9. Error in the Surface Potential Between the GCA and the Asymptotic Theories

In deriving the boundary condition for the potential at the interface, it was assumed that the potential drop in the middle of the oxide was entirely one-dimensional. However, in the linear regime, the surface potential varies with the position along the channel. To resolve this apparent inconsistency, we consider a higher order expansion for the potential in the aspect ratio $d = t_{ox}/L \ll 1$ in the middle of the oxide. Retaining the same notation as in Chapter 1, the outer

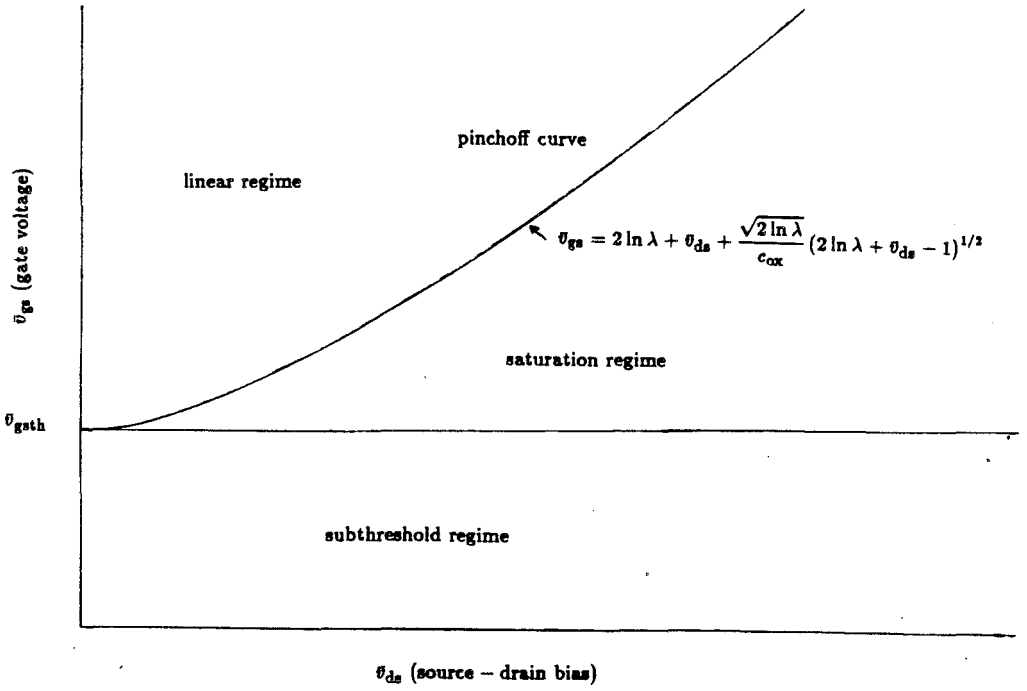

FIGURE 5.10. Control Plane Illustrating the Different Bias Regimes

solution in the oxide to second order in d is

$$\hat{\psi}(\hat{x}, y) = \psi_s(y) - (\bar{v}_{gs} - (\psi_s(y) + \ln\lambda))\hat{x} + d^2\psi_s''(y)(1+\hat{x})\left(1 - (1+\hat{x})^2\right) + \cdots,$$

where $\hat{x} = x_1/t_{ox}$. The expansion is seen to be valid provided that $\psi_s''(y)\, d^2 \ll 1$. For small source-drain biases in the linear regime, the surface potential is roughly linear in y, and thus the above condition is easily satisfied. However, for large transverse fields in the oxide a full numerical approach, coupling the potential in the oxide to the potential in the semiconducting material, is required. This significant complication in the analysis is not covered here.

For fixed gate voltage, the minimum source-drain bias such that pinchoff occurs at the end of the channel can easily be found from the depletion approximation. By definition, pinchoff occurs at the end of the channel when the dominant balance there for $\lambda \gg 1$ changes from strong to weak inversion, i.e.,

$$w_s - \phi_n^0 = 1 \quad \text{at} \quad y = 1 - O(\varepsilon) \quad \text{where} \quad \phi_n^0 = \frac{\bar{v}_{ds}}{\ln\lambda}.$$

Using the mixed boundary condition for the potential that holds along the interface combined with the potential in weak inversion, the pinchoff curve in the $(\bar{v}_{gs}, \bar{v}_{ds})$

plane for constant doping is

$$\bar{v}_{\rm gs} = 2\ln\lambda + \bar{v}_{\rm ds} + \frac{\sqrt{2\ln\lambda}}{c_{\rm ox}}(2\ln\lambda + \bar{v}_{\rm ds} - 1)^{1/2}\,.$$

This curve delineates the boundary between the linear and saturation regimes, as shown in Figure 5.10. A similar relationship can also be found for variable doping.

As a first step to determining the current, we notice that for constant mobility, $\mu_n^0 = 1$, (5.13) reduces to

$$\ln\lambda\phi_n'^0\, e^{-\phi_n^0\ln\lambda}\int_0^{x^*} e^{w^0\ln\lambda}dx = \frac{I_{\rm ds}}{I_{\rm c}}\left(\frac{\lambda}{\ln\lambda}\right)^{1/2}. \tag{5.35}$$

As in Chapter 2, the integral appearing above can be computed asymptotically for $\lambda \gg 1$ using the parametrized potential, w^0, in the inversion layer (5.30). Provided an inversion layer exists, i.e., $w_s - \phi_n^0 > 1$, we have

$$\left(\frac{\ln\lambda}{\lambda}\right)^{1/2}\int_0^{x^*} e^{w^0\ln\lambda}dx \sim \sqrt{2}\,e^{(w_s+\phi_n^0)\ln\lambda/2}\left[(1+\alpha^2)^{1/2} - \alpha\right], \tag{5.36}$$

where α is given by (5.32*b*). In the linear regime, this expression is valid throughout the channel. However, in the saturation regime, the above expression does not apply throughout the channel as we have $w_{sp} \equiv w_s(y^*) = 1 + \phi_n^0(y^*)$ for some y^*. At the pinchoff position y^*, $\alpha = \alpha_0(\ln\lambda)^{1/2} \gg 1$, and thus using $(1+\alpha^2)^{1/2} - \alpha \sim 1/2\alpha$, and assuming constant doping, (5.36) reduces to

$$\left(\frac{\ln\lambda}{\lambda}\right)^{1/2}\int_0^{x^*} e^{w^0\ln\lambda}dx \sim \frac{e^{w_{sp}\ln\lambda}}{\sqrt{2\lambda\,\ln\lambda}\,(1 + w_{sp} - 1/\ln\lambda)^{1/2}} \tag{5.37}$$

in the post-pinchoff region $y > y^*$. Since in the post-pinchoff region the asymptotic potential for $\lambda \gg 1$ is independent of y, the differential equation for ϕ_n^0 given by (5.35) in this region is identical to that studied in the subthreshold regime. Therefore, in the region $y^* < y < 1 - O(\varepsilon)$, the flow of current is due to diffusion.

We now solve the coupled system (5.35), (5.34) for $\phi_n^0(y)$ and $w_s(y)$ and determine the current $I_{\rm ds}$ subject to the boundary conditions $\phi_n^0(0) = 0$ and $\phi_n^0(1) = \bar{v}_{\rm ds}/\ln\lambda$ in both the linear and saturation regimes.

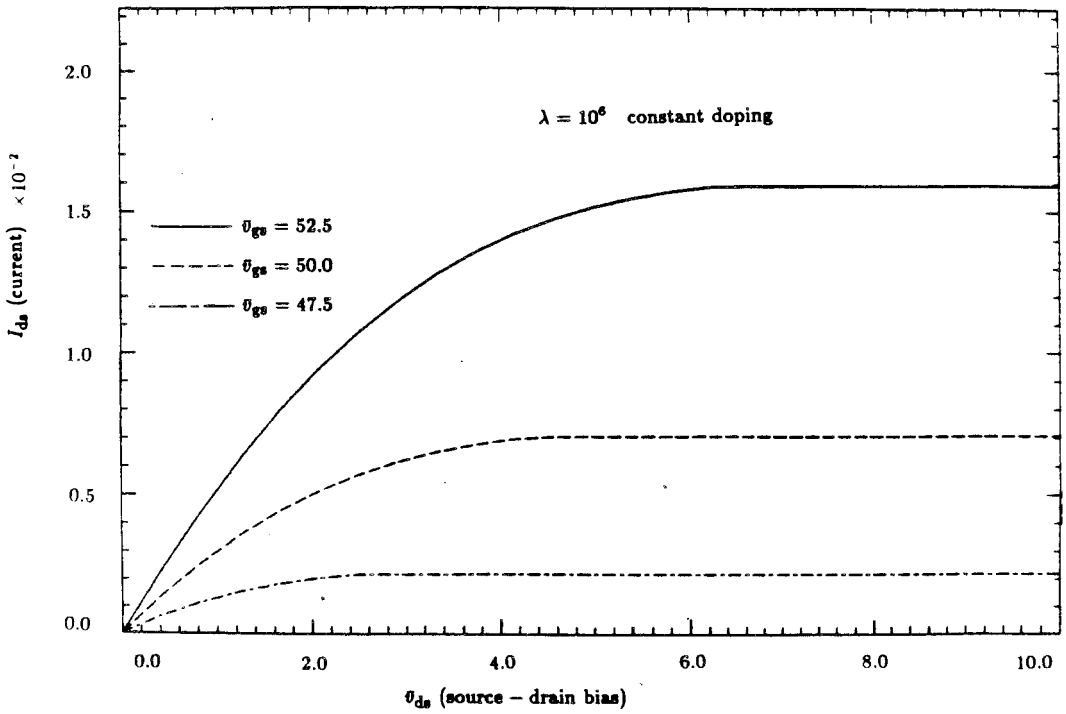

FIGURE 5.11. Current Versus Source-Drain Bias for Constant Doping

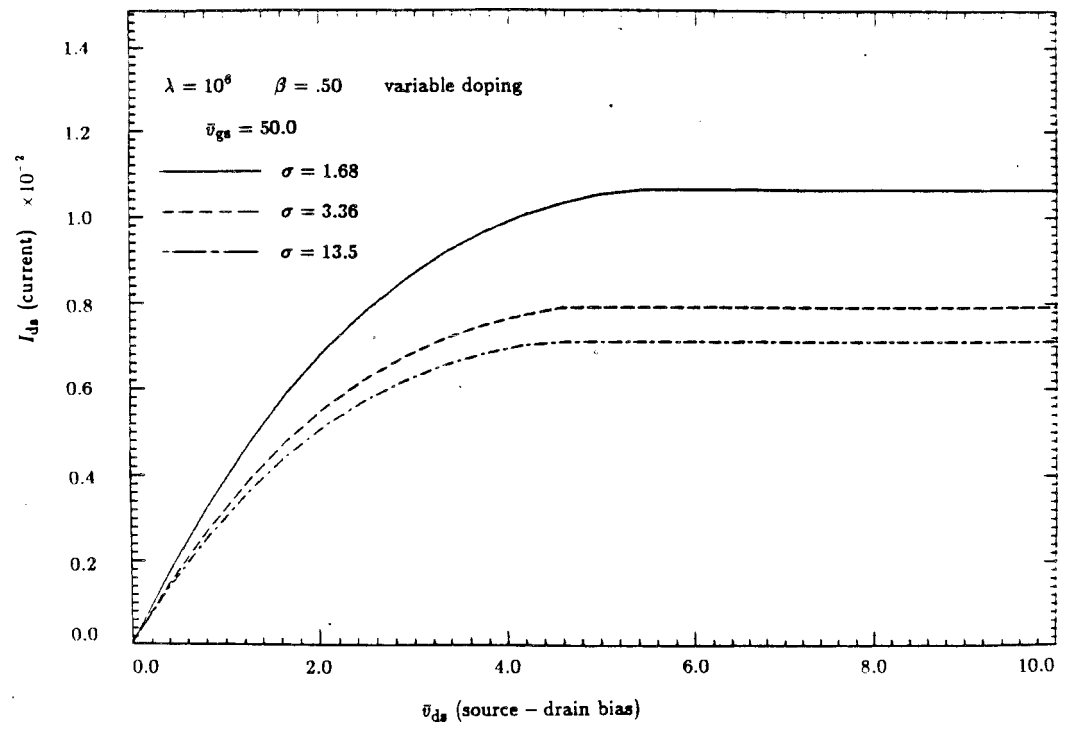

FIGURE 5.12. Current Versus Source-Drain Bias for Variable Doping

Since $\phi_n^{'0} > 0$, it is convenient to consider $y = y(\phi_n^0)$ where from (5.35)

$$I_{\rm ds}\, y'(\phi_n^0) = -I_{\rm c}\, Q_c(w_s(\phi_n^0), \phi_n^0)\, \ln\lambda\,. \tag{5.38}$$

As shown above, the mobile charge, Q_c, is known asymptotically for $\lambda \gg 1$ in the channel in both the linear and saturation regimes. By the implicit function theorem, the surface potential $w_s = w_s(\phi_n^0)$ is found from (5.34) using the asymptotic total charge Q_s, i.e., $F(w_s(\phi_n^0), \phi_n^0) = 0$.

The source-drain current is then found by integrating (5.38) from $\ln\lambda\,\phi_n^0 = 0$ to $\ln\lambda\,\phi_n^0 = \bar{v}_{\rm ds}$;

$$I_{\rm ds} = -I_{\rm c} \int_0^{\bar{v}_{\rm ds}} Q_c(w_s(u/\ln\lambda), u/\ln\lambda)du\,, \tag{5.39}$$

where we use the asymptotic expressions for the mobile charge. The electron quasi-Fermi potential $\phi_n^0(y)$ is then found from the implicit relationship

$$I_{\rm ds}\, y = -I_{\rm c} \int_0^{\phi_n^0} Q_c(w_s(\eta), \eta)\, \ln\lambda\, d\eta\,. \tag{5.40}$$

These integrals are evaluated numerically by Romberg's method as a function of the source-drain bias for various gate voltages. A plot of the current versus source-drain bias for constant channel doping and for various $\bar{v}_{\rm gs}$ is shown in Figure 5.11. From this figure, we notice that as the gate voltage increases the current saturates at larger source-drain biases. This feature is in direct contrast to the subthreshold characteristics. The device characteristics for various straggles in the variable implant are shown in Figure 5.12. As anticipated from the equilibrium problem, the device characteristics in the linear regime are relatively insensitive to variations in the straggle. However, the saturation behavior depends strongly on the parameters characterizing the channel implant.

It is important to emphasize that the pinchoff position, y^*, in the channel is quite insensitive to source-drain biases in the saturation regime. This is owing to the fact that the current increases only marginally once saturation has occurred as the dominant contribution to the mobile charge integral arises from those electrons closer to the source. Thus, the pinchoff region $y^* < y < 1 - O(\varepsilon)$ is, in general, quite thin.

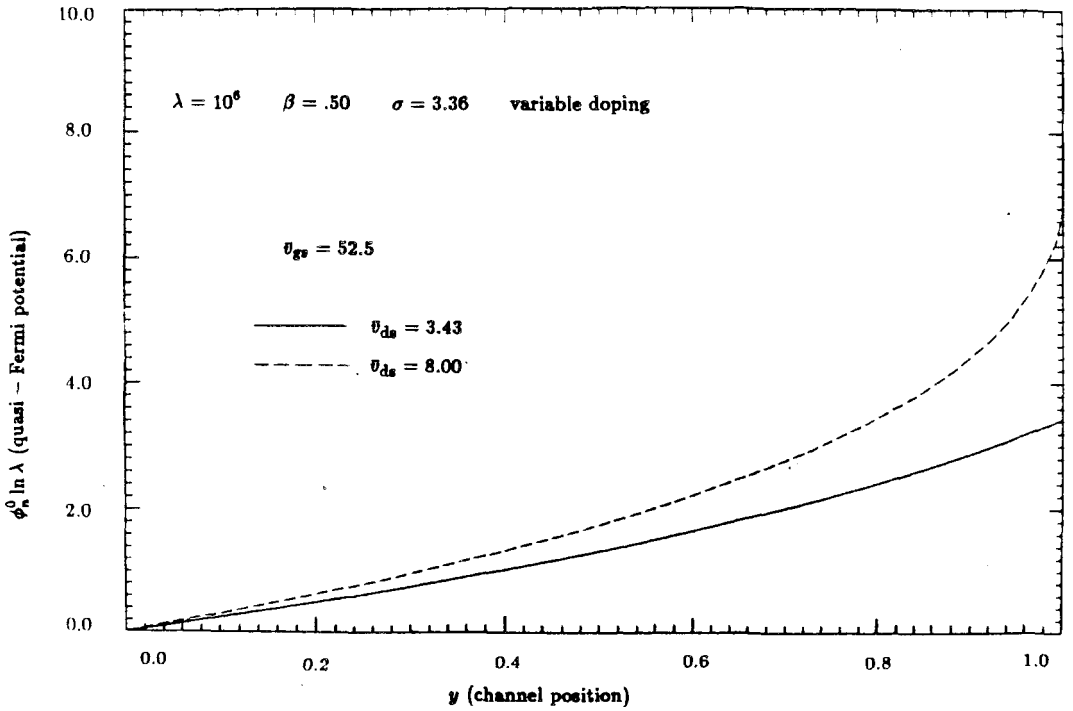

FIGURE 5.13. Electron Quasi-Fermi Potential (Various $\bar{v}_{ds}$)

Using the source-drain current in (5.40), $\phi_n^0 = \phi_n^0(y)$ can be found numerically as a function of y in the channel. A plot of the electron quasi-Fermi potential in the channel for various $\bar{v}_{ds}$ is shown in Figure 5.13. The logarithmic singularity in the electron quasi-Fermi potential just outside the domain that was found in the subthreshold case is also apparent in this case as well. Finally, with $\phi_n^0(y)$ the surface potential $w_s(y)$ and, hence, the parametrized potential $w^0(x, y)$ is known as a function of position in the region $O(\varepsilon) < y < 1 - O(\varepsilon)$.

5.3 Built-in Channel Device – Pinchoff Analysis

Owing to the many gate bias regimes in equilibrium, as seen in Figure 3.3, the pinchoff analysis for the built-in channel device is more complicated than for the enhancement device. The qualitative definition of pinchoff, however, remains the same. Pinchoff occurs in the channel at some $y = y^*$ where the dominant balance in the Poisson equation in the $\lambda \gg 1$ limit changes. Typically the mobile electron concentration dominates the space charge density in some x region for $y < y^*$ but is subdominant everywhere to the impurity concentration for $y > y^*$.

There are several different pinchoff possibilities depending on the relative magnitude of the gate voltage and source-drain bias and the location of the junction depth. For $x_0 \leq \sqrt{2}$, a transition between inversion (small x_0) and full depletion is possible. However, the analysis for this case closely parallels that of the enhancement device and is not considered here. Likewise, for $x_0 > 2 + \sqrt{2}$, a transition between inversion (large x_0) and partial depletion is also possible but is again not considered here. The case that we shall focus on in this section is the transition between partial and full depletion. Pinchoff for this case is defined to occur when the channel width $x_c(y)$ vanishes at some position y^* in the channel.

The potential from (5.5a) in the partial depletion mode for $\lambda \gg 1$ with ϕ_n^0 as a parameter, with the assumption that $x_0 \in (\sqrt{2}, 2 + \sqrt{2})$, is easily constructed using the asymptotic theory of the potential presented in Chapter 3. Assuming the channel width satisfies $x_c > 0$ near the source, and referring to the notation of Figure 3.1, the leading order asymptotic potential for $\ln \lambda \gg 1$ is

$$
\begin{aligned}
w_d(x, \phi_n^0) &= -\frac{1}{2}(x - x_d)^2 + 1 + \phi_n^0 \quad \text{for} \quad 0 \leq x \leq x_d - O((\ln \lambda)^{-1/2}), \\
w_c(x, \phi_n^0) &= 1 + \phi_n^0 \quad \text{for} \quad x_d + O((\ln \lambda)^{-1/2}) \leq x \leq x_{jl} - O((\ln \lambda)^{-1/2}), \\
w_l(x, \phi_n^0) &= -\frac{1}{2}(x - x_{jl})^2 + 1 + \phi_n^0 \quad \text{for} \quad x_{jl} + O((\ln \lambda)^{-1/2}) \leq x \leq x_0, \\
w_r(x, \phi_n^0) &= \frac{1}{2}(x - x_{jr})^2 + 1 \quad \text{for} \quad x_0 \leq x \leq x_{jr} - O((\ln \lambda)^{-1/2}), \\
w_b(x, \phi_n^0) &= -1 \quad \text{for} \quad x_{jr} + O((\ln \lambda)^{-1/2}) \leq x < \infty,
\end{aligned}
$$

where

$$x_d = \sqrt{2}(1 + \phi_n^0 - w_s)^{1/2},$$
$$x_{jl} = x_0 - \sqrt{2 + \phi_n^0},$$
$$x_{jr} = x_0 + \sqrt{2 + \phi_n^0}.$$

As in Chapter 3, there are transition layers connecting the depletion layers to both the channel region and the bulk. The analysis is valid provided $x_c = x_{jl} - x_d > 0$. When pinchoff occurs, $x_c(y^*) = 0$ for some y^*, and thus at this position in the channel, we have

$$w_s = w_{sp} \equiv 1 + \phi_n^0(y^*) - \frac{\left(x_0 - \sqrt{2 + \phi_n^0(y^*)}\right)^2}{2}. \tag{5.41}$$

After pinchoff has occurred, the contribution to the space charge density of the mobile electrons becomes subdominant to the impurities everywhere and thus the potential is given by the potential in the full depletion mode and is consequently independent of ϕ_n^0. Therefore, in this post-pinchoff region $y > y^*$ we have to leading order in $\ln \lambda$

$$w(x) = \begin{cases} -\frac{1}{2}x^2 + x_m x + w_{sp} & \text{for} \quad x < x_0, \\ \frac{1}{2}x^2 - x_j x + (w_{sp} + x_0^2) & \text{for} \quad x > x_0, \end{cases}$$

where $x_j = \sqrt{2}(1 + w_{sp} + x_0^2)^{1/2}$ and $x_m = 2x_0 - x_j$. There is again a transition layer connecting the depletion layer potential furthest from the interface to the bulk.

To invert the $w_s = w_s(\phi_n^0)$ relationship for various $\bar{v}_{gs}$, we first compute the total charge in the two regimes on either side of the pinchoff point. Evaluating the slope at the origin provides

$$Q_s = (\lambda \ln \lambda)^{1/2} \begin{cases} \sqrt{2}(1 + \phi_n^0 - w_s)^{1/2} & \text{for} \quad y < y^*, \\ 2x_0 - \sqrt{2}(1 + w_{sp} + x_0^2)^{1/2} & \text{for} \quad y > y^*. \end{cases} \tag{5.42}$$

From this expression we note that the total charge as a function of the surface potential is continuous but is not differentiable across $w_s = w_{sp}$. The relationship $w_s = w_s(\phi_n^0)$ is then found from the mixed boundary condition

$$F(w_s, \phi_n^0) \equiv (w_s + 1) \ln \lambda - \frac{Q_s(w_s, \phi_n^0)}{c_{ox}} - \bar{v}_{gs} = 0, \tag{5.43}$$

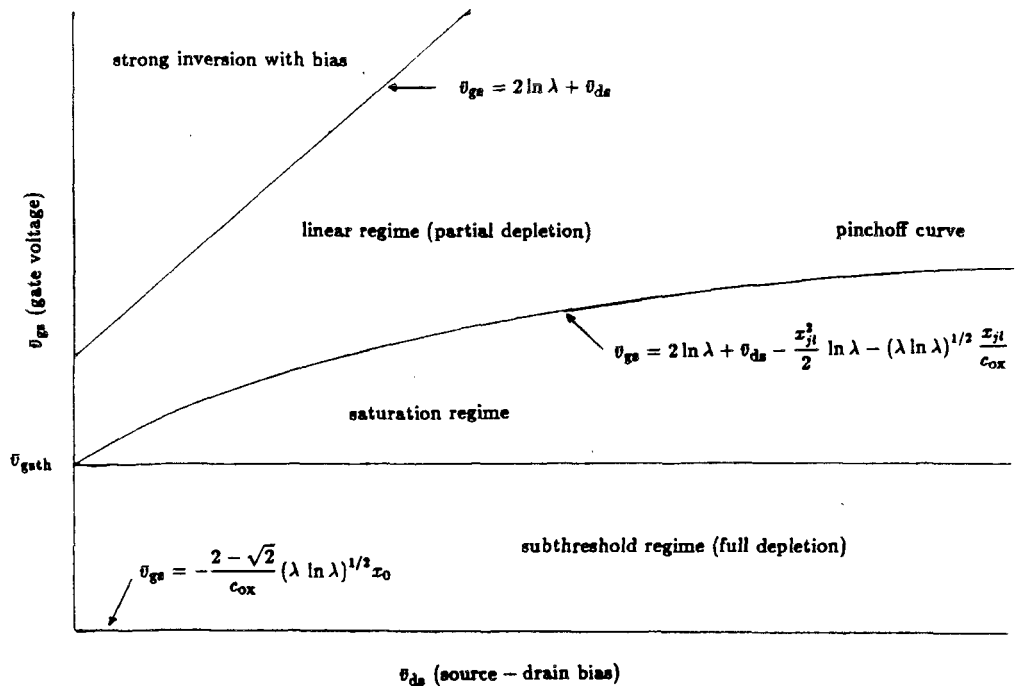

FIGURE 5.14. Control Plane for $x_0 \in (\sqrt{2}, 2+\sqrt{2})$

with Q_s as given in (5.42).

Once again, the condition that pinchoff occurs at the end of the channel gives a curve in the $(\bar{v}_{\rm gs}, \bar{v}_{\rm ds})$ control plane. Setting $\phi_n^0 = \bar{v}_{\rm ds}/\ln\lambda$ in (5.41) and substituting w_{sp} into (5.43) gives the minimum conditions for pinchoff at the end of the channel

$$\bar{v}_{\rm gs} = 2\ln\lambda + \bar{v}_{\rm ds} - \frac{x_{jl}^2}{2}\ln\lambda - \frac{\sqrt{\lambda}}{c_{\rm ox}}x_{jl}(\ln\lambda)^{1/2}.$$

Notice that $x_{jl}(y^*) = x_0 - \sqrt{2+\phi_n^0(y^*)} \geq 0$ since $x_{jl} > x_c$. The boundaries in the $(\bar{v}_{\rm gs}, \bar{v}_{\rm ds})$ control plane for fixed x_0 between full depletion, partial depletion and inversion are shown in Figure 5.14. From this figure, we see that provided $x_0 \in (\sqrt{2}, 2+\sqrt{2})$, pinchoff beween partial depletion and full depletion will always occur at the end of the channel for some sufficiently large $\bar{v}_{\rm ds}$. It is to be noticed that the pinchoff curve between partial and full depletion increases monotonically with increasing x_0 for $x_0 \in (\sqrt{2}, 2+\sqrt{2})$.

To compute the source-drain current, the averaged channel conductivity must be computed asymptotically, as in Chapter 3, using the parametrized potential.

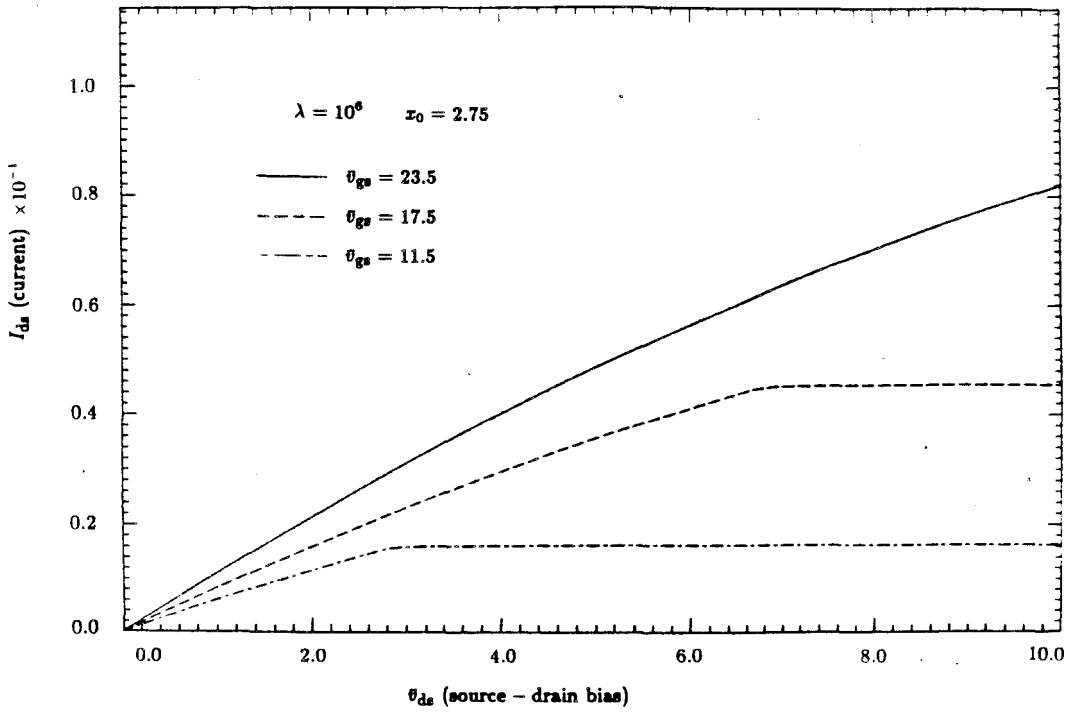

FIGURE 5.15. Current Versus Source-Drain Bias for Various $\bar{v}_{gs}$

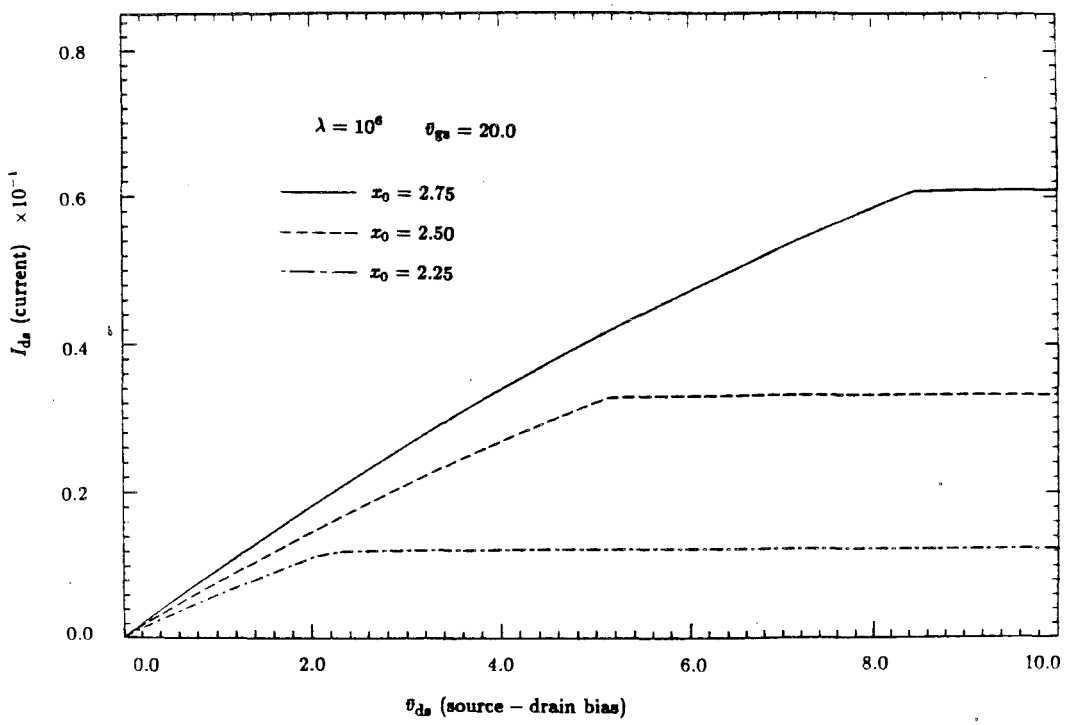

FIGURE 5.16. Current Versus Source-Drain Bias for Various x_0

Defining the mobile charge as usual by

$$Q_c \equiv -\left(\frac{\ln\lambda}{\lambda}\right)^{1/2}\int_0^{x^*} e^{(w-\phi_n^0)\ln\lambda}dx\,,$$

the leading order expansion for $\ln\lambda \gg 1$ to the integral on either side of the pinchoff location provides

$$Q_c \sim -\begin{cases} (\lambda\ln\lambda)^{1/2}x_c + (\pi\lambda/2)^{1/2}\left[1+\mathrm{erf}\left(x_d(\ln\lambda/2)^{1/2}\right)\right] & y < y^*, \\ (\pi\lambda/2)^{1/2}e^{-(\phi_n^0(y)-\phi_n^0(y^*))\ln\lambda}\left[1+\mathrm{erf}\left(x_{jl}(y^*)\,(\ln\lambda/2)^{1/2}\right)\right] & y > y^*. \end{cases}$$

If pinchoff does not occur, the expression for $y < y^*$ is valid throughout the channel. The above two expressions agree asymptotically at the pinchoff location.

Using the asymptotic mobile and total charge, the source-drain current is determined from (5.40) as for the enhancement device. A plot of the source-drain current as a function of $\bar{v}_{\mathrm{ds}}$ for various $\bar{v}_{\mathrm{gs}}$ and x_0 is given in Figures 5.15 and 5.16, respectively. The apparent non-differentiability of the I-V curve at the pinchoff location is due to the non-smooth transition in the surface potential across the boundary between the partial and full depletion regimes discussed earlier in Chapter 3. Finally, using the computed source-drain current, $\phi_n^0(y)$, $w_s(y)$ and hence, the leading order potential $w^0(x,y)$, are easily computed in the channel.

5.4 Extensions

In this section, we briefly discuss the generalization of the asymptotic techniques to include a simple recombination and mobility model. The breakdown of the asymptotic expansions in the middle of the channel for large source-drain biases is also illustrated.

A Simple Recombination Model. In real devices, the lifetimes of carriers are not infinite but are limited by the recombination processes that are prevalent. For current flow dominated by n-carriers under moderate biasing conditions, the model

$$R_n = \frac{n-n_0}{\tau_{\mathrm{n}}}\,, \tag{5.44}$$

where

$\tau_{\mathrm{n}} =$ carrier lifetime for electrons,

$n_0 =$ equilibrium electron concentration,

is often used to discuss the qualitative effect of recombination in other devices. We shall briefly discuss the effect of this simple recombination model on the structure of the solutions to $(5.1a,b)$. The full Shockley-Read-Hall (SRH) recombination model set forth in Chapter 1 is used by Please [23] in his asymptotic study of the one-dimensional diode.

The effect of a bulk recombination model of the form (5.44) in MOSFETs does not significantly alter the behavior of the n-carriers near the interface but rather introduces a length scale of decay onto the equilibrium electron concentration in the bulk. This additional length scale in the problem set by the n-carrier lifetime is, however, in general much larger than the depth of the n-well reservoirs. Consequently, an equilibrium boundary condition of $\phi_n = 0$ on $x = x^*$ is not appropriate, as the asymptotic boundary condition for ϕ_n should instead be imposed at a distance normal to the interface satisfying $x \gg \sqrt{D_n \tau_n}$. The need to impose $\phi_n = 0$ deep in the bulk makes the analysis very difficult, as the geometry of the n-well reservoirs plays an important role in determining the structure of the solutions to the governing equations in the bulk. To circumvent these difficulties, we shall alter the no flux boundary conditions on $x = 0$ and $x = x^*$ to allow for some current flux normal to the interface leaving the rectangular domain BGHC. This simplification is anticipated to give some insight into the effect of bulk and surface recombination for MOSFETs.

The scaled electron transport equation analogous to $(5.1b)$ under (5.44) and for constant mobility is

$$\tilde{\nabla}^2 \phi_n + \ln \lambda \tilde{\nabla} \phi_n \cdot \tilde{\nabla}(w - \phi_n) = \frac{\tau_{\rm rel}}{\lambda \tau_{\rm n}} \left(e^{\phi_n \ln \lambda} - 1 \right), \tag{5.45}$$

where $\tau_{\rm rel} = 1/\omega$ is the dielectric relaxation time defined in Table 1.1. In order to avoid a multi-parameter expansion, we assume $\tau_{\rm rel}/\lambda\, \tau_{\rm n} = O(\varepsilon^2)$ so that (5.45) takes the form

$$\tilde{\nabla}^2 \phi_n + \ln \lambda \tilde{\nabla} \phi_n \cdot \tilde{\nabla}(w - \phi_n) = \theta \varepsilon^2 (e^{\phi_n \ln \lambda} - 1), \tag{5.46}$$

where $\theta > 0$ satisfies $\theta = O(1)$ as $\varepsilon \to 0$. This assumption is not entirely unreasonable, as the n-carrier lifetime can in general depend on the doping level and from the definition of ε, we have $\varepsilon \propto 1/\lambda$.

The boundary conditions imposed on ϕ_n are

$$\begin{aligned} \frac{\partial \phi_n}{\partial x} &= s_n \varepsilon^2 (e^{\phi_n \ln \lambda} - 1) \qquad \text{on } x = 0\,, \\ \frac{\partial \phi_n}{\partial x} &= -\theta \varepsilon^2 (e^{\phi_n \ln \lambda} - 1) \qquad \text{on } x = x^*\,, \end{aligned} \tag{5.47}$$

where $s_n > 0$, referred to as the surface recombination velocity, is assumed to be $O(1)$. The signs of the coefficients θ and s_n are chosen so that some current can leave the box BGHC in the direction perpendicular to the oxide. The analysis that follows is restricted to moderate source-drain biases satisfying $\varepsilon^2 e^{v_{ds}} \ll 1$.

Expanding both

$$\begin{aligned} w(x,y) &= w^0(x,y) + \varepsilon^2 w^1(x,y) + \cdots\,, \\ \phi_n(x,y) &= \phi_n^0(x,y) + \varepsilon^2 \phi_n^1(x,y) + \cdots\,, \end{aligned}$$

and the boundary conditions (5.47) in powers of ε^2, we obtain to leading order the equations $(5.5a,b)$ from which we again conclude $\phi_n^0 \equiv \phi_n^0(y)$ only. Thus the leading order Poisson equation is still parametrized by $\phi_n^0(y)$ as the flow of current is still directed primarily parallel to the interface. The differential equation satisfied by ϕ_n^0 is again determined by a Fredholm alternative condition applied at the next order in the expansion of the electron quasi-Fermi potential. Expanding (5.46) and the boundary conditions to $O(\varepsilon^2)$ and integrating once gives

$$\frac{\partial \phi_n^1}{\partial x} = e^{-w^0(x,\phi_n^0)\ln\lambda} \left[\int_0^x B(\eta, \phi_n^0)\, e^{w^0(\eta,\phi_n^0)\ln\lambda}\, d\eta + s_n (e^{\phi_n^0 \ln\lambda} - 1)\, e^{w_* \ln\lambda} \right], \tag{5.48}$$

where the boundary condition on $x = 0$ has been satisfied and where

$$B(x, \phi_n^0) \equiv -\left[\phi_n^{''0} + \ln\lambda \left(\frac{\partial w^0}{\partial y} - \phi_n^{'0} \right) \phi_n^{'0} - \theta (e^{\phi_n^0 \ln\lambda} - 1) \right].$$

Imposing the boundary condition on $x = x^*$ for ϕ_n^1 and defining $w_*^0 \equiv w^0(x^*, y)$ provides

$$\begin{aligned} \phi_n^{''0} - \ln\lambda\, (\phi_n^{'0})^2 + \phi_n^{'0} \frac{\partial}{\partial y} \ln \left(\int_0^{x^*} e^{w^0(\zeta,\phi_n^0)\ln\lambda} d\zeta \right) \\ = (e^{\phi_n^0 \ln\lambda} - 1) \left[\theta + \frac{(\theta e^{w_*^0 \ln\lambda} + s_n e^{w_* \ln\lambda})}{Q_{c0}} \right], \end{aligned}$$

where Q_{c0} is proportional to the amount of mobile electrons in the channel in equilibrium;

$$Q_{c0} \equiv \int_0^{x^*} e^{w^0 \ln \lambda} d\zeta \, .$$

To obtain some insight into the effect of bulk and surface recombination, we now solve this equation for ϕ_n^0 asymptotically in the weak inversion regime of the enhancement device under constant doping. Since $w_y^0 \approx 0$ and $w_*^0 \sim -1$ in weak inversion, the differential equation for ϕ_n^0 reduces asymptotically for $\lambda \gg 1$ to

$$\phi_n^{''0} - \ln \lambda \, (\phi_n^{'0})^2 = c(e^{\phi_n^0 \ln \lambda} - 1) \quad \text{where} \quad c = c(w_s) \equiv \left[\theta + \frac{s_n e^{w_s \ln \lambda}}{Q_{c0}} \right] .$$

Now, evaluating the mobile charge integral asymptotically in weak inversion with constant doping, we obtain

$$c \sim \theta + \sqrt{2} s_n \, (1 + w_s - 1/\ln \lambda)^{1/2} \ln \lambda \, .$$

Thus since w_s increases with $\bar{v}_{gs}$, the surface currents induced by the surface recombination will be larger for larger gate voltages.

This simplified equation for ϕ_n^0 is easy to solve via the transformation $v = e^{-\phi_n^0 \ln \lambda}$, which gives the linear equation

$$v'' - c \ln \lambda \, v = c \ln \lambda \quad \text{with} \quad v(0) = 1 \text{ and } v(1) = e^{-\bar{v}_{ds}} \, . \tag{5.49}$$

The solution to this equation gives

$$\phi_n^0(y) = -\frac{1}{\ln \lambda} \ln \left(1 + (e^{-\bar{v}_{ds}} - 1) \frac{\sinh(\sqrt{c \ln \lambda} \, y)}{\sinh(\sqrt{c \ln \lambda})} \right) .$$

In the limit $c \ln \lambda \ll 1$, this expression agrees with $\phi_n^0(y)$ in weak inversion with no recombination given previously by (5.17). Alternatively, for large surface recombination such that $c \ln \lambda \gg 1$, a boundary layer of thickness $(c \ln \lambda)^{-1/2}$ exists near the drain. In this limit, an evaluation of the current density vector shows that there are large surface currents normal to the insulator in this region. A similar qualitative analysis can also be performed for other bias regimes.

A Variable Mobility Model. For the class of mobility models (5.22), the expression for the source-drain current (5.13) becomes

$$\frac{\phi_n'^0 \ln\lambda}{(1+\theta(\phi_n'^0)^m)^{1/m}}|Q_c(w_s,\phi_n^0)| = \frac{I_{ds}}{I_c}.$$

Solving for $\phi_n'^0$ then gives

$$\ln\lambda\,\phi_n'^0 = \frac{I_{ds}}{I_c|Q_c|}\left((\ln\lambda)^m - (\frac{I_{ds}}{I_c})^m \frac{\theta}{(\ln\lambda)^m|Q_c|^m}\right)^{-1/m}.$$

Integrating along the channel, the current is then found to satisy the nonlinear algebraic equation

$$N(\frac{I_{ds}}{I_c}) \equiv \int_0^{\bar v_{ds}/\ln\lambda} \ln\lambda|Q_c|\left(1-(\frac{I_{ds}}{I_c})^m\frac{\theta}{(\ln\lambda)^m|Q_c|^m}\right)^{1/m} d\phi_n^0 - \frac{I_{ds}}{I_c} = 0\,, \quad (5.50)$$

where $Q_c = Q_c(w_s(\phi_n^0),\phi_n^0)$ is the asymptotic mobile charge. Although this equation for the current can easily be solved numerically for both the built-in channel and enhancement devices for various m and θ values, qualitatively, it is more informative to consider the case $m=1$ and $\theta \ll 1$. Solving (5.50) in this limit, we find

$$I_{ds} = \frac{I_c}{1+\theta\bar v_{ds}/\ln\lambda}\int_0^{\bar v_{ds}/\ln\lambda}|Q_c|\,\ln\lambda\,d\phi_n^0\,.$$

Therefore, the current for both the built-in channel and enhancement devices shown in Figures 5.11, 5.12, 5.15, 5.16 is reduced by the factor $1+\theta\bar v_{ds}/\ln\lambda$ at each bias point $\bar v_{ds}$.

As alluded to in section §5.1, it can also be shown that there is no solution to (5.50) for sufficiently large $\bar v_{ds}$ in the saturation regime. Therefore as remarked in section §5.1, the class of mobility models of the form (5.22) should not be used in this regime.

In addition to field dependent mobility models the scattering of electrons near the interface, leading to a lower effective mobility, is often important in real devices. In the numerical simulations of Price [25], the phemenological position dependent mobility model

$$\mu_n = \mu_{nb} + (\mu_{na}-\mu_{nb})e^{-x/\delta}\,, \qquad \text{with } \mu_{nb} > \mu_{na}\,,$$

was used to investigate the influence of mobility degradation in the inversion layer due to surface scattering effects. The variation of the mobility, δ, was assumed

to occur on the order of an inversion width. Even though the spatial dependence of the mobility in this model is quite simple, any analytical investigation of the current flow with this model within our formulation is limited by the need to compute the averaged channel conductivity appearing in (5.13) in closed form. Unfortunately, the averaged channel conductivity can not be computed in closed form with the above mobility model, even though the asymptotic inversion layer potential is available.

Breakdown Of Expansions For Large Source-Drain Biases. As discussed in Chapter 1, even though the aspect ratio ε may be very small, the asymptotic expansions in the middle of the channel can become invalid for $\bar{v}_{ds}$ sufficiently large. Specifically, the regular expansion in the middle of the channel is no longer valid when, in some region of the channel, $\varepsilon \phi_n^{\prime 0} = O(1)$. The breakdown of the expansion will first be observed in the drain end of the channel. To obtain some insight into the range of source-drain biases for which $\varepsilon \phi_n^{\prime 0} \ll 1$, it is convenient to use the simple analytical expression for ϕ_n^0 in weak inversion given by (5.17). Since $\phi_n^{\prime\prime 0} > 0$, setting $\varepsilon \phi_n^{\prime 0}(1) = 1$ for small fixed ε gives a crude criterion for the maximum source-drain bias for which the long-channel theory is expected to be valid. Using (5.17) and setting $\varepsilon \phi_n^{\prime 0}(1) = 1$ implies $e^{\bar{v}_{ds}} L_d / L = (\lambda \ln \lambda)^{1/2}$. Therefore, for $\bar{v}_{ds} \gg \ln \lambda / 2$, the regular expansion is suspect in the drain end of the channel. This estimate, though, is rather conservative since there is a logarithmic singularity in $\phi_n^0(y)$ just outside the domain that primarily influences the gradients of $\phi_n^0(y)$ only near $y = 1 - O(\varepsilon)$.

In addition to the possible breakdown of the regular expansions in the drain end of the channel for sufficiently large $\bar{v}_{ds}$, the drain depletion width increases with increasing $\bar{v}_{ds}$, and thus, the drain region may occupy a significant fraction of the total channel length. As a result of the expanding drain region, deviations from the long-channel I-V curve previously constructed will occur. To determine the departure from the long-channel behavior, it is essential to compute the potential in the inner region near the drain to find the total mobile charge. The analytical construction of the potential in these inner regions near the source and drain and the resulting departure from long-channel behavior is one of the topics of the next chapter.

CHAPTER 6

Asymptotic Theory Of The Two-Dimensional Equilibrium Potential

In this chapter, some analytical methods are used to construct the equilibrium potential in the vicinity of the source and the drain. Referring to Figure 6.1 and defining the scaled variable $\tilde{y} = (1-y)/\varepsilon$, the potential in equilibrium near the drain for constant doping is given by

$$\nabla^2 w = \frac{1}{\lambda}\left(\exp(w\,\ln\lambda) - \exp(-w\,\ln\lambda)\right) + \begin{cases} 1 & \text{in region I,} \\ -\lambda_+/\lambda & \text{in region II,} \end{cases} \tag{6.1}$$

where $\lambda_+/\lambda \gg 1$, $\lambda \gg 1$ and λ_+ is ratio of the doping level of the heavily doped n-well to the intrinsic concentration. The asymptotic structure of the potential along with the appropriate boundary conditions is shown in Figure 6.1.

As remarked in Chapter 1, the surface potential along the semiconductor-insulator in the vicinity of the drain is taken to be

$$w(0,\tilde{y}) = w_s + (w_{\rm bi} - w_s)\exp(-\pi\varepsilon\tilde{y}/2d)\,.$$

It is also assumed that the depth of the n-well is sufficiently large so that a one-dimensional solution as $x \to \infty$ is the appropriate asymptotic boundary condition for the potential. In §6.5, we will derive a rough estimate of how deep the n-well must be so that the one-dimensional asymptotic boundary condition is appropriate.

Although this problem is not difficult to solve numerically, some analytical results are possible if we limit ourselves to constructing a leading order match. As was shown for the one-dimensional potential in Chapter 2, a leading order match between the depletion layer and the bulk can be obtained by simply patching the potential for C^1 continuity at some unknown location. For the two-dimensional situation shown above, this procedure leads to the study of the model free boundary problem shown in Figure 6.2. The two conditions on the unknown free boundary are that $u = -1$ and the normal derivative of u vanishes across the boundary. With this approach, the details of the transition layer for (6.1) near the depletion

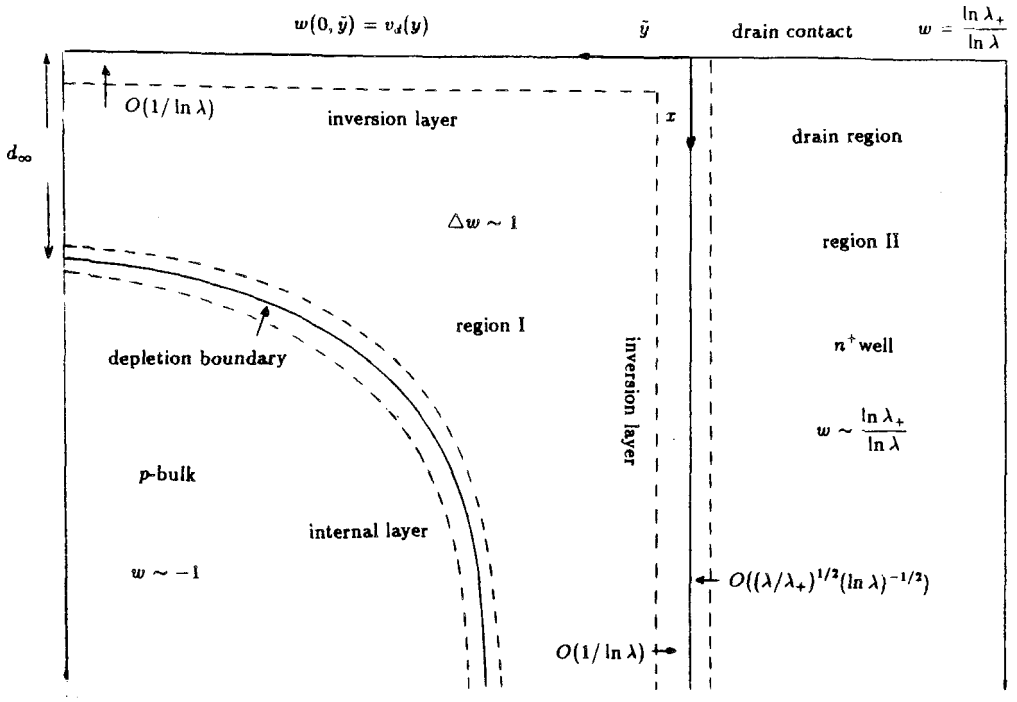

FIGURE 6.1. Structure of the Asymptotic Potential in Equilibrium near the Drain

edge are lost. The constant potential u_b will be found later by matching to the inversion layers.

As a remark, to further illustrate why the free boundary model problem plays a central role in the analysis of (6.1), consider

$$\triangle w_\lambda = 1 + \beta_\lambda(w) \quad \text{with} \quad \beta_\lambda(w) = -\frac{1}{\lambda} e^{-w \ln \lambda}.$$

Then since

$$\beta_\lambda(w) \to \begin{cases} -\infty & \text{for } w < -1 \text{ as } \lambda \to \infty, \\ 0 & \text{for } w > -1 \text{ as } \lambda \to \infty, \end{cases}$$

β_λ can be viewed as a penalty term of the type used to establish existence of solutions of variational inequalities (see [14] and [32]). Therefore it is plausible, although not proven rigorously, that as $\lambda \to \infty$, $w_\lambda \to u$ where u is the solution of the free boundary model problem shown in Figure 6.2.

Free boundary problems of the type shown in Figure 6.2 were considered by Tuck et al. [32] in their study of gravity driven unidirectional viscous flows. The physical situation concerned the coating of a corner of a plate as the plate moved upward, opposed by gravity, through a bath filled with some molten material. The

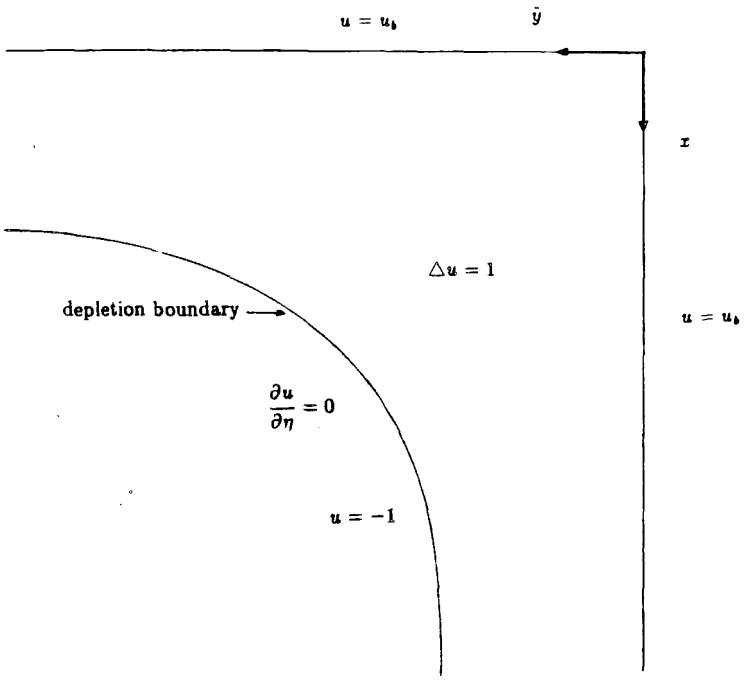

FIGURE 6.2. Model Free Boundary Problem in a 90° Corner

coating thickness, defined as the distance from the corner to the free boundary, was the parameter of interest. Numerical techniques based on an elaborate finite difference calculation were used to find the upward velocity u and the coating thickness for a 90°, 270° and a 360° corner.

Motivated by the work of Tuck et al. [32] and some diffusion problems in semiconductor process modeling, Howison and King [17] have provided analytical solutions for six free boundary problems including those considered by Tuck et al.. Of primary interest for their application was the determination of the explicit shape of the free boundary. The complex variable method they use to solve their free boundary problems is based on a method, introduced by Polubarinova-Kochina [24], originally developed to solve the simple rectangular dam problem in ground-water flow. A review of her method is provided in Crank [9] and Howison and King [17].

The analytical construction of the asymptotic potential in the $\lambda \gg 1$ limit near the source and drain relies heavily on the solution of one of the free boundary problems solved explicitly by Howison and King. The explicit solution to the model free boundary problem shown in Figure 6.2 provides the outer solution to the asymptotic potential away from both the semiconductor-insulator interface

and the boundary of the n-well. By matching the outer potential to quasi one-dimensional inversion layers near the coordinate axes, the asymptotic potential for (6.1) will be constructed.

Although from the solution of Howison and King, a complete pointwise description of the outer potential is available only up to a quadrature, to accomplish the matching of the outer potential to the quasi one-dimensional inversion layers, the normal derivative of the outer potential along both coordinate axes must be provided analytically. Using the explicit solution of Howison and King as well as by manipulating some identities concerning elliptic integrals of complex modulus, the normal derivative information required for the matching will be obtained.

Before constructing the asymptotic potential in equilibrium near the drain, we briefly review the method of Polubarinova-Kochina and the construction of the solution of the model free boundary problem by Howison and King in a 90°, 270° and 360° corner.

6.1 The Method of Polubarinova-Kochina (P-K Method)

The P-K method, which is reviewed briefly below, can be used to find an analytic function, $f(z) = \phi + i\psi$, in some physical domain, Ω, whose boundary consists of $N+1$ segments, each of which is either a free surface or a fixed straight line segment. Corresponding to the physical domain, Ω, there also exists a potential plane, $\bar{\Omega}$, whose boundary may be unknown. On each segment of $\partial\Omega$, two conditions of the form

$$a_{ij}\phi + b_{ij}\psi + c_{ij}x + d_{ij}y = 0 \quad \text{for } i \in 0,..,N \quad \text{and } j = 1,2 \tag{6.2}$$

are assumed to hold. As a remark, the P-K method also applies if (6.2) has a constant inhomogeneous term, e_{ij}; but this freedom will not be needed to solve the model problems. For convenience, (6.2) is written as

$$\mathrm{Im}(k_i z + l_i f) = 0 \quad \text{and} \quad \mathrm{Im}(m_i z + n_i f) = 0 \tag{6.3}$$

on the i'th segement of $\partial\Omega$ where the complex constants k_i, l_i, m_i and n_i are related to a_{ij}, b_{ij}, c_{ij} and d_{ij}.

Now, map the boundaries $\partial\Omega$ of the physical plane and $\partial\bar{\Omega}$ of the potential plane to the real axis of an intermediate ξ plane, so that both Ω and $\bar{\Omega}$ are

mapped conformally to $\mathrm{Im}(\xi) > 0$ by the unknown mapping functions $z = Z(\xi)$ and $f = F(\xi)$. Once the mapping functions Z and F are determined, $w(z)$ can in principle be found by eliminating ξ.

In the mappings, the intersection points of the various segments of the physical plane and the corresponding points of the physical plane are mapped onto the points $\xi = \xi_0 = 0$, $\xi = \xi_1 = 1$, $\xi = \xi_2, .., \xi = \xi_{N-1}$ and $\xi = \xi_N = \infty$. The points $\xi = \xi_2, .., \xi = \xi_{N-1}$ with $\xi = \xi_2, .., \xi = \xi_{N-1}$ purely real, cannot be prescribed. Under this mapping, (6.3) becomes

$$\mathrm{Im}(k_i Z + l_i F) = 0 \quad \text{and} \quad \mathrm{Im}(m_i Z + n_i F) = 0 \tag{6.4}$$

for each i and for $\mathrm{Re}(\xi) \in (\xi_i, \xi_{i+1})$, $\mathrm{Im}(\xi) = 0$.

From (6.4) and using the Schwartz reflection principle, it is possible to determine the nature of the singularities in Z and F at $\xi = \xi_i$ from knowledge of k_{i-1}, k_i, l_{i-1}, l_i, m_{i-1}, m_i and n_{i-1}, n_i. Then, as described in Polubarinova-Kochina [24], setting a certain determinant to zero gives two numbers α_i, β_i, called the exponents, such that near $\xi = \xi_i$ there exists numbers a_i, b_i and functions $h_i(\xi)$, $g_i(\xi)$ such that

$$\begin{aligned} Z(\xi) &\sim a_1(\xi - \xi_i)^{\alpha_i} h_i(\xi) + b_1(\xi - \xi_i)^{\beta_i} g_i(\xi)\,, \\ F(\xi) &\sim a_2(\xi - \xi_i)^{\alpha_i} h_i(\xi) + b_2(\xi - \xi_i)^{\beta_i} g_i(\xi)\,, \end{aligned} \tag{6.5}$$

where g_i and h_i are analytic in discs centered at $\xi = \xi_i$ extending at least to the nearest singularity of Z and F. In the exceptional case when $\alpha_i = \beta_i$ is an integer, we have a logarithmic singularity and so (6.5) takes on a more complicated form.

Thus, we know that all singularities of Z and F are algebraic or logarithmic branch points. Therefore, since we have only regular singular points, Z and F are branches of the Rienmann P-function

$$P\begin{pmatrix} \xi_0 & \xi_1 & \dots & \infty & \\ \alpha_0 & \alpha_1 & \dots & \alpha_\infty & \xi \\ \beta_0 & \beta_1 & \dots & \beta_\infty & \end{pmatrix},$$

which has precisely the required singular behavior at $\xi_0, .., \xi_N$.

The main emphasis with this technique is in relating the appropriate P-function to known special functions that can easily be manipulated. For $N > 2$, this problem can be very difficult. Fortunately, for the model problems to be considered, $N = 2$, so that Z and F are branches of

$$P\begin{pmatrix} 0 & 1 & \infty & \\ \alpha_0 & \alpha_1 & \alpha_\infty & \xi \\ \beta_0 & \beta_1 & \beta_\infty & \end{pmatrix},$$

which can easily be related to the hypergeometric function. To make the comparison between this latter P-function and the hypergeometric function we must arrange for one exponent at $\xi = 0$ and $\xi = 1$ to vanish. Using the well known property of P-functions (see Carrier et al. (8)),

$$P\begin{pmatrix} 0 & 1 & \infty & \\ \alpha_0 & \alpha_1 & \alpha_\infty & \xi \\ \beta_0 & \beta_1 & \beta_\infty & \end{pmatrix} = \xi^{\alpha_0}(\xi-1)^{\alpha_1} \; P\begin{pmatrix} 0 & 1 & \infty & \\ 0 & 0 & \hat{\alpha}_\infty & \xi \\ \hat{\beta}_0 & \hat{\beta}_1 & \hat{\beta}_\infty & \end{pmatrix},$$

where

$$\hat{\alpha}_\infty = \alpha_0 + \alpha_1 + \alpha_\infty \quad \hat{\beta}_0 = \beta_0 - \alpha_0\,,$$
$$\hat{\beta}_\infty = \alpha_0 + \alpha_1 + \beta_\infty \quad \hat{\beta}_1 = \beta_1 - \alpha_1\,,$$

then Z and F are branches of the hypergeometric function $F(a, b, c : \xi)$ with

$$a = \hat{\alpha}_\infty \qquad b = \hat{\beta}_\infty \qquad c = 1 - \hat{\beta}_0\,.$$

The arguments a, b and c can be found knowing only the local behavior of the maps near $\xi = 0$, $\xi = 1$, and $\xi = \infty$. In contrast to the more difficult dam problems considered by Polubarinova-Kochina, the local behavior of the mapping functions near the singular points for the model problems considered by Howison and King can be determined basically by inspection.

6.2 Solution of Three Model Free Boundary Problems

To apply the P-K method to the model free boundary problem, Howison and King noticed that, if u solves the free boundary problem shown in Figure 6.2, then

$f(z)$, defined by

$$f(z) = \phi + i\psi = \bar{z} - 2\left(\frac{\partial u}{\partial x} - i\frac{\partial u}{\partial y}\right), \tag{6.6}$$

is an analytic function in Ω. By means of this ingenious trick, the complex function, $f(z)$, can be found by the P-K method for various geometries by knowing only the local behavior of u and the mapping functions near A,B and O (see Figure 6.3). It is to be noticed, however, that the method applies only for the case of constant doping.

Referring to Figure 6.3a, the local behavior of the potential for the 90° corner near A,B and O is

$$\begin{aligned}
&\text{A}: \quad u \sim \frac{1}{2}y^2 - d_\infty y + u_b \quad \text{so that} \quad f(z) \sim z - 2id_\infty\,, \\
&\text{B}: \quad u \sim \frac{1}{2}x^2 - d_\infty x + u_b \quad \text{so that} \quad f(z) \sim -z + 2d_\infty\,, \\
&\text{0}: \quad u \sim u_b + \frac{r^2}{4}(1 - \cos 2\theta) + \frac{1}{\pi}\mathrm{Im}(z^2 \ln z) + \text{h.o.t.} \quad \text{so that} \quad f(z) \sim cz \ln z\,,
\end{aligned}$$

where $d_\infty = \sqrt{2}(1 + u_b)^{1/2}$, $z = r\exp(i\theta)$ and $r^2 = x^2 + y^2$.

Now the behavior of the mapping functions $f = F(\xi)$ and $z = Z(\xi)$ are easily found near A,B and O. Since infinite strips in the z plane near A and B are mapped to $\xi = 0$ and $\xi = 1$, respectively, we have

$$\begin{aligned}
&\text{A}: \quad Z(\xi) \sim -\frac{d_\infty}{\pi}\left[\ln \xi - i\pi\right] \quad \text{so that} \quad F(\xi) \sim -\frac{d_\infty}{\pi}\left[\ln \xi + i\pi\right], \\
&\text{B}: \quad Z(\xi) \sim -\frac{i\,d_\infty}{\pi}\left[\ln(1 - \xi) + i\pi\right] \quad \text{so that} \quad F(\xi) \sim \frac{i\,d_\infty}{\pi}\left[\ln(1 - \xi) - i\pi\right], \\
&\text{0}: \quad Z(\xi) \sim \xi^{-1/2} \quad \text{so that} \quad F(\xi) \sim c\xi^{-1/2} \ln \xi\,,
\end{aligned} \tag{6.7}$$

where in all cases the principal value of the logarithm is taken. Thus, the exponents at A,B and O are $(0,0)$, $(0,0)$ and $(1/2,1/2)$ so that $Z(\xi)$ and $F(\xi)$ are branches of the hypergeometric function $F(1/2,1/2,1:\xi)$. Two linearly independent branches of this function are $K(\xi)$ and $K(1-\xi)$ where $K(m)$ denotes the complete elliptic integral of the first kind with modulus $m^{1/2}$. Therefore, from the general theory presented earlier, we have

$$Z(\xi) = a_1 K(\xi) + a_2 K(1 - \xi) \quad \text{and} \quad F(\xi) = b_1 K(\xi) + b_2 K(1 - \xi)$$

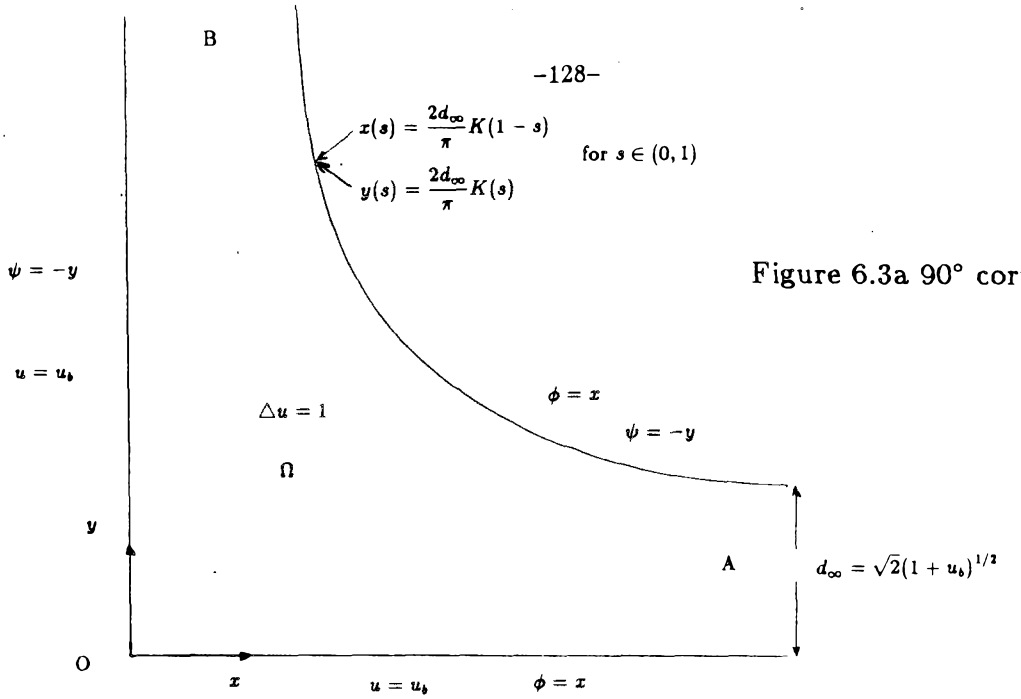

Figure 6.3a 90° corner

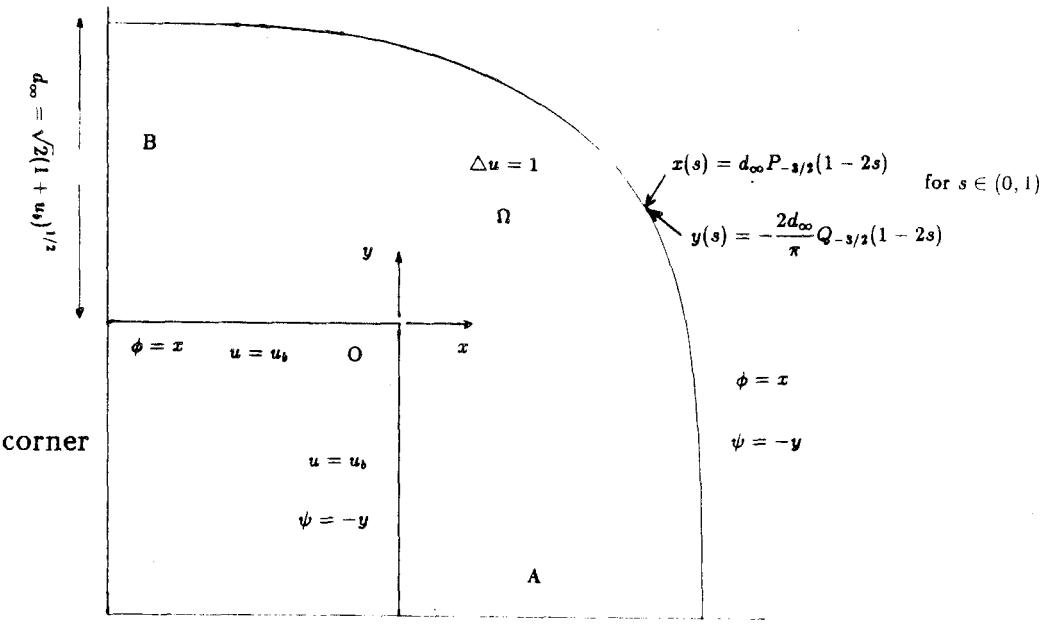

Figure 6.3b 270° corner

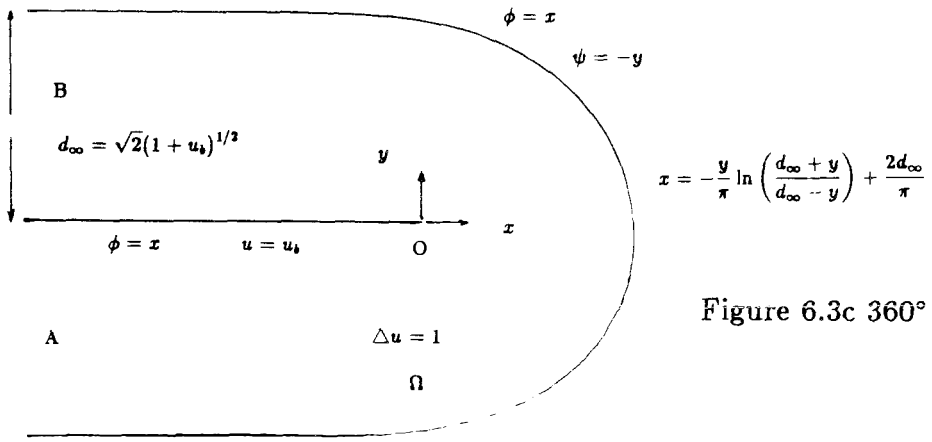

Figure 6.3c 360° corner

FIGURE 6.3. Model Free Boundary Problem For Three Geometries

in the upper half plane $\mathrm{Im}(\xi) \geq 0$ for some coefficients a_j, b_j. Expanding Z and F near the singular points $\xi = 0$ and $\xi = 1$ by using the following limiting expressions for the complete elliptic integral of the first kind

$$\begin{aligned} K(m) &\sim \frac{\pi}{2}(1 + m/4) \quad \text{as } m \to 0\,, \\ K(m) &\sim -\frac{1}{2}\ln\left((1-m)/16\right) \quad \text{as } m \to 1\,, \end{aligned} \tag{6.8}$$

we find

$$a_1 = -b_1 = \frac{2d_\infty i}{\pi} \qquad a_2 = b_2 = \frac{2d_\infty}{\pi}$$

upon comparison with (6.7). Therefore, the mapping functions Z and F are given by

$$Z(\xi) = \frac{2d_\infty}{\pi}\left(K(1-\xi) + iK(\xi)\right) \quad \text{and} \quad F(\xi) = \frac{2d_\infty}{\pi}\left(K(1-\xi) - iK(\xi)\right) \tag{6.9}$$

and the shape of the free boundary is given parametrically by

$$x(s) = \frac{2d_\infty}{\pi}K(1-s) \quad \text{and} \quad y(s) = \frac{2d_\infty}{\pi}K(s) \quad \text{for } s \in (0,1)\,. \tag{6.10}$$

Although the shape of the entire free boundary cannot be expressed explicitly in the form $\tilde{y} = f(x)$, the asymptotic form of the free boundary for $\tilde{y} \to \infty$ out of the corner region can easily be obtained. Letting $s \to 1$ in (6.10) and using the limiting expressions (6.8), we obtain $x/d_\infty \sim 1 + 4\exp(-\tilde{y}\pi/d_\infty)$ as $\tilde{y} \to \infty$ upon eliminating the parametrization, s. The decay of the free boundary onto the simple one-dimensional result is thus exponential with decay factor π/d_∞.

Not surprisingly, the decay constant onto the one-dimensional solution can easily be found without the detailed knowledge of the specific shape of the free boundary. This is accomplished by a simple linearization about the one-dimensional solution. Assuming a solution of the form

$$\begin{aligned} u(x,\tilde{y}) &= u_0(x) + \delta e^{-\sigma\tilde{y}}u_1(x) + \cdots\,, \\ \tilde{y}_d &= d_\infty + \delta e^{-\sigma\tilde{y}}d_1 + \cdots\,, \end{aligned}$$

for the potential and the shape of the free boundary $\tilde{y}_d$ for large $\tilde{y}$, substitution into $\triangle u = 1$ then gives a linear eigenvalue problem for $u_1(x)$:

$$u_1'' + \sigma^2 u_1 = 0 \quad \text{with } u_1 = 0 \quad \text{on} \quad x = 0,\, d_\infty\,.$$

Expanding the vanishing normal derivative condition, we also have $u_1'(d_\infty) = -d_1$. Using only the dominant mode of the above eigenvalue problem, we find

$$u(x,\tilde{y}) \sim u_0(x) + \delta \exp(-\pi\tilde{y}/d_\infty)\, \sin(\pi x/d_\infty)\,,$$
$$\tilde{y}_d \sim d_\infty + \delta \frac{\pi}{d_\infty} \exp(-\pi\tilde{y}/d_\infty)\,.$$

Confirming our expectations, the dominant mode $\sigma = \pi/d_\infty$ does agree with the decay constant found from the explicit shape of the free boundary in the limit $\tilde{y} \to \infty$.

For the 270° corner problem as shown in Figure 6.3b, the local behavior of the potential near A,B and O is

$$\text{A}: \quad u \sim \frac{1}{2}x^2 - d_\infty x + u_b \quad \text{so that} \quad f(z) \sim -z + 2d_\infty\,,$$
$$\text{B}: \quad u \sim \frac{1}{2}y^2 - d_\infty y + u_b \quad \text{so that} \quad f(z) \sim z - 2id_\infty\,,$$
$$0: \quad u \sim u_b + cr^{3/2}\sin\left(\frac{2}{3}(\theta - \pi)\right) + \text{h.o.t.} \quad \text{so that} \quad f(z) \sim cz^{-1/3}\,,$$

while the local behavior of the mapping functions $f = F(\xi)$ and $z = Z(\xi)$ is

$$\begin{aligned}
&\text{A}: \quad Z(\xi) \sim \frac{i\,d_\infty}{\pi}\,[\ln\xi - i\pi] \quad \text{so that} \quad F(\xi) \sim -\frac{i\,d_\infty}{\pi}\,[\ln\xi + i\pi]\,,\\
&\text{B}: \quad Z(\xi) \sim \frac{d_\infty}{\pi}\,[\ln(1-\xi) + i\pi] \quad \text{so that} \quad F(\xi) \sim \frac{d_\infty}{\pi}\,[\ln(1-\xi) - i\pi]\,,\\
&0: \quad Z(\xi) \sim \xi^{-3/2} \quad \text{so that} \quad F(\xi) \sim c\xi^{1/2}\,.
\end{aligned} \tag{6.11}$$

Thus, the exponents at A,B and O are $(0,0)$, $(0,0)$ and $(3/2,-1/2)$, so that $Z(\xi)$ and $F(\xi)$ are branches of the hypergeometric function $F(3/2,-1/2,1:\xi)$. Two linearly independent branches of this function are $P_{-3/2}(1-2\xi)$ and $Q_{-3/2}(1-2\xi)$ where P and Q are Legendre's functions of the first and second kind of order $-3/2$. By using some identities for hypergeometric functions from Erdelyi [12], we derive the identities

$$P_{-3/2}(1-2\xi) = \frac{2}{\pi}\,[2E(\xi) - K(\xi)] \quad \text{and} \quad Q_{-3/2}(1-2\xi) = K(1-\xi) - 2E(1-\xi)\,,$$

where $E(m)$ is the complete elliptic integral of the second kind with modulus $m^{1/2}$. Therefore the mapping functions $F(\xi)$ and $Z(\xi)$ are given by

$$Z(\xi) = a_1\frac{2}{\pi}\,[2E(\xi) - K(\xi)] + a_2\,[K(1-\xi) - 2E(1-\xi)]\,,$$
$$F(\xi) = b_1\frac{2}{\pi}\,[2E(\xi) - K(\xi)] + b_2\,[K(1-\xi) - 2E(1-\xi)]\,,$$

in the upper half plane $\mathrm{Im}(\xi) \geq 0$ for some coefficients a_j, b_j. Expanding Z and F near the singular points $\xi = 0$ and $\xi = 1$ by using (6.8) and

$$E(m) \sim 1 \text{ as } m \to 1 \quad \text{and} \quad E(m) \sim \frac{\pi}{2}(1 - \frac{m}{4}) \text{ as } m \to 0\,, \tag{6.12}$$

we find

$$a_1 = b_1 = d_\infty \qquad a_2 = -b_2 = -\frac{2id_\infty}{\pi}$$

upon comparison with (6.11). Therefore, the mapping functions Z and F are given by

$$\begin{aligned} Z(\xi) &= d_\infty \left[P_{-3/2}(1-2\xi) - \frac{2i}{\pi} Q_{-3/2}(1-2\xi) \right], \\ F(\xi) &= d_\infty \left[P_{-3/2}(1-2\xi) + \frac{2i}{\pi} Q_{-3/2}(1-2\xi) \right], \end{aligned} \tag{6.13}$$

so that the shape of the free boundary is given parametrically by

$$x(s) = d_\infty P_{-3/2}(1-2s) \quad \text{and} \quad y(s) = -\frac{2d_\infty}{\pi} Q_{-3/2}(1-2s) \quad \text{for } s \in (0,1)\,. \tag{6.14}$$

Finally, for the 360° corner problem as shown in Figure 6.3c, the local behavior of the potential near A,B and O is

$$\begin{aligned} &\text{A}: \quad u \sim \frac{1}{2}y^2 + d_\infty y + u_b \quad \text{so that} \quad f(z) \sim z + 2id_\infty\,, \\ &\text{B}: \quad u \sim \frac{1}{2}y^2 - d_\infty y + u_b \quad \text{so that} \quad f(z) \sim z - 2id_\infty\,, \\ &0: \quad u \sim u_b + \frac{1}{2}y^2 + cr^{1/2}\sin(\theta/2) + \text{h.o.t.} \quad \text{so that} \quad f(z) \sim cz^{-1/2}\,, \end{aligned}$$

while the local behavior of the mapping functions $f = F(\xi)$ and $z = Z(\xi)$ is

$$\begin{aligned} &\text{A}: \quad Z(\xi) \sim +\frac{d_\infty}{\pi}[\ln\xi - i\pi] \quad \text{so that} \quad F(\xi) \sim \frac{d_\infty}{\pi}[\ln\xi + i\pi]\,, \\ &\text{B}: \quad Z(\xi) \sim \frac{d_\infty}{\pi}\ln(\xi - 1) \quad \text{so that} \quad F(\xi) \sim \frac{d_\infty}{\pi}[\ln(\xi-1) - 2\pi i]\,, \\ &0: \quad Z(\xi) \sim \xi^{-2} \quad \text{so that} \quad F(\xi) \sim c\xi\,, \end{aligned} \tag{6.15}$$

where the principal value of the logarithm has been taken. Thus, the exponents at A,B and O are $(0,0)$, $(0,0)$ and $(2,-1)$, so that $Z(\xi)$ and $F(\xi)$ are branches of

the hypergeometric function $F(2,-1,1:\xi)$. Two linearly independent branches of this function are $y_1(\xi) = 1-2\xi$ and $y_2(\xi) = (1-2\xi)\ln(\xi/(\xi-1))+2$, so that

$$Z(\xi) = a_1(1-2\xi) + a_2\left[(1-2\xi)\ln(\xi/(\xi-1))+2\right],$$
$$F(\xi) = b_1(1-2\xi) + b_2\left[(1-2\xi)\ln(\xi/(\xi-1))+2\right],$$

in the upper half plane $\mathrm{Im}(\xi) \geq 0$ for some coefficients a_j, b_j. Expanding Z and F near the singular points $\xi = 0$ and $\xi = 1$ and comparing with (6.15), we find

$$a_1 = 0 \quad b_1 = 2id_\infty \quad a_2 = b_2 = \frac{d_\infty}{\pi}.$$

Therefore, the mapping functions Z and F are given by

$$\begin{aligned} Z(\xi) &= \frac{d_\infty}{\pi}\left[(1-2\xi)\ln(\xi/(\xi-1))+2\right], \\ F(\xi) &= -2id_\infty(1-2\xi) + \frac{d_\infty}{\pi}\left[(1-2\xi)\ln(\xi/\xi-1)+2\right], \end{aligned} \tag{6.16}$$

so that the shape of the free boundary is given parametrically by

$$x(s) = \frac{d}{\pi}\left[(1-2s)\ln(s/(1-s))+2\right] \quad \text{and} \quad y(s) = -d_\infty(1-2s) \quad \text{for } s \in (0,1). \tag{6.17}$$

Eliminating s from the above two equations, the free boundary is given explicitly by

$$x = -\frac{y}{\pi}\ln\left(\frac{d_\infty + y}{d_\infty - y}\right) + \frac{2d_\infty}{\pi}.$$

In the next few sections, we will use the solutions of the model free boundary problems to compute the asymptotic potential for the semiconductor device problem in several geometries.

6.3 Asymptotic Equilibrium Potential Near The Drain in Strong Inversion

In this section, we compute the potential, defined by (6.1), asymptotically using the solution of the model free boundary problem in the 90° corner. To accomplish a leading order match of the quasi one-dimensional inversion layers near the coordinate axes to the two-dimensional free boundary solution, the normal derivative of the outer potential along the two coordinate axes must be found. Even though the outer solution, defined up to a quadrature by (6.9), is known only

very implicitly, fortunately, this normal derivative information is easily available with the help of some identities.

Using Byrd [7], the following identities for the complete elliptic integral of the first kind for $\mathrm{Im}(\xi) \geq 0$ can be derived:

$$\begin{aligned} K(\xi) - iK(1-\xi) &= \frac{1}{\sqrt{\xi}} K(\frac{1}{\xi}) = -\frac{i}{\sqrt{1-\xi}} K(\frac{1}{1-\xi}) \\ K(1-\xi) &= \frac{1}{\sqrt{\xi}} K(\frac{\xi-1}{\xi}) = \frac{1}{\sqrt{1-\xi}} \left[K(\frac{1}{1-\xi}) - iK(\frac{\xi}{\xi-1}) \right] . \end{aligned} \tag{6.18}$$

Using these identities in (6.9) and (6.6) to seperate the real and imaginary parts of F and Z and using the fact that the coordinate axis $\tilde{y} = 0$ is mapped to the real segment $\xi = s \in (-\infty, 0)$, we find

$$u_{\tilde{y}}(x(s), 0) = -\frac{2d_\infty}{\pi} \frac{1}{\sqrt{1-s}} K(\frac{s}{1-s}) \quad \text{for } s \in (-\infty, 0) , \tag{6.19}$$

where $x = x(s)$ is determined implicitly from

$$x(s) = \frac{2d_\infty}{\pi} \frac{1}{\sqrt{1-s}} K(\frac{1}{1-s}) \quad \text{for } s \in (-\infty, 0) .$$

As a partial check, the one-dimensional result is obtained from the limit $s \to 0^-$. Similarly, since the coordinate axis $x = 0$ is mapped to the real segment $\xi = s \in (1, \infty)$, using the identities (6.18) in (6.9) and (6.6), we obtain

$$u_x(0, \tilde{y}(s)) = -\frac{2d_\infty}{\pi} \frac{1}{\sqrt{s}} K(\frac{s-1}{s}) \quad \text{for } s \in (1, \infty) , \tag{6.20}$$

where $\tilde{y} = \tilde{y}(s)$ is determined implicitly from

$$\tilde{y}(s) = \frac{2d_\infty}{\pi} \frac{1}{\sqrt{s}} K(\frac{1}{s}) \quad \text{for } s \in (1, \infty) .$$

As a partial check, a simple redefinition of the parametrization, s, shows the required symmetry about $x = \tilde{y}$.

Not only is this normal derivative information crucial to the matching for (6.1), but it is also needed for the computation of the asymptotic mobile charge by Laplace's method. Before computing the mobile charge, we now construct the asymptotic potential for the 90° corner with inversion layers.

Referring to Figure 6.1, in the inversion layer near the boundary between the oxide and the semiconductor region, we take $\hat{x} = x \ln \lambda$ and assume $\tilde{y} = O(1)$ so that posing $w = v(\hat{x}, \tilde{y}) + \cdots$ gives the familiar equation

$$v_{\hat{x}\hat{x}} = \frac{1}{\lambda(\ln \lambda)^2} e^{v \ln \lambda} \quad \text{with} \quad v(0, \tilde{y}) \equiv v_d(\tilde{y}) = w_s + (w_{\rm bi} - w_s) e^{-\epsilon \pi \tilde{y}/2d} ,$$

where $w_s = w_s(\bar{v}_{\rm gs})$ is found from the one-dimensional theory valid in the middle of the channel. The exact solution of this equation is

$$v = 1 + \frac{\ln(\ln \lambda)}{\ln \lambda} + \frac{2}{\ln \lambda} \ln(\alpha_0) - \frac{2}{\ln \lambda} \ln \left(\sinh(\frac{\alpha_0 \hat{x}}{\sqrt{2}} + \gamma_x) \right) , \tag{6.21}$$

where

$$\gamma_x = \sinh^{-1}(\alpha) \quad \text{and} \quad \alpha = \alpha_0 \, (\ln \lambda)^{1/2} \, \lambda^{(1 - v_d(\tilde{y}))/2} , \tag{6.22}$$

and $\alpha_0 = \alpha_0(\tilde{y})$ will be found by matching to the outer solution found from the two-dimensional free boundary problem. In terms of an intermediate variable x_η, the expansion out of the inversion layer is

$$v \sim 1 + \frac{\ln(\ln \lambda)}{\ln \lambda} - \sqrt{2} \alpha_0(\tilde{y}) x_\eta \eta + O(\ln \alpha_0 / \ln \lambda) . \tag{6.23}$$

Before matching to the free boundary solution, we construct the quasi one- dimensional inversion layer near the axis $\tilde{y} = 0$.

Near the axis $\tilde{y} = 0$, we have a planar n^+-p junction and so the potential is constructed in a similar manner as in §4.2. On the n^+-side (for $\tilde{y} < 0$), we take the scalings

$$\bar{y} = \tilde{y} \, (\lambda_+ / \lambda)^{1/2} (\ln \lambda)^{1/2} \quad x = O(1) \quad \text{and} \quad w(x, \tilde{y}) = \frac{\ln \lambda_+}{\ln \lambda} - \frac{h(x, \bar{y})}{\ln \lambda} ,$$

so that to leading order we have

$$h_{\bar{y}\bar{y}} = 1 - e^{-h} \quad \text{on } \bar{y} < 0 ,$$

with $h \to 0$ as $\bar{y} \to \infty$ needed to match to the constant potential in the drain region. Integrating once and defining $h(0, x) = h_0(x)$, we have

$$\sqrt{2} \bar{y} = \int_{h_0(x)}^{h} (t + e^{-t} - 1)^{-1/2} \, dt .$$

Now on the p-side for $\tilde{y} > 0$, we take the scalings $\hat{y} = \tilde{y} \ln \lambda$, $x = O(1)$, and we pose $w = u(x, \hat{y}) + \cdots$. Therfore in the inversion layer along $\tilde{y} = 0$, we have

$$u_{\hat{y}\hat{y}} = \frac{1}{\lambda (\ln \lambda)^2} e^{u \ln \lambda} \quad \text{with} \quad u(x,0) \equiv u_d(x) = \frac{\ln \lambda_+}{\ln \lambda} - \frac{h_0}{\ln \lambda} ,$$

so that

$$u = 1 + \frac{\ln(\ln \lambda)}{\ln \lambda} + \frac{2}{\ln \lambda} \ln(\beta_0) - \frac{2}{\ln \lambda} \ln \left(\sinh(\frac{\beta_0 \hat{y}}{\sqrt{2}} + \gamma_y) \right) , \tag{6.24}$$

where

$$\gamma_y = \sinh^{-1}(\beta) \quad \text{and} \quad \beta = \beta_0 \, (\ln \lambda)^{1/2} \, \lambda^{(1-u_d(x))/2} ,$$

and $\beta_0(x)$ and $h_0(x)$ are to be found by matching.

Patching the potential for C^1 continuity across $\tilde{y} = 0$ gives the transcendental equation

$$(h_0 - 1 + e^{-h_0})^{1/2} = e^{-h_0/2} \cosh(\gamma_y) . \tag{6.25}$$

Since $\lambda_+/\lambda \gg 1$, γ_y is transcendentally small, and thus from (6.25), $h_0(x) \sim 1$. Therefore, the potential along $\tilde{y} = 0$ is essentially constant even though there are significant two-dimensional fields in the corner region. This result clearly illustrates the shielding behavior of the inversion layer mentioned in Chapter 2. Finally, expanding out of the inversion layer as $\hat{y} \to \infty$, we find that with $\hat{y} = y_\eta \eta \ln \lambda$ we have

$$u \sim 1 + \frac{\ln(\ln \lambda)}{\ln \lambda} - \sqrt{2} \beta_0(x) y_\eta \eta + O(\ln \beta_0 / \ln \lambda) . \tag{6.26}$$

Ignoring terms of order $O(1/\ln \lambda)$, matching the quasi one-dimensional inversion layers u and v to the outer two-dimensional potential found from the solution of the free boundary problem involves matching the function values and their derivatives across the layer.

Matching the constant term implies

$$u_b \sim 1 + \frac{\ln(\ln \lambda)}{\ln \lambda} \quad \text{so that} \quad d_\infty \sim \sqrt{2}(2 + \ln(\ln \lambda)/\ln \lambda)^{1/2} .$$

The above expression for the depletion width agrees up to $O((\ln \lambda)^{-1/2})$ with the expression for the one-dimensional depletion width found in Chapter 2 from constructing the internal layer near the depletion edge.

Finally, matching the derivatives determines $\alpha_0(\tilde{y})$ and $\beta_0(x)$ according to

$$-\sqrt{2}\alpha_0(\tilde{y}) = \lim_{x\to 0} \frac{\partial u_{out}}{\partial x} \quad \text{and} \quad -\sqrt{2}\beta_0(x) = \lim_{\tilde{y}\to 0} \frac{\partial u_{out}}{\partial \tilde{y}}\,,$$

where u_{out} denotes the outer free boundary solution found earlier. Using (6.20), (6.19), (6.23) and (6.26) then gives

$$\begin{aligned} \alpha_0(\tilde{y}) &= \frac{\sqrt{2}d_\infty}{\pi\sqrt{s}}\, K(\frac{s-1}{s}) \quad \text{with} \quad \tilde{y}(s) = \frac{2d_\infty}{\pi\sqrt{s}}\, K(\frac{1}{s})\,, \\ \beta_0(x) &= \frac{\sqrt{2}d_\infty}{\pi\sqrt{s}}\, K(\frac{s-1}{s}) \quad \text{with} \quad x(s) = \frac{2d_\infty}{\pi\sqrt{s}}\, K(\frac{1}{s})\,, \end{aligned} \tag{6.27}$$

for $s \in (1, \infty)$, which completes the matching of the free boundary solution to the quasi one-dimensional inversion layers.

As a remark, the quasi one-dimensional inversion layer potential is invalid in the inner corner region where both $x = O(1/\ln\lambda)$ and $\tilde{y} = O(1/\ln\lambda)$. To see why the inversion layer expansion breaks down as $\tilde{y} \to 0$, we see that from (6.27) we have

$$\alpha_0(\tilde{y}) \sim -\frac{\sqrt{2}}{\pi}\tilde{y}\ln\tilde{y} \quad \text{as} \quad \tilde{y} \to 0\,.$$

Since $\alpha_0(\tilde{y}) \to 0$ as $\tilde{y} \to 0$, the $O(1/\ln\lambda)$ term in (6.23) cannot be neglected as $\tilde{y} \to 0$, and so the inversion layer breaks down when $\tilde{y} = O(1/\ln\lambda)$.

In the two-dimensional inversion layer in the inner region, the space charge density is dominated by the mobile n-carriers. In this region, we take the scalings $\xi = x\ln\lambda$, $\eta = \tilde{y}\ln\lambda$, so that to leading order

$$w_{\xi\xi} + w_{\eta\eta} = \frac{e^{w\ln\lambda}}{\lambda(\ln\lambda)^2} \quad \text{with } w(\xi,0) = w(0,\eta) = w_{\rm bi}\,. \tag{6.28}$$

Using Liouville's formula [2], every solution to (6.28) is of the form

$$w\ln\lambda = \ln\left(\frac{|f'(z)|^2}{(1+\frac{\alpha}{8}|f(z)|^2)^2}\right) \quad \text{with } \alpha = -(\ln\lambda)^{-3}/\lambda\,,$$

and $z = \xi + i\eta$, where $f(z)$ is any meromorphic function with simple poles and simple zeroes. Although this result is theoretically interesting, finding the meromorphic function satisfying the boundary conditions and matching to the quasi

one-dimensional inversion layers is no easy task, and in fact, such an explicit solution has not been found. Keeping in mind that our results are not valid in this inner corner region, we now proceed to find the mobile charge.

To compute asymptotically the integral defining the mobile charge, we proceed as in Chapter 2. Defining

$$Q_c = -\left(\frac{\ln\lambda}{\lambda}\right)^{1/2}\int_0^{x^*} e^{w\ln\lambda}\,dx\,,$$

we notice that the contribution to the mobile charge on the interval $[0,1]$ arises from three regions: the source region, the drain region and the gate controlled middle region.

To find the contribution to the mobile charge from the drain region, we integrate the normalized electron concentration over the inversion layer using the quasi one-dimensional inversion layer potential near the drain. A simple calculation gives

$$Q_{cd}(\tilde{y}) \sim -\sqrt{2}e^{v_d(\tilde{y})\ln\lambda/2}\left(\sqrt{1+\alpha^2(\tilde{y})}-\alpha(\tilde{y})\right) \quad \text{with} \quad \tilde{y}=(1-y)/\varepsilon \quad \tilde{y}\ln\lambda \gg 1\,, \tag{6.29}$$

where $v_d(\tilde{y})$ is the surface potential near the drain given by

$$v_d(\tilde{y}) = w_s + (w_{\rm bi} - w_s - \frac{1}{\ln\lambda})e^{-\varepsilon\pi\tilde{y}/2d}\,, \tag{6.30}$$

α is given by (6.22), and $\alpha_0(\tilde{y})$ is given implicitly by (6.27).

Similarly, the contribution to the mobile charge from the source region can also be found. Assuming that the doping levels of the n-wells near the source and drain are equal, symmetry requires $v_s(\tilde{y}) = v_d(\tilde{y})$, so that

$$Q_{cs}(\tilde{y}) \sim -\sqrt{2}e^{v_d(\tilde{y})\ln\lambda/2}\left(\sqrt{1+\alpha^2(\tilde{y})}-\alpha(\tilde{y})\right) \quad \text{with} \quad \tilde{y}=y/\varepsilon \quad \tilde{y}\ln\lambda \gg 1\,. \tag{6.31}$$

Therefore, defining the contribution to the mobile charge from the gate controlled region by Q_m, where Q_m is given by (2.37), a composite expansion for the mobile charge on $O(\varepsilon/\ln\lambda) < y < 1-O(\varepsilon/\ln\lambda)$ can be written. Adding the three contributions to the mobile charge and subtracting the common parts gives

$$Q_c(y) \sim Q_{cd}\left(\frac{1-y}{\varepsilon}\right) + Q_{cs}\left(\frac{y}{\varepsilon}\right) - Q_m(y) \quad \text{on} \quad O(\varepsilon/\ln\lambda) < y < 1-O(\varepsilon/\ln\lambda)\,. \tag{6.32}$$

As a partial check, in the middle of the channel we have $Q_c(y) \sim Q_m(y)$ as anticipated. In §6.4 we derive the expression for the mobile charge under source-drain bias, and show how it is possible to compute the I-V curves in the linear regime taking the two-dimensional end effects into account.

Finally, it should be emphasized that it does not appear possible to construct analytically the potential near the drain in weak inversion. This is owing to the fact that the P-K method for the solution of the free boundary model problem not only requires constant doping but also requires a constant and equal potential along both coordinate axes. Since in weak inversion there is no inversion layer near the semiconductor-insulator interface, the outer potential must satisfy the non-constant boundary data (6.30) along $x = 0$. Therefore the P-K method is not applicable in this regime.

Although analytical progress near the source and drain seems limited in the case of weak inversion, it should, however, be possible to numerically solve for the potential in the inner regions by finite differences and numerically match to the behavior in the middle of the channel. This task is left to future investigators.

6.4 The I-V Curves In The Linear Regime Including End Effects

In this section, we derive the asymptotic expression for the mobile charge, taking into account end effects, that is needed to compute the I-V curves in the linear regime of the enhancement device for constant doping. As shown in Chapter 5, under the appropriate boundary conditions, the leading order potential and electron quasi-Fermi potential for constant mobility are the solutions of

$$\begin{aligned} w_{xx} + \varepsilon^2 w_{yy} &= \frac{1}{\lambda}\left(e^{(w-\phi_n)\ln\lambda} - e^{-w\ln\lambda}\right) + 1\,, \\ \ln\lambda\,\phi_n'^0\,Q(y) &= -\frac{I_{\rm ds}}{I_{\rm c}}\,, \end{aligned} \tag{6.33}$$

where $Q(y)$ is the amount of mobile charge under source-drain bias

$$Q(y) = -\left(\frac{\ln\lambda}{\lambda}\right)^{1/2} \int_0^{x^*} e^{(w(x,y)-\phi_n^0(y))\ln\lambda}\,dx\,.$$

The asymptotic mobile charge for $\lambda \gg 1$ is denoted by Q_u. In contrast to Chapter 5, a uniform expansion for the asymptotic mobile charge, valid throughout the

channel, is now calculated retaining the contributions from the inner regions near the source and drain.

In the outer gate controlled region, the $w_s = w_s(\phi_n^0)$ relationship in the linear regime is found from (5.34). To match to the inner regions near the source and drain, it is convenient to define

$$w_{sr} = \lim_{\ln\lambda\phi_n^0 \to \bar{v}_{\rm ds}} w_s(\phi_n^0) \quad \text{and} \quad w_{sl} = \lim_{\phi_n^0 \to 0} w_s(\phi_n^0)$$

so that the phemenological surface potential profiles near the source and drain are

$$w(0, 1-\varepsilon\tilde{y}) \equiv v_d(\tilde{y}) = w_{sr} + (w_{\rm bi} + \frac{\bar{v}_{\rm ds}}{\ln\lambda} - w_{sr}) \exp(-\frac{\pi\tilde{y}}{2d}) \quad \text{near the drain},$$

$$w(0, \varepsilon\tilde{y}) \equiv v_s(\tilde{y}) = w_{sl} + (w_{\rm bi} - w_{sl}) \exp(-\frac{\pi\tilde{y}}{2d}) \quad \text{near the source}.$$

As $\tilde{y} \to \infty$, we see that the surface potential in the inner regions matches identically to the surface potential in the outer gate controlled region. As a remark, both w_{sl} and w_{sr}, which depend also on the gate voltage, must be found numerically from the expression for the gate controlled total charge (5.34).

In the inner region near the source, $\phi_n^0(y) = \phi_n^0(\varepsilon\tilde{y}) \approx \phi_n^0(0) \approx 0$ so that the potential in the stretched variable $\tilde{y} = y/\varepsilon$ is given by

$$w_{xx} + w_{\tilde{y}\tilde{y}} = \frac{1}{\lambda}(e^{w\ln\lambda} - e^{-w\ln\lambda}) + 1.$$

Since the gate voltage is assumed to be above threshold, we have $w_{sl} > 1$, and thus an inversion layer exists near the semiconductor-insulator interface. Using exactly the same reasoning as in the previous section, the asymptotic mobile charge in the source region is given by

$$Q_{cs}(\tilde{y}) \sim -\sqrt{2}e^{v_s(\tilde{y})\ln\lambda/2}\left(\sqrt{1+\alpha_l^2(\tilde{y})} - \alpha_l(\tilde{y})\right) \quad \text{with} \quad \tilde{y} = y/\varepsilon \quad \tilde{y}\ln\lambda \gg 1$$

where

$$\alpha_l(\tilde{y}) = \alpha_{0l}(\ln\lambda)^{1/2}\lambda^{(1-v_s(\tilde{y})/2},$$

$$\alpha_{0l}(\tilde{y}) = \frac{\sqrt{2}d_{\infty l}}{\pi\sqrt{s}} K(\frac{s-1}{s}) \quad \text{with} \quad \tilde{y}(s) = \frac{2d_{\infty l}}{\pi\sqrt{s}} K(\frac{1}{s}),$$

and $d_{\infty l} = \sqrt{2}(2 + \ln(\ln\lambda)/\ln\lambda)^{1/2}$ is the one-dimensional depletion width near the source.

Similarly, in the inner region near the drain, $\phi_n^0(y) = \phi_n^0(1-\varepsilon\tilde{y}) \approx \bar{v}_{\rm ds}/\ln\lambda$ so that the potential in the stretched variable $\tilde{y} = (1-y)/\varepsilon$ is given by

$$w_{xx} + w_{\tilde{y}\tilde{y}} = \frac{1}{\lambda}(e^{w\ln\lambda - \bar{v}_{\rm ds}} - e^{-w\ln\lambda}) + 1\,.$$

Since, by assumption, we are in the linear regime where $w_{sr}\ln\lambda - \bar{v}_{\rm ds} > \ln\lambda$, pinchoff does not occur, and an inversion layer exists near the semiconductor-insulator interface. Using a similar reasoning as in §6.3, the asymptotic mobile charge, taking carefully into account the dependence on $\bar{v}_{\rm ds}$, is given by

$$Q_{cd}(\tilde{y} : \bar{v}_{\rm ds}) \sim -\sqrt{2}e^{v_d(\tilde{y})\ln\lambda/2}\left(\sqrt{1+\alpha_r^2(\tilde{y})} - \alpha_r(\tilde{y})\right)$$

with $\tilde{y} = (1-y)/\varepsilon$, $\tilde{y}\ln\lambda \gg 1$, and where

$$\alpha_r(\tilde{y}) = \alpha_{0r}(\ln\lambda)^{1/2}\lambda^{(1-v_d(\tilde{y}))/2}e^{\bar{v}_{\rm ds}/2}\,,$$
$$\alpha_{0r}(\tilde{y}) = \frac{\sqrt{2}d_{\infty r}}{\pi\sqrt{s}}K(\frac{s-1}{s}) \quad \text{with} \quad \tilde{y}(s) = \frac{2d_{\infty r}}{\pi\sqrt{s}}K(\frac{1}{s})\,,$$

and $d_{\infty r} = \sqrt{2}(2 + \bar{v}_{\rm ds}/\ln\lambda + \ln(\ln\lambda)/\ln\lambda)^{1/2}$ is the one-dimensional depletion width valid near the drain. The explicit dependence on the source-drain bias $\bar{v}_{\rm ds}$ has been shown.

It is to be remarked that the above expression for the mobile charge near the drain becomes invalid for $\bar{v}_{\rm ds}$ sufficiently large because of two effects. Firstly, for $\bar{v}_{\rm ds}$ sufficiently large, the depletion width near the drain can exceed the depth of the n-well thereby invalidating the boundary condition as $x \to \infty$ used for the construction of the asymptotic potential near the drain. Secondly, for $\bar{v}_{\rm ds}$ sufficiently large, $\varepsilon\phi_n^{0\prime}(1) = O(1)$ so that the approximation that ϕ_n^0 is locally constant in an $O(\varepsilon)$ neighborhood of the drain, which was crucial in finding the asymptotic potential, becomes invalid. From an analytical approach, there appears to be no remedy for either of these difficulties.

Now that the asymptotic mobile charge has been computed in the inner regions, a uniform expansion for the asymptotic mobile charge Q_u, valid along the full extent of the channel to within an inversion layer width of the source and drain, can be written.

Using the the asymptotic mobile charge $Q_c(w_s(\phi_n^0), \phi_n^0)$ controlled by the gate in the linear regime found in §5.3, upon defining $Q_m(y) \equiv Q_c(w_s(\phi_n^0(y)), \phi_n^0(y))$, we see

$$\lim_{\tilde{y}\to\infty} Q_{cd}(\tilde{y} : v_{\rm ds}) = \lim_{y\to 1} Q_m(y) = \lim_{\ln\lambda\phi_n^0 \to v_{\rm ds}} Q_c(w_s(\phi_n^0), \phi_n^0) = Q_c(w_{sr} : \bar{v}_{\rm ds}/\ln\lambda)\,,$$

$$\lim_{\tilde{y}\to\infty} Q_{cs}(\tilde{y}) = \lim_{y\to 0} Q_m(y) = \lim_{\phi_n^0 \to v_{\rm ds}} Q_c(w_s(\phi_n^0), \phi_n^0) = Q_c(w_{sl} : 0)\,.$$

Adding the three contributions to the mobile charge and subtracting the common parts, a uniform expression Q_u for the asymptotic mobile charge is

$$Q_u(y) = Q_{cs}(y/\varepsilon) + Q_{cd}((1-y)/\varepsilon : \bar{v}_{\rm ds}) + Q_m(y) - Q_c(w_{sl} : 0) - Q_c(w_{sr} : \bar{v}_{\rm ds}/\ln\lambda) \tag{6.34}$$

As a partial check, we notice that in the middle of the channel $Q_u(y) \sim Q_m(y)$ and that when $\bar{v}_{\rm ds} = 0$, $Q_u(y)$ is identical to the asymptotic mobile charge in equilibrium given by (6.32). Using this uniform expression for the mobile charge in (6.33) the problem of determining the I-V curves in the linear regime has been reduced to quadrature.

6.5 Asymptotic Equilibrium Potential For a 270° Corner

In this section, we briefly show how the free boundary model problem (6.3*b*) is useful in finding the asymptotic equilibrium potential in a 270° corner. The asymptotic construction of the equilibrium potential for such a geometry is relevant to the study of the two-dimensional n^+-p junction away from the semiconductor-insulator interface. A schematic plot of the geometry, layer structure and local coordinate system for

$$\nabla^2 w = \frac{1}{\lambda}\left(\exp(w\,\ln\lambda) - \exp(-w\,\ln\lambda)\right) + \begin{cases} 1 & \text{in region I,} \\ -\lambda_+/\lambda & \text{in region II,} \end{cases} \tag{6.35}$$

with $\lambda_+/\lambda \gg 1$, $\lambda \gg 1$ and $\lambda_+ \gg 1$ is shown in Figure 6.6.

For the case of a 270° corner, the outer solution for (6.35) is given up to a quadrature by (6.13). Matching the outer solution to the inversion layers near the coordinate axes again requires explicit knowledge of the normal derivative of the outer solution along both coordinate axes. Although the details of the calculation are more involved than for a 90° corner, we again must seperate real and imaginary parts in (6.13) for various ranges along $\mathrm{Im}(\xi) = 0$.

implicit relation along $y = 0$ for $s \in [1, \infty)$:

$$\begin{aligned} \frac{\partial u}{\partial y}(x(s),0) &= \frac{2d_\infty}{\pi}\left[\frac{1}{\sqrt{s}}K(\frac{s-1}{s}) - 2\sqrt{s}E(\frac{s-1}{s})\right], \\ x(s) &= \frac{2d_\infty}{\pi}\left[2\sqrt{s}\left(E(\frac{1}{s}) - K(\frac{1}{s})\right) + \frac{1}{\sqrt{s}}K(\frac{1}{s})\right]. \end{aligned} \tag{6.36}$$

Similarly, along $x = 0$ for $s \in (-\infty, 0)$, we have

$$\begin{aligned} \frac{\partial u}{\partial x}(0,y(s)) &= \frac{2d_\infty}{\pi}\left[\frac{1}{\sqrt{1-s}}K(\frac{s}{s-1}) - 2\sqrt{1-s}E(\frac{s}{s-1})\right], \\ y(s) &= \frac{2d_\infty}{\pi}\left[2\sqrt{1-s}\left(E(\frac{1}{1-s}) - K(\frac{1}{1-s})\right) + \frac{1}{\sqrt{1-s}}K(\frac{1}{1-s})\right]. \end{aligned} \tag{6.37}$$

As a partial check, we notice that a simple redefinition of the parametrization, s, shows the required symmetry. In addition, using the asymptotic relations for small and large argument of K and E, we see that

$$x(s) \to -\infty \quad \text{and} \quad \frac{\partial u}{\partial y}(x(s),0) \to -d_\infty \quad \text{as } s \to 1\,,$$

which agrees with the one-dimensional result. Finally, near the origin, we have

$$x(s) \sim -\frac{3d_\infty}{8}s^{-3/2} \quad \text{and} \quad \frac{\partial u}{\partial y} \propto x^{-1/3} \quad \text{as } s \to \infty\,,$$

which has the correct singular behaviour.

Now that the normal derivative information for the outer potential has been obtained, the procedure for constructing the asymptotic potential for (6.35) is virtually identical to that of the 90° corner. Constructing inversion layers near the coordinate axes and transition layers in the n-well and matching to the outer solution, we again find

$$d_\infty \sim \sqrt{2}(2 + \ln(\ln\lambda)/\ln\lambda)^{1/2}\,.$$

Likewise, we can easily determine the unknown constants in both inversion layers using (6.36) and (6.37). Since the details are very similar to §6.3, they will not be repeated here. Recall that the quasi two-dimensional inversion layer expansion breaks down in an $O(1/\ln\lambda)$ neighborhood of the origin.

As a remark, the solution near the n^+-p junction is only valid provided that the depth of the n-well is sufficiently large so that there is no interaction with the fields near the semiconductor-insulator interface. We now provide a simple estimate, based on the equilibrium potential, that gives a rough measure of the minimum depth of the n-well for which there is little interaction between the fields in the 90° and 270° corner.

Using the asymptotic expressions for large and small argument of $K(\xi)$ and $E(\xi)$ for the 90° and 270° corner problems, it can be shown that the minimum depth of the n-well for which the no interaction assumption is satisfied is roughly .50 microns for $\lambda = 10^6$ for silicon at room temperature. The above estimate is based on the somewhat arbitrary requirement that the two-dimensional free boundaries for the 90^0 and 270° corners must each approach the one-dimensional limit of d_∞ to within 2 percent. For n-well depths less than this rough cutoff value, the geometry of the free boundary problem becomes much more complex, and thus applying the P-K method requires the determination of the appropriate P-function with four singular points. Because of the difficulty in finding the P-function with $N = 3$, the shape of the free boundary over a step geometry has not been found.

Finally, a viable application of the 270° corner solution is the possibility of finding the breakdown voltage for a reverse biased two-dimensional n^+-p junction. Using the free boundary solution with the quasi one-dimensional inversion layers, it should be possible to find analytically, in contrast to Greenfield's [15] elaborate numerical calculation, the breakdown voltage of a reverse biased two-dimensional n^+-p junction.

6.6 Asymptotic Potential For The JFET

For other devices such as the junction field effect transisitor (JFET), the model free boundary problem (6.3c) for a 360° corner plays an important role in constructing the asymptotic potential for long-channel devices. In this section, we briefly remark on how our singular perturbation arguments are easily adapted to the new geometry and can provide the I-V relations incorporating the effect of regions with distinctly two-dimensional behavior.

The scaled semiconductor equations for the unipolar n-channel JFET under

constant doping and no recombination are

$$\tilde{\nabla}^2 w = \frac{1}{\lambda}(e^{\ln\lambda(w-\phi_n)} - e^{-\ln\lambda w}) - 1\,,$$

$$\tilde{\nabla}^2\phi_n + \tilde{\nabla}\phi_n \cdot \left(\frac{\tilde{\nabla}\mu_n}{\mu_n} + \ln\lambda\tilde{\nabla}(w-\phi_n)\right) = 0\,,$$

where

$$\tilde{\nabla} \equiv \left(\varepsilon\frac{\partial}{\partial x}, \frac{\partial}{\partial y},\right) \qquad \text{with} \qquad \varepsilon = \frac{L_d}{L_g}\sqrt{\frac{\ln\lambda}{\lambda}}\,,$$

and L_g is the physical gate length. As for the MOSFET, the scaling has been chosen so that the depletion width directly under the gate is $O(1)$ as $\lambda \gg 1$. The other symbols have the same meaning as in Chapter 1. The simplified scaled geometry of the JFET and the relevant boundary conditions are shown schematically in Figure 6.7.

There are several qualitative differences between the MOSFET and the JFET. For the JFET the gate voltage modulates the depletion width and thus controls the amount of cross sectional area available for the passage of current. For these devices, we need not worry about the presence of inversion layers directly under the gate, and there is no oxide between the gate and the semiconducting material. This is in contrast to the enhancement type MOSFET where, by a field effect mechanism, the gate modulates the amount of mobile carriers and hence the conductivity of the thin inversion layer near the interface. Another difference between the JFET and the MOSFET is in the different geometry and thus the different structure in the inner two-dimensional regions near the edges of the gate. In these inner regions for the JFET, the model free boundary problem (6.3*c*) plays an important role in determining the asymptotic potential.

In equilibrium, $\phi_n \equiv 0$, and in the normal operating regime of the JFET, $-1 < w_s(\bar{v}_{gs}) < 1$, the contribution to the space charge of the holes can be neglected so that the potential is given asymptotically by

$$w_{yy} + \varepsilon^2 w_{xx} = \frac{1}{\lambda}e^{w\ln\lambda} - 1\,, \tag{6.38}$$

with boundary conditions as shown in Figure 6.7. As in the case of the MOSFET, in the limit $\varepsilon \to 0$, there is a region directly under the gate where the potential

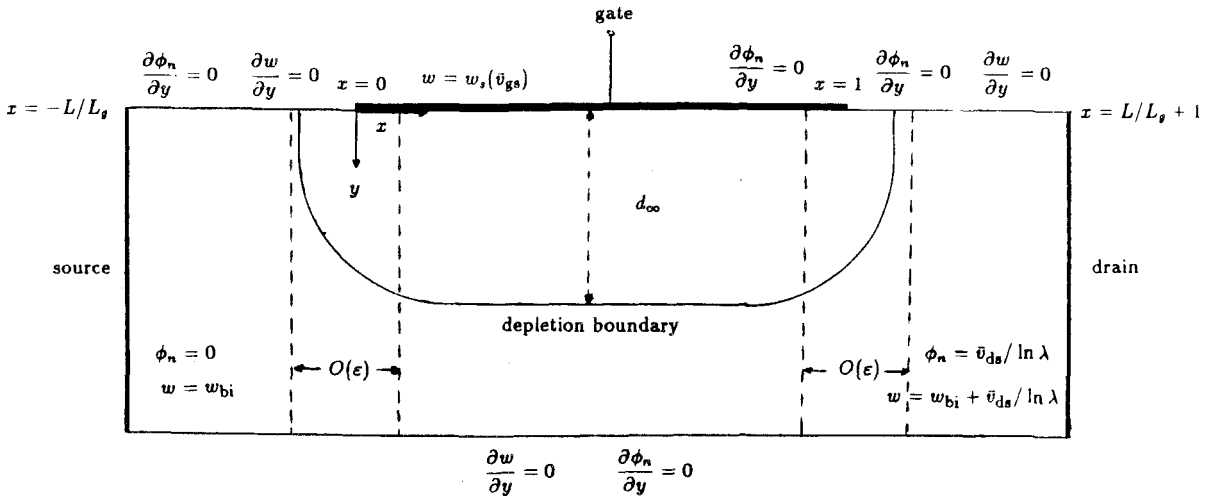

FIGURE 6.5. Schematic Plot of the Geometry of the JFET

is one-dimensional and can easily be constructed in the limit $\lambda \gg 1$. In the inner region near the left edge of the gate, we scale by $\tilde{x} = x/\varepsilon$ and let $u(\tilde{x}, y) = -w(\tilde{x}, y)$ so that (6.38) becomes fully two-dimensional

$$u_{\tilde{x}\tilde{x}} + u_{yy} = 1 - \frac{1}{\lambda} e^{-u \ln \lambda} . \tag{6.39}$$

Although the geometry and boundary conditions are different, the equation for u is identical to that encountered for the 90° corner problem near the drain away from the inversion layers. Ignoring the details of the transition layer near the depletion edge and noticing the symmetry about $y = 0$, which allows the normal derivative condition on w for $\tilde{x} < 0$ to be satisfied, the leading order asymptotic potential to (6.39) as $\lambda \gg 1$ is given up to a quadrature by (6.16). Thus, the explicit shape of the depletion boundary is simply

$$\frac{x}{\varepsilon} = \frac{y}{\pi} \ln\left(\frac{d_\infty + y}{d_\infty - y}\right) - \frac{2d_\infty}{\pi} \quad \text{for } 0 \le y < d_\infty , \tag{6.40}$$

where $d_\infty \sim \sqrt{2}(1 - w_s)^{1/2}$ is found by matching to the one-dimensional potential under the gate. A similar expression holds for the shape of the free boundary near

$x = 1$. As shown in §6.3 and Chapter 5, the asymptotic potential under moderate source-drain bias can easily be constructed in the inner and outer regions, respectively, once the equilibrium asymptotic potential is known.

As a remark, to obtain a simple estimate of how small ε must be so that the basic structure of outer and inner regions for the potential is appropriate, suppose that at $x = 1/2$ we require that the two-dimensional free boundary $y = y_d(x)$ given implicitly by (6.40) satisfy $(d_\infty - y_d(x))/d_\infty \leq f$, where f is some specified tolerance. Then using (6.40), we easily derive the rough estimate that $1/\varepsilon \geq 2d_\infty \ln(2/f)/\pi$. Setting $d_\infty = \sqrt{2}$ and $f = .01$, the rough estimate requires $\varepsilon \leq 1/3$. Recalling the definition of ε, we find that for silicon at room temperature with a normalized doping level of 10^5 we require that the gate length satisfy $L \geq 1.0$ microns. Therefore only for devices with submicron gate lengths or devices under very large source-drain bias is a full numerical simulation of the semiconductor equations necessary.

Finally, we remark that the framework developed in Chapters 3 and 5 for long-channel modeling can be used as in §6.4 to compute asymptotically the I-V curves for the JFET incorporating the two-dimensional edge effects of the gate.

References

[1] U. Ascher, J. Christiansen, R. Russell, Collocation Software for Boundary Value ODE's, ACM TOMS 7 No. 2 209 1981.

[2] C. Bandle, Solutions of a Nonlinear Dirchlet Problem for Nearly Circular Domains, SIAM J. Numer. Anal. Vol. 20 No. 6 (1983) pp. 1094-1098.

[3] R. Bank, D. Rose, W. Fichtner, Numerical Methods for Semiconductor Device Simulation, SIAM J. Sci. Stat. Comput. Vol. 4 No. 3 (1983) pp. 416-435.

[4] M. Barron, Low Level Currents in Insulated Gate Field Effect Transistors, Solid State Electronics 15 (1972) pp. 293-302.

[5] J. Brews, Physics of the MOS transistor, Applied Solid State Supplement 2A, Academic Press (1981) pp. 1-119.

[6] J. Brews, A Charge-Sheet Model of the MOSFET, Solid-State Electronics 21 (1978) pp. 345-355.

[7] P. Byrd, M. Friedman, Handbook of Elliptic Integrals for Engineers and Scientists, Springer-Verlag, Berlin 1954.

[8] G. Carrier, M. Krook, C. Pearson, Functions of a Complex Variable, McGraw-Hill, New York 1966.

[9] J. Crank, Free and Moving Boundary Problems, Oxford University Press, Oxford 1984.

[10] A. Demari, An Accurate Numerical Steady-State One-Dimensional Solution of the P-N Junction, Solid-State Electronics 11 (1968) pp. 33-58.

[11] W. Engl, H.Dirks, B.Meinerzhagen, Device Modeling, Proc. IEEE 71 No. 1 (1983) pp. 10-33.

[12] A. Erdelyi, Higher Transcendental Functions Vol. 2, Bateman Manuscript Project, McGraw-Hill 1953.

[13] W. Fichtner, D. Rose, R. Bank, Semiconductor Device Simulation, SIAM J. Sci. Stat. Comp. Vol. 4 No. 3 (1983) pp. 391-415.

[14] A. Friedman, Variational Inequalities and Free Boundary Problems, Wiley-Interscience, New York 1982.

[15] J. Greenfield, Analysis of Intrinsic MOS Devices and Parasitic Effects Using Solutions of Poisson's Equation, Ph.D. Dissertation, Stanford Electronics Lab, Stanford (1982).

[16] H. Gummel, A Self-Consistent Iterative Scheme for One-Dimensional Steady State Transistor Calculations. IEEE Trans. Electron Devices ED-11 (1964) pp. 455-465.

[17] S. Howison, J. King, Explicit Solutions to Six Free Boundary Problems, Preprint (1988).

[18] P. Markovich, A Singular Perturbation Analysis of the Fundamental Semiconductor Device Equations, SIAM J. Appl. Math 44 No.5 (1984) pp. 896-928.

[19] P. Markovich, The Stationary Semiconductor Device Equations, Springer Verlag, Wien-New York 1986.

[20] M. Mock, A Two-Dimensional Mathematical Model of the Insulated-Gate Field-Effect Transistor, Solid-State Electronics 16 (1973) pp 601-609.

[21] H. Pao and C. Sah, Effects of Diffusion Current on Characteristics of Metal-Oxide Semiconductor Transistors, Solid-State Electronics, Vol. 9 (1966) pp. 927-937.

[22] C. Please, An Analysis of Semiconductor P-N Junctions, D. Phil Thesis, Oxford University, Oxford 1978.

[23] C. Please, An Analysis of Semiconductor P-N Junctions, IMA J. of Applied Math. 28 (1982) pp. 301-318.

[24] P. Polubarinova-Kochina, Theory of Ground Water Movement,

Princeton University Press, Princeton 1962.

[25] C. Price, Two-Dimensional Numerical Simulation of Semiconductor Devices, Ph.D. Dissertation, Stanford University, Stanford (1982).

[26] M. Protter, H. Weinberger, Maximum Principles in Differential Equations, Prentice-Hall, Englewood Cliffs 1967.

[27] I. Rubinstein, Multiple Steady States in One-Dimensional Electrodiffusion with Local Electroneutrality, SIAM J. Appl. Math Vol. 47 No. 5 (1987) pp 1076-1093.

[28] K. Seeger, Semiconductor Physics, Springer-Verlag, Berlin, 1985.

[29] S. Selberherr, Analysis and Simulation of Semiconductor Devices, Springer Verlag, Wien-New York, 1984.

[30] W. Shockley, The Theory of P-N Junctions in Semiconductors and P-N Junction Transistors, Bell Syst. Tech J., 28 435 (1949).

[31] S. Sze, Physics of Semiconductor Devices, John Wiley, New York 1969.

[32] E. Tuck, M. Bentwich, J. Van Der Hoek, The Free-Boundary Problem for Gravity-Driven Unidirectional Viscous Flows, IMA J. of Applied Math 30 (1983) pp. 191-208.